

Working Paper

A Set of Climate Models for Integrated Modelling of Climate Change Impacts

*Part II: A 2.5-Dimensional
Dynamical-Statistical
Climate Model (2.5-DSCM)*

*Vladimir K. Petoukhov
Andrey V. Ganopolski*

WP-94-39
May, 1994



International Institute for Applied Systems Analysis □ A-2361 Laxenburg □ Austria

Telephone: +43 2236 715210 □ Telex: 079 137 iiasa a □ Telefax: +43 2236 71313

A Set of Climate Models for Integrated Modelling of Climate Change Impacts

Part II

A 2.5-Dimensional Dynamical-Statistical Climate Model (2.5-DSCM)

*Vladimir K. Petoukhov
Andrey V. Ganopolski*

May 1994

Working Papers are interim reports on work of the International Institute for Applied Systems Analysis and have received only limited review. Views or opinions expressed herein do not necessarily represent those of the Institute, its National Member Organizations, or other organizations supporting the work.



International Institute for Applied Systems Analysis □ A-2361 Laxenburg □ Austria

Telephone: +43 2236 71521 □ Telex: 079 137 iiasa a □ Telefax: +43 2236 73147

FOREWORD

The climate research component of the Forestry and Climate Change Project has had as one of the objectives to develop a series of simplified climate models which can be part of integrated models for analyses of climate change. This Working Paper describes climate simulations with a 2.5-Dimensional Dynamic-Statistical Climate Model.

Table of Contents

1. Summary	2
2. Introduction and overview.	4
3. Description of the 2.5-DSCM	7
3.1 Approach	10
3.2 Atmospheric component of the model	11
3.3 Oceanic component	29
3.4 Land component	32
3.5 Linkage of climate components	33
3.5.1 Atmosphere and ocean	33
3.5.2 Atmosphere and land	34
3.6 Present status of the model	34
4. Model results	36
4.1 Overview of results	36
4.2 Simulation of present climate	37
4.3 Equilibrium response to a doubling of CO ₂ content in the atmosphere	48
4.4 Time dependent runs	48
5. Multilayer isopycnal ocean model	53
5.1 Physical background	53
5.2 Model description	54
5.3 Numerical methods	60
5.4 Model results	63
5.4.1 Description of the numerical experiments	63
5.4.2 Oceanic circulation	64
5.4.3 Thermohaline structure of the ocean	67
5.4.4 Heat and salt balance	71
5.4.5 Tracers distribution	77
6. Integrated Assessment of Climate Change Impacts on European Forests (ICCF): A projected application to integrated modelling of climate change impact	78
7. Conclusion	81
Appendix. The structure of the global scale coupled climate model and preliminary results	84
References	90

1. Summary

Projections of changes in climate are valuable in their own right, but they raise another, perhaps more important set of questions: What effects might such changes have on food production, on forests, on insect life, energy demand, and fresh water supply - on dozens of factors that directly and indirectly affect human well-being?

To address these questions, specialists must link ecological models with climate models; to assess policies, the climate models must in turn be driven by accounting frameworks that calculate total emissions and concentrations of greenhouse gases, depending on policy scenarios. This chain - from policy-oriented accounting tool to climate model to ecological impact model, with feedback, possibly supported by a model for socioeconomic analyses - comprises an integrated assessment model or an integrated model of climate change, as it is also called.

In terms of running time a climate model can easily play a dominant role within an integrated model of climate change. General Circulation Models are the state of the art for studying and projecting climate, but for integrated assessments they are impractical: they are not computer-efficient with respect to both running time and hardware. They can take weeks, running on a super computer, to calculate one complete scenario. Many ecologists and policy analysts, however, wish to assess a great number of scenarios and therefore need a suitable climate model that can give results within hours, possibly within a day, using a workstation or a PC.

In fact, the needs of impact modellers and other model users are very often antagonistic to each other, like, e.g., their desire for both a quick turnaround time and climatic information with a high spatial and temporal resolution. Therefore, the choice of a proper climate model is crucial for the entire integrated model. In principle, it is the environmental impact one wishes to assess that determines the degree of sophistication of the climate model and thus its computing time requirements. But environmental impact modellers or assessors, on the other hand, must be prepared to answer questions of great consequence. They might be asked, e.g., whether the environmental impact under discussion could also be studied having less climate variables available as input information, and which spatial

and temporal resolution of these climate variables would still be acceptable.

The Working Paper summarizes the status of two climate models out of a set of four of graded complexity that are available or under development at IIASA, and describes the envisaged position of these climate models in the context of an integrated model of climate change. The climate models mentioned in Part I and II of the Working Paper are a 2-dimensional Zonal Climate Model and a 2.5-dimensional Dynamical-Statistical Climate Model, respectively. They offer different sets of climatic information with different spatial and temporal resolutions and thus allow a choice depending on the environmental impact to be studied in an integrated fashion.

The Working Paper also sheds light on a projected application to integrated modelling of climate change impacts, which forms one of the focal points of IIASA's environmental research until 1996 and involves five collaborating research teams from Australia, Finland and Sweden. This will be an integrated assessment of climate change impacts on European forests. A two-step approach employing both the Zonal Climate Model and the Dynamical-Statistical Climate Model is outlined. An important feature of the integrated assessment is that the ecophysiology of a single plant up to that of aggregated forest ecosystems will be considered. This provides a linkage to the climate models mentioned and thus, in combination with a policy-oriented accounting tool for greenhouse gas emissions and concentrations, an integrated assessment becomes feasible.

2. Introduction and overview.

Current studies in the field of climate modelling are carried out using five basic methods depending on the scientific tool of investigation.

The first approach uses highly sophisticated climate models which simulate the general circulation of the atmosphere and/or the ocean. These are the so-called general circulation models (GCMs) (e.g., Manabe *et al.*, 1992; Hansen *et al.*, 1983; Cubasch *et al.*, 1991). The thermodynamical approach is based on simplified energy balance models (e.g., Budyko, 1969; Sellers, 1969; North, 1975; Rasool and Schneider, 1971). Radiative-convective and radiative-turbulence models form the third type of climate modelling (e.g., Karol and Rozanov, 1982; Hummel and Kuhn, 1981; Ou and Liou, 1984). Empirical-statistical models are the basis for the so-called statistical method of climate research (e.g., Vinnikov, 1986; Polyak, 1975). The fifth type of climate modelling, finally, is represented by the so-called statistical-dynamical (or, equivalently, dynamical-statistical) models (see, e.g., Saltzman, 1978; Adem, 1964; Petoukhov, 1976).

Three-dimensional GCMs are the state of the art for present studies of climate and climate change. Most of them use the primitive hydrothermodynamical equations for both the atmosphere and the ocean. These models have a high spatial and temporal resolution (in the best GCMs the latitudinal and longitudinal resolution is up to 1° , the temporal resolution is up to 10 minutes, and the number of vertical levels is more than 20). The most sophisticated GCMs explore the atmospheric and oceanic interaction. GCMs are widely used for simulating present climate in terms of its annual cycle and its intraseasonal and interannual variability, as well as for evaluating natural and anthropogenic impacts on climate.

However, GCMs have some shortcomings which make them inconvenient for climate change impact studies. Due to their degree of complexity they have a relatively long turnaround time, even on the most advanced computer systems. This fact places certain limitations on the application of GCMs in integrated models in the cases of polyvariant analysis of climate change scenarios. Different parts of GCMs are not equally developed (e.g., cloudiness being an important component of the climate system

is one of the relatively weak points of these models). The accuracy of simulating basic present climate conditions (e.g., surface air temperature) at a grid-point level is not very high, especially in polar regions. A noticeable concurrence seems to exist between the uncertainty of simulating current temperature and the uncertainty of temperature sensitivity due to standard experiments (see Figures 2.2 and 2.3 in Part I of this Working Paper, hereafter referred to as WP1).

The second type of climate modelling is represented by energy balance models (EBMs). They are less sophisticated, have a sound physical bases, and are computer efficient in terms of running time. Restrictions to applying these models in climate change impact investigations are connected with the small number of climate output variables (see Table 2.4 in WP1), and with their relatively low spatial resolution (they are mainly zonal; in nonzonal models of this type oceanic and atmospheric modules are generally not separated).

Radiative-convective models (RCMs) and radiative-turbulence models (RTMs) are the best tool for investigating the radiative effect of greenhouse gases and aerosols and for evaluating their influence on the mean global and zonal temperatures at various pressure levels. But these models cannot be used for regional climate responses to, for instance, anthropogenic impacts. RCMs and RTMs are very limited also as to the number of climatic variables they deal with. For these reasons the application of RCMs and RTMs in integrated models is restrictive.

Empirical-statistical climate models that are based on empirical climatic information are useful when elucidating the various spatial/temporal correlations which exist between climatic variables under present climatic conditions. At the same time, the possibility of using them for estimating correlation trends under a changing climate is doubtful. In this sense, relatively simple statistical models derived from GCM results seems to have a perspective. These statistical models (see, e.g., Hasselmann and von Storch, 1992) represent what we call the top-down approach with regard to the climate module design for an integrated model of climate change impacts (see Table 2.2 of WP1).

Dynamical-statistical climate models (DSCMs) occupy an intermediate position in the hierarchy of climate models between GCMs and EBMs. On the one hand, DSCMs are rather sophisticated (in comparison with EBMs), comprise the most important feedbacks, and a large number of climate output

variables. Their spatial and temporal resolution is adequate to many environmental impact problems (see Table 2.5 in WP1). On the other hand, they are not as complicated as GCMs and can process many model experiments in a computer-efficient manner. This is very important for assessing the influence of various climate change scenarios on man/biota life aspects. The weakest point of DSCMs is basically the heuristic character of the spatial and temporal averaging procedure which is applied to the original set of primitive hydrothermodynamical equations (for atmosphere, ocean and land) and which results in the working equations of these models.

The DSCM includes all major components of the climate system: atmosphere, land, and ocean. Nevertheless we envisage to use instead of original oceanic module of DSCM, more sophisticated ocean model, namely oceanic GCM, called MILE¹. The main reason for that is the recognized importance of oceanic processes for climate changes. MILE was specially designed for long-term climate simulation and it has rather quick turnaround time. Thus, coupling atmosphere/land modules of DSCM with MILE does not increase significantly projected computer resources.

The structure of the paper is as follows. The concept and structure (climate components) of the 2.5-DSCM of the Institute of Atmospheric Physics (IAP, Moscow) are described in Chapter 3. Chapter 4 reviews the results of simulations with this model of present climate, of a transient experiment (instantaneous doubling of atmospheric CO₂), and of a time-dependent climate change experiment (increase of the atmospheric greenhouse gases content according to the 1990 IPCC scenario A, Houghton *et al.*, 1990). A multilayer isopycnal oceanic model (MILE) developed in the Computer Center of the Russian Academy of Sciences (CC, Moscow) which is envisaged to be coupled with 2.5-DSCM is described in Chapter 5. A brief description and perspective of the improved global version of the 2.5-DSCM are given in Chapter 6 and Appendix. Possible applications of the 2.5-DSCM in the framework of climate change impact studies, as well as the envisaged use of the DSCM in an Integrated Assessment of Climate Change Impacts on European Forests (ICCF) are also discussed. Chapter 7 summarizes the status of the 2.5-DSCM and its position in the context of an integrated model of climate change impacts.

¹ Multilayer Isopycnal Largescale ocean model

3. Description of the 2.5-DSCM

The main concept of the 2.5-DSCM described below is that the evolution of the climate system on spatial scales ≥ 500 – 1000 km (in the atmosphere) and ≥ 300 – 500 km (in the ocean) and with a time scale ≥ 10 days is the result of the nonlinear interaction between a limited number of large-scale climate-forming objects (CFOs). In accordance with this concept, the minimum CFOs are synoptic-scale eddies and waves as well as ensembles of dry and moist (cumulus) convection, in the atmosphere, and synoptic-scale eddies and waves as well as convective ensembles, in the ocean. Small-scale and mesoscale eddies and waves of the atmosphere and ocean are treated in the model as vertical and horizontal of "turbulence."

The second important point of the concept is that the vertical structure of the main climatic variables of the atmosphere and ocean is considered to be universal, i.e., it is supposed to have stable features (to be represented by stable thermodynamical structural elements, TSEs) under a broad range of climatic states, even somewhat away from present climate conditions. For example, vertical temperature profiles in the free troposphere and stratosphere are considered to be quasi-linear, in the mixed layer of the ocean quasi-isothermal, and so on (a more detailed description of the TSEs with respect to the main climatic variables of the model is given below in this chapter). The number and composition of CFOs and TSEs are also considered to be universal in the above-mentioned sense, as well as physical mechanisms of their generation, interaction, and feedbacks between various chains (components, modules, variables) of the climate system.

The main temperature-related feedbacks taken into account in the 2.5-DSCM are listed in Table 2.6 of WP1. In Figure 3.1 the general structure of the 2.5-DSCM is shown (Petoukhov, 1991). The spatial and temporal resolution of the 2.5-DSCM and the number and composition of the climate components and feedbacks, as well as of the climate output elements of the model (see Tables 2.3, 2.4, 2.6 of WP1 and Table 3.1), are anticipated to be appropriate for assessing already quite a few climate change impacts and for incorporating the model into different integrated models (see, e.g., Tables 2.1, 2.4, 2.5 and 5.3 of WP1).

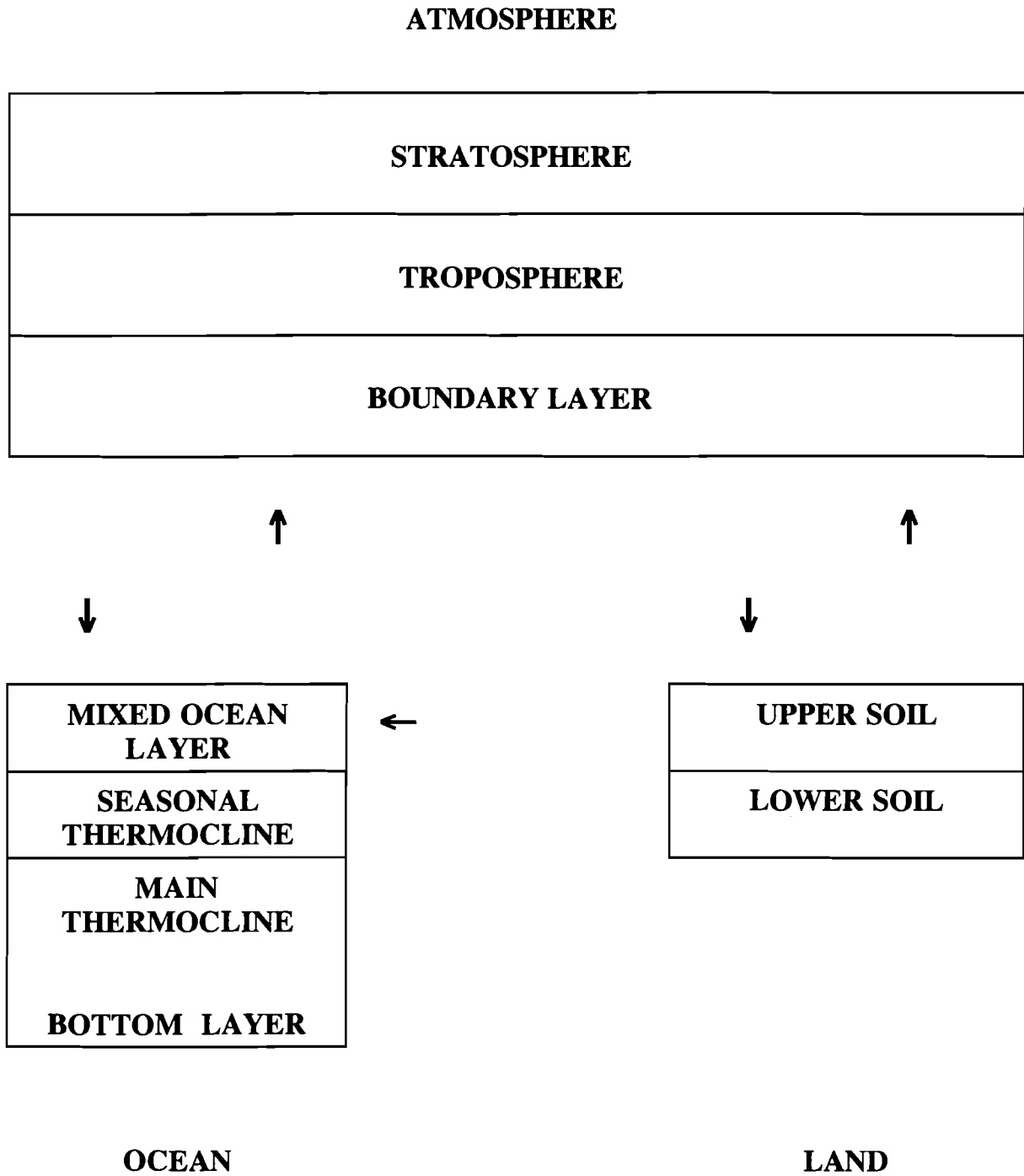


Figure 3.1. Structure of the 2.5 DSCM

Table 3.1 Main features of the present version of the 2.5-DSCM

Spatial resolution	18° x 4.5° (18° on λ and 4.5° on θ ; 3 layers in atmospheric module (20 layers for radiative transfer calculations); 3 layers in oceanic module; 2 layers in land module; simplified geographical distribution of ocean and land; hemispheric ¹⁾ .
Temporal resolution	Seasonal (time step $\sim 1 \div 3$ days).
Governing equations	Prognostic equations for atmospheric temperature and specific humidity; energy balance equations for land and sea ice temperatures; prognostic equation for oceanic temperature and sea ice thickness; diagnostic equations for atmospheric and oceanic large-scale long-term circulation patterns, auto- and cross-correlation functions of atmospheric and oceanic synoptic components (e.g T'^2 , $T'q'_v$, q'^2_v , etc.), soil moisture.
Prescribed parameters	Optical parameters of atmospheric gases, water droplets, crystals and aerosols in solar and terrestrial radiation bands; aerosols and greenhouse gases concentrations; soil and vegetation parameters; oceanic salinity.
Computed climate elements	T , Pr , WV , R , H , E , Cl , Sn , SI , T'^2 , q'^2 , $u'T'$, $v'T'$, $u'q'_v$, $v'q'_v$, u'^2 , v'^2 , Pr'^2 .
Main processes	
Atmosphere	Radiation transfer; large-scale circulation and macroscale eddy/wave horizontal and vertical transport of momentum; heat and moisture (MHM); MHM small/mesoscale "turbulent diffusion"; large-scale condensation, deep and shallow convection.
Ocean	Horizontal and vertical momentum and heat exchange by means of large-scale circulation, synoptic eddies, convection, and small mesoscale "diffusion".
Land	Soil/vegetation/atmospher heat and moisture exchange.
Explicit temperature-related feedbacks	Water vapor; snow and ice albedo; cloudiness; lapse rate; horizontal and vertical transport processes in the atmosphere and ocean; vegetation/soil moisture.
Surface types	Eight vegetation/land-cover and soil types (with and without snow cover); open ocean; sea ice; Antarctic sheet.
Orography	None.
Greenhouse gases	LW calculations: H_2O , CO_2 , CH_4 , O_3 . SW calculations: H_2O , O_3 , aerosols ²⁾ .
Running time	ca 15 minutes on a SUN SPARC 2 workstation for one model year.

- 1) The global version of the model with realistic geography is now under development. For the geographical distribution of ocean and land, grid spacing, and preliminary results of global versions runs see Appendix.
- 2) The global version of the model will also include the most radiatively active CFCs in the SW radiation scheme, using the same procedure as in the 2-D ZCM (see Chapter 3 of WP1)

3.1. Approach

The IAP 2.5-dimensional climate model belongs to a class of grid (with respect to λ and θ , where λ is longitude and θ is co-latitude), multilayer (with respect to z , where z is geometrical height or depth) dynamical-statistical climate models. The vertical structure of the main variables in the atmospheric, oceanic and land boxes is represented in the model by several integral layers (see Figure 3.1 and description below). This spatial λ , θ , z resolution is reflected in the name of the model (2.5-dimensional DSCM, or 2.5-DSCM). Any dependent variable φ_i entering the set of primitive hydrothermodynamical equations for atmosphere, ocean, and land is represented in the model by the sum of the large-scale, long-term component $\hat{\varphi}_i$ (with spatial and temporal scales $\hat{L} \geq 500$ km, $\hat{\tau} \geq 10$ days) and the deviation $\varphi_i' = \varphi_i - \hat{\varphi}_i$. The latter is considered to be connected mainly with synoptic processes in the atmosphere and ocean.

The initial primitive equations of motion, energy, and state, as well as the continuity equation, are subjected to spatial and temporal $(\hat{L}, \hat{\tau})$ averaging. The hydrostatic and quasi-solenoidal approximation for synoptic component φ_i' is used under this procedure. The close to normal (Gaussian) distribution with respect to time and space of the ensembles of synoptic eddies and waves is supposed (Golitsyn and Demchenko, 1980; Lemke, 1977). This allows for omitting the third and all other high odd moments of synoptic component φ_i' in the averaged equations for $\hat{\varphi}_i$ and for representing the fourth and other high even moments of φ_i' as products of second moments.

As a result, the equations for large-scale long-term components of wind speed, vertical velocity, temperature, density, pressure, specific humidity, and salinity are obtained (Petoukhov, 1991). These averaged equations include, besides $\hat{\varphi}_1, \hat{\varphi}_2, \dots, \hat{\varphi}_N$, the products of synoptic components $\overline{\varphi_i' \varphi_j'}$ (auto- and cross-correlation functions). To deduce the corresponding equations for $\overline{\varphi_i' \varphi_j'}$ from the original

(primitive) equations, one of the common methods of statistical fluid dynamics (Monin and Yaglom, 1965, 1967) is applied (Petoukhov, 1990). Namely, the set of primitive equations for $\varphi_1, \varphi_2, \dots, \varphi_N$ is multiplied, for example, by φ_1' and the $(\hat{L}, \hat{\tau})$ average is used. Then the original (primitive) equation for φ_1 is multiplied by $\varphi_1', \varphi_2', \dots, \varphi_N'$, and again the $(\hat{L}, \hat{\tau})$ average is applied. The averaged equations, including $\overline{\varphi_1' \frac{\partial \varphi_j'}{\partial t}}$ and $\overline{\varphi_j' \frac{\partial \varphi_1'}{\partial t}}$, respectively are then summarized to obtain the nonstationary (in the general case) equation in partial derivatives for $\overline{\varphi_1' \varphi_j'}$ (Petoukhov, 1990, 1991). The same procedure is applied to φ_2', φ_3' and any other $\varphi_i' (i = 1, 2, \dots, N)$, which gives the corresponding equations for $\overline{\varphi_2' \varphi_j'}, \overline{\varphi_3' \varphi_j'}, \dots, \overline{\varphi_N' \varphi_j'}$ ($j = 1, 2, \dots, N$). The above-mentioned features of synoptic components are taken into account under this procedure and two additional assumptions are used: (1) the synoptic component in high and middle latitudes is considered to be quasi-geostrophic in free atmosphere; and (2) of all the nonadiabatic processes only phase transition of water vapor and surface friction are considered to be energetically important in the synoptic component of Q , where Q is the sum of nonadiabatic sources and sinks in the atmosphere and the ocean. Let us now describe the model equations in detail.

3.2 Atmospheric component of the model

The set of basic equations of the model for the atmospheric component, resulting from the above-mentioned $(\hat{L}, \hat{\tau})$ averaging is as follows (Petoukhov, 1991):

$$c_p \hat{\rho} \frac{\partial \hat{T}}{\partial t} + c_v \nabla \cdot (\hat{V} \hat{T} \hat{\rho} + \overline{V' T' \hat{\rho}} - \hat{V} \hat{\alpha} \overline{T'^2 \hat{\rho}}) = - \hat{R} \hat{\rho} \hat{T} \nabla \cdot \hat{V} + \hat{Q}_R + \hat{Q}_{PH} + \hat{Q}_H \quad (3.2.1)$$

$$\hat{\rho} \frac{\partial \hat{q}_v}{\partial t} + \nabla \cdot (\hat{V} \hat{q}_v \hat{\rho} + \overline{V' q_v' \hat{\rho}}) = \hat{Q}_v + \hat{M} \quad (3.2.2)$$

$$\hat{\rho} \frac{\partial \hat{u}}{\partial t} + \frac{\partial}{\partial z} \hat{w} \hat{u} \hat{\rho} + \underline{\underline{\nabla_{\theta} \hat{v} \hat{u} \hat{\rho}}} = - f \hat{\rho} \hat{v} - \underline{\underline{\frac{1}{a \sin \theta} \frac{\partial \hat{p}}{\partial \lambda}}} + \underline{\underline{\hat{F}_{wz}}} + \underline{\underline{\hat{F}_{u\theta}}} \quad (3.2.3)$$

$$\hat{\rho} \frac{\partial \hat{v}}{\partial t} + \frac{\partial}{\partial z} \hat{w} \hat{v} \hat{\rho} + \underline{\underline{\nabla_{\theta} \hat{v}^2 \hat{\rho}}} = f \hat{\rho} \hat{u} - \frac{1}{a} \frac{\partial \hat{p}}{\partial \theta} + \hat{F}_{vz} + \underline{\underline{\hat{F}_{v\theta}}} \quad (3.2.4)$$

$$\frac{\partial \hat{p}}{\partial z} = - \hat{\rho} g \quad (3.2.5)$$

$$\hat{\rho} = \hat{R} (\hat{\rho} \hat{T} - \hat{\alpha} \hat{\rho} \overline{T'^2}) \quad (3.2.6)$$

$$\frac{\partial \hat{\rho}}{\partial t} = - \nabla \cdot (\hat{\rho} \hat{V}) - \frac{\partial}{\partial z} \hat{\rho}' w' \quad (3.2.7)$$

In equations (3.2.1)–(3.2.7) $\hat{T}, \hat{q}_v, \hat{u}, \hat{v}, \hat{w}, \hat{p},$ and $\hat{\rho}$ are temperature, specific humidity, zonal, meridional, and vertical components of velocity vector \hat{V} , pressure, and density, $\hat{\alpha} = 1/\hat{T}$,

$$\nabla \cdot (Ax) = \frac{1}{a \sin \theta} \frac{\partial A_{\lambda} x}{\partial x} + \frac{\partial (A_{\theta} x \sin \theta)}{a \partial \theta} + \frac{\partial (A_z x)}{\partial z} \equiv \nabla_{\lambda} (A_{\lambda} x) + \nabla_{\theta} (A_{\theta} x) + \nabla_z (A_z x) \quad ,$$

$$A \cdot \nabla x = A_{\lambda} \frac{\partial x}{a \sin \theta \partial \lambda} + A_{\theta} \frac{\partial x}{a \partial \theta} + A_z \frac{\partial x}{\partial z} \quad ,$$

where $A = \{A_{\lambda}, A_{\theta}, A_z\}$ (any vector); x is any scalar; \hat{Q}_R and \hat{Q}_{PH} are heating rates per unit volume due to radiative transfer and water vapor phase transition, $\hat{Q}_H, \hat{Q}_v, \hat{F}_{uz}, \hat{F}_{u\theta}, \hat{F}_{vz},$ and $\hat{F}_{v\theta}$ describe small-scale and mesoscale "turbulence" heating rate, water vapor influx, z and θ components of frictional force acting on \hat{u} and \hat{v} components of \hat{V} ; \hat{M} is water vapor influx due to phase transition; the other designations in equations (3.2.1) to (3.2.7) are evident. The single-underlined terms in equations (3.2.3) and (3.2.4) are important only in the boundary layer, while the double-underlined terms are important only in the equatorial regions (see text below). The term $\underline{\underline{\frac{1}{a \sin \theta} \frac{\partial \hat{p}}{\partial \lambda}}}$ in equation

(3.2.3) is important outside the equatorial regions only.

Equations (3.2.1) to (3.2.7) contain, besides the large-scale long-term components, the auto- and cross-correlation functions of synoptic-scale component: $\overline{u'T'}, \overline{v'T'}, \overline{w'T'}, \overline{u'q'_v}, \overline{v'q'_v}, \overline{w'q'_v},$

and $\overline{T'^2}$. The set of equations for these variables using the above-mentioned method can be written as follows (Petoukhov, 1990, 1991):

$$-\overline{u'T'} \frac{\partial}{\partial z} \overline{\rho'w'} = -c_{uT} \hat{\rho} \overline{u'^2} \nabla_\lambda \hat{T} \quad (3.2.8)$$

$$-\overline{v'T'} \frac{\partial}{\partial z} \overline{\rho'w'} = -c_{vT} \overline{v'^2} \nabla_\theta \hat{T} \quad (3.2.9)$$

$$-\overline{u'q'_v} \frac{\partial}{\partial z} \overline{\rho'w'} = -c_{uq} \hat{\rho} \overline{u'^2} \nabla_\lambda \hat{q}_v \quad (3.2.10)$$

$$-\overline{v'q'_v} \frac{\partial}{\partial z} \overline{\rho'w'} = -c_{vq} \hat{\rho} \overline{v'^2} \nabla_\theta \hat{q}_v \quad (3.2.11)$$

$$\overline{T'^2} \frac{\partial}{\partial z} \overline{\rho'w'} = -c_T \hat{\rho} (\overline{T'u'} \nabla_\lambda \hat{T} + \overline{T'v'} \nabla_\theta \hat{T}) + \frac{1}{c_v} \overline{T'Q_{PH}} \quad (3.2.12)$$

$$\overline{u'^2} \frac{\partial}{\partial z} \overline{\rho'w'} = \hat{\alpha} \hat{R} \hat{\rho} \left[\frac{c_{uT} \hat{\rho} \frac{1}{2} \sqrt{\hat{u}^2 + \hat{v}^2}}{\frac{\partial}{\partial z} \overline{\rho'w'}} \right] (\nabla_\lambda \hat{T})^2 \quad (3.2.13)$$

$$\overline{v'^2} \frac{\partial}{\partial z} \overline{\rho'w'} = \hat{\alpha} \hat{R} \hat{\rho} \left[\frac{c_{vT} \hat{\rho} \frac{1}{2} \sqrt{\hat{u}^2 + \hat{v}^2}}{\frac{\partial}{\partial z} \overline{\rho'w'}} \right] (\nabla_\theta \hat{T})^2 \quad (3.2.14)$$

$$\overline{\rho'w'} = -K_{\rho z} \frac{\partial \hat{\rho}}{\partial z} \quad (3.2.15)$$

$$\overline{\psi'w'} = \frac{1}{\hat{\rho} g} \left\{ \overline{\psi'V_H'} \cdot \nabla_H \hat{\rho} - (\gamma - 1) \overline{\psi'Q_{PH}} + \gamma \hat{\rho} \frac{\overline{\psi'V'} \cdot \nabla_H \hat{\rho}}{\hat{\rho}} \right\} \quad (3.2.16)$$

In equations(3.2.8) to (3.2.16) $c_{uT} > 0$, $c_{vT} > 0$, $c_{uq} > 0$, $c_{vq} > 0$, and $c_T > 0$ are dimensionless functions of θ , λ , and z (Petoukhov, 1980, 1990, 1991; Mokhov *et al.*, 1992),

$$K_{\rho z, e} = c_{\rho w, e} L_{RO}^{-1} (H_0 R_0)^2 (\hat{u}^2 + \hat{v}^2)^{1/2} > 0$$

at high and middle latitudes and

$$K_{\rho z} = K_{\rho z, e} = c_{\rho w, e} L_{RO, e}^{-1} (H_0 R_{0, e})^2 (\hat{u}^2 + \hat{v}^2)^{1/2} > 0$$

in equatorial regions, where $c_{\rho w}$ and $c_{\rho w, e}$ are dimensionless functions of θ , λ , and z ; Ro , Ro_e , L_{Ro} and $L_{Ro, e}$ are, respectively, Rossby number, equatorial Rossby number, Rossby deformation radius and equatorial Rossby deformation radius (Pedlosky, 1979); H_0 is the scale height for the atmospheric density; ∇_λ and ∇_θ are, λ and θ components of ∇ vector operator; ψ' in equation (3.2.16) stands for T' or q_v' (Petoukhov, 1980, 1991).

The term \hat{Q}_R in equation (3.2.1) comprises the upward and downward fluxes of solar $\hat{F}_{RS}^{\uparrow\downarrow}$ and terrestrial $\hat{F}_{RT}^{\uparrow\downarrow}$ radiation. The $\hat{F}_{RS}^{\uparrow\downarrow}$ fluxes are computed in the model using the method described in Tarasova and Feigelson (1981), Veltishev *et al.* (1990), and Tarasova (1992). The method is based on two-stream δ -Eddington approximation of the transport equation solution in gas-aerosol atmosphere in spectrum ranges outside the water vapor absorption bands. In the NI region of the solar spectrum the combined δ -Eddington method is applied taking into account the water vapor absorption calculated by use of integral transmission function (Veltishev *et al.*, 1990; Tarasova, 1992). Cloud droplets and crystals absorption computation was conducted using the integral transmission function for liquid water and crystals (Tarasova, 1992). The terrestrial radiation fluxes $\hat{F}_{RT}^{\uparrow\downarrow}$ were calculated in the model by the method suggested in Mokhov and Petoukhov (1978) utilizing the integral transmission function approximation.

The term \hat{Q}_{PH} in (3.2.1) is represented in the model by two items: one of them $\left(\hat{Q}_{PH}^{LS}\right)$ describes the phase transition of water vapor due to large-scale condensation in stratus cloud systems; the other one $\left(\hat{Q}_{PH}^{cu}\right)$ represents the processes of deep and shallow (not precipitating) moist convection. No liquid and crystal water storage is assumed to occur in stratus and cumulus cloud systems on the above-mentioned spatial and temporal \bar{L} , $\hat{\tau}$ scales, so that precipitation is supposed to be equal to condensation.

The large-scale stratus cloudiness lower boundary in the model is suggested to be disposed at three atmospheric levels: (1) at the top of atmospheric boundary layer \hat{h}_b ; (2) at the level of maximum value of large-scale vertical flux of water vapor $\hat{F}_{zq} = \hat{w}\hat{q}_v + \overline{w'q_v'}$; (3) at the level of maximum value of water vapor influx due to large-scale vertical motions $\hat{R}_{zq} = \frac{\partial}{\partial z} (\hat{w}q_v + \overline{w'q_v'})$.

The cloud amount \hat{n}_i , and liquid water content \hat{M}_{wi} in each layer are calculated in the model as functions of large-scale temperature \hat{T}_i , relative humidity $\hat{f}_q = \hat{q}/\hat{q}_{v,sat}$, and of vertical velocity $\hat{w}^{LS} = \hat{w} + (\overline{w'^2})^{1/2}$ (Dushkin *et al.*, 1960; Petoukhov, 1991):

$$\hat{n}_i = \hat{n}_i(\hat{f}_q, \hat{w}_i^{LS}) \quad (3.2.17a)$$

$$\hat{M}_{wi} = \hat{M}_{wi}(\hat{T}_i, \hat{f}_{qi}, \hat{w}_i^{LS}, n_i) \quad (3.2.17b)$$

The expression for $\overline{w'^2}$ is obtained in the model using the above-mentioned method of synoptic-scale component description by multiplying the barical tendency equation (see, for example, Lorenz, 1967) by w' and then using the $(\hat{L}, \hat{\tau})$ average procedure (Petoukhov, 1991).

The overlap of stratus cloudiness deposited in different layers is suggested to be statistically independent under $|\hat{w}^{LS}| < w_{LS0}$, highly correlated under $|\hat{w}^{LS}| > w_{LS1}$, with linear dependence of the correlation on $|\hat{w}^{LS}|$ in the range $w_{LS0} < |\hat{w}^{LS}| < w_{LS1}$, where w_{LS0} and w_{LS1} are functions of minimum and maximum life cycle duration for stratus cloud systems (Petoukhov, 1991; Manuilova *et al.*, 1992). The term \hat{Q}_{PH}^{LS} (equal to large-scale precipitation rate, as has already been mentioned) in the model is the function of cloud amount \hat{n}_i , large-scale vertical velocity \hat{w}_i^{LS} , and water vapor content $\hat{q}_v^{LS} = \hat{q}_v + (\overline{q_v'^2})^{1/2}$ (Petoukhov, 1980, 1991):

$$\hat{Q}_{PH_i}^{LS} = \hat{Q}_{PH_i}^{LS}(\hat{n}_i, \hat{w}_i^{LS}, \hat{q}_v^{LS}) \quad , \quad i = 1, 2, 3 \quad (3.2.18)$$

The quantity $\overline{q_v'^2}$ in equation (3.2.18) is calculated using the formula analogous to (3.2.12) in which

$\overline{T'^2}$, $\overline{T'u'}$, $\overline{T'v'}$, $\nabla_\lambda \hat{T}$, $\nabla_\theta \hat{T}$, and $\overline{T'Q_{PH}'}$ are replaced, respectively, by $\overline{q'^2}$, $\overline{q'u'}$, $\overline{q'v'}$, $\nabla_\lambda \hat{q}_v$, and $\overline{q'_v Q_{PH}'}$. The quantities $\overline{T'Q_{PH}'}$ and $\overline{q'_v Q_{PH}'}$ are calculated as $(\hat{L}, \hat{\tau})$ averaged products of T' (or q'_v) and Q_{PH} computed by (3.2.18), in which \hat{n} , \hat{w}^{LS} , \hat{q}_v^{LS} are replaced by $n = \hat{n} + n'$, $w = \hat{w} + w'$, and $q_v = \hat{q}_v + q'_v$.

The second item \hat{Q}_{PH}^{cu} in \hat{Q}_{PH} is represented in the model by the schemes of deep and shallow moist convection, which are close to Betts (1986) parameterizations. The main assumptions used in these schemes are (1) the simultaneous relaxation of temperature and moisture fields in deep and shallow convective ensembles toward the large-scale long-term (quasi-equilibrium) hydrothermodynamical fields of the atmosphere. (2) the closeness of the vertical structure of quasi-equilibrium fields toward the phenomenological universal vertical profiles - quasi-linear for temperature and wind, quasi-exponential for density, pressure, and specific humidity (Petoukhov, 1991). Under these assumptions the simple mathematical procedure of the \hat{Q}_{PH}^{cu} computation is described in Petoukhov (1991) using the so-called parcel method, but taking into account the dry air entrainment and evaporation of rainfall. The latter is calculated using Schlesinger *et al.*, (1988) scheme. This procedure comprises calculation of \hat{n}_{cu} and \hat{M}_{wcu} - cumulus cloud amount and liquid water content. The quantities $\overline{T'Q_{PH}'^{cu}}$ and $\overline{q'_v Q_{PH}'^{cu}}$ are calculated using the same method as when computing the terms $\overline{T'Q_{PH}'^{LS}}$ and $\overline{q'_v Q_{PH}'^{LS}}$. Let us note that the term \hat{M} in (3.2.2) is equal to \hat{Q}_{PH}/L_e , where L_e is the latent heat of evaporation or sublimation (under negative temperatures).

The terms \hat{Q}_H (in 3.2.1), \hat{Q}_v (in 3.2.2), \hat{F}_{uz} , and $\hat{F}_{u\theta}$ (in 3.2.3), and \hat{F}_{vz} , $\hat{F}_{v\theta}$ (in 3.2.4) represent, correspondingly, the heating rate, influx of water vapor, z and θ components of frictional forces applied to \hat{u} and \hat{v} components of motion due to small scale (mainly vertical) and mesoscale (mainly

quasi-horizontal) "turbulent" fluxes. The term \hat{Q}_H is described in the model as follows:

$$\hat{Q}_H = c_p \left\{ \frac{\partial}{\partial \lambda} \left[k_{\lambda T} \hat{\rho} \frac{\partial \hat{\Theta}_e}{\partial \lambda} \right] + \frac{\partial}{\partial \theta} \left[k_{\theta T} \hat{\rho} \frac{\partial \hat{\Theta}_e}{\partial \theta} \sin \theta \right] + \frac{\partial}{\partial z} \left[k_{zT} \hat{\rho} \frac{\partial \hat{\Theta}_e}{\partial z} \right] \right\} \quad (3.2.19)$$

In equation (3.2.19) $\hat{\Theta}_e$ is effective potential temperature including the so-called counter gradient factor (Deardorff, 1972). The coefficients $k_{\lambda T}$ and $k_{\theta T}$ in the high and middle latitude troposphere model are phenomenological constants taken from (Vinnuchenko *et al.*, 1968). The coefficient k_{zT} is computed using the turbulent kinetic energy balance equation under unstable neutral and stable stratification in the boundary layer and stable stratification in free troposphere (Zilitinkevitch, 1970; Deardorff, 1972; Vinnichenko *et al.*, 1968). The term \hat{Q}_v has the same structure as \hat{Q}_H , but for \hat{q}_v instead of $\hat{\Theta}_e$, as well as the terms \hat{F}_{uz} , $\hat{F}_{u\theta}$ and \hat{F}_{vz} , $\hat{F}_{v\theta}$ for \hat{u} and \hat{v} [the last four taking into account only the second and the third items in equation (3.2.19), with \hat{u} and \hat{v} instead of $\hat{\Theta}_e$].

Equations (3.2.1) to (3.2.7) and (3.2.8) to (3.2.16) represent the basic equations of the atmospheric box of the model. To get the set of working equations of the model the following stable phenomenological features of the vertical structure of the atmosphere are used. The atmosphere is supposed to be represented in broad range of climatic states by several stable vertical layers: boundary layer, free troposphere, stratosphere, mesosphere, etc.

The vertical profiles of temperature, \hat{T} , and specific humidity, \hat{q}_v , in these layers are supposed to have universal general structure for current climate conditions and for climatic states far enough from it. Namely, temperature vertical distribution is suggested to be quasi-linear in troposphere, stratosphere, and higher layers, while q_v is considered to be quasi-exponential in these layers. In the boundary layer (BL) the vertical profiles of these variables are also supposed to be well described by universal functions of height depending on stable, neutral and unstable stratification of the BL

(Zilitinkevitch, 1970; Deardorff, 1972). The vertical profile of $\hat{\rho}$ is suggested to be quasi-exponential through the whole atmosphere:

$$\hat{\rho} = \hat{\rho}(0) \exp \left\{ -z/\hat{H}_0 \right\} , \quad (3.2.20)$$

where $\hat{H}_0 = \hat{R}\hat{T}(0)/g$, with only slight dependence of $\hat{\rho}(0)$ on λ and θ .

The height of boundary layer \hat{h}_b is described in the model using the corresponding formulae from Deardorff (1972) in stationary approximation according to $(\hat{L}, \hat{\tau})$ average. The height of tropopause \hat{H}_{tr} is represented by the following expression (Mokhov and Petoukhov, 1978):

$$\hat{H}_{tr} = K_H \frac{\hat{T}(\hat{h}_b)}{\hat{\Gamma}_{tr}} \left[1 - \left[\frac{\hat{D}}{1 + \hat{D}} \right]^{1/4} \right] , \quad (3.2.21)$$

where $\hat{\Gamma}_{tr}$ is the temperature lapse rate in free troposphere, \hat{D} is integral transmission function for thermal radiation of the entire vertical column of the atmosphere, $K_H \sim 0.8$ (Mokhov and Petoukhov, 1978). Formula (3.2.21) is obtained in Mokhov and Petokhov (1978) using the corresponding expression for the upward flux of thermal radiation at the tropopause under assumption of linear vertical profile of \hat{T} in the troposphere, blackbody approximation for clouds emissivity, and radiative equilibrium of the stratospheric layer as a whole with a small temperature lapse rate in it.

The temperature lapse rate in free troposphere $\hat{\Gamma}_{tr}$ is described in the model using the results obtained in Petoukhov (1980, 1991). In these papers the similarity theory was developed of free troposphere as boundary layer, but with mesoscale and large-scale (synoptic) eddies and waves (at high and moderate latitudes) and Hadley cell and deep cumulus convection (in tropics) as the main subjects (instead of small-scale turbulence) of energy, momentum, and latent heat vertical transfer:

$$\hat{\Gamma}_{ir} = \frac{1}{\frac{c_v}{c_p} \frac{\bar{K}_{TZ}}{k_{zT}(\hat{h}_b)} + 1} \left[\Gamma_a (1 - \hat{n}_{cu}^d) + \Gamma_{wa} \hat{n}_{cu}^d \right], \quad (3.2.22)$$

where Γ_a , Γ_{wa} are adiabatic and moist adiabatic lapse rates,

$$\bar{K}_{TZ} = c_{TW} L_{RO}^{-1} (H_0 Ro)^2 \left(\overline{u'^2} + \overline{v'^2} + \hat{u}^2 + \hat{v}^2 \right)^{1/2},$$

\hat{n}_{cu}^d -cumulus cloud amount in free troposphere, $c_{TW} > 0$ — dimensionless function of λ, θ , and z of the order of unity. In equatorial regions L_{RO} and Ro should be replaced by $L_{RO,e}$, and Ro_e , correspondingly. All the variables in equation (3.2.22) [except $k_{zT}(\hat{h}_b)$] are calculated at $z = \frac{\hat{H}_0}{2}$.

Using the same approach, the expression for vertical profile of specific humidity in free troposphere is obtained in Petoukhov (1980, 1991):

$$\hat{q}_v(z) = \hat{q}_v(\hat{h}_b) \exp \left\{ - \hat{\beta}_{v,ir} z' \right\}, \quad (3.2.23)$$

where

$$z' = z - \hat{h}_b$$

$$\hat{\beta}_{v,ir} = \frac{W_1 c_{Dq} \left(\hat{u}^2 + \overline{u'^2} + \hat{v}^2 + \overline{v'^2} \right)^{1/2} \Big|_{z = \hat{h}_b}}{K_{qz} \left[\frac{\hat{H}_0}{2} \right]} \left[\frac{\hat{q}_{v,sat}(\hat{T}(\hat{h}_b), \hat{p}(\hat{h}_b))}{\hat{q}_v(\hat{h}_b)} - 1 \right] - \frac{\hat{w} \left[\frac{\hat{H}_0}{2} \right]}{K_{qz} \left[\frac{\hat{H}_0}{2} \right]}, \quad (3.2.24)$$

where $K_{qz} = c_{qw} L_{RO}^{-1} (H_0 Ro)^2 \left(\overline{u'^2} + \overline{v'^2} \right)^{1/2}$ in high and middle latitudes (in equatorial regions

L_{RO} , RO should be replaced by $L_{RO,e}$, RO_e); $c_{qw} > 0$ -dimensionless functions of λ , θ , and z of the order of unity; W_1 is the wetness of the upper soil layer or of oceanic and sea ice surfaces (for the ocean $W_1 = 1$; c_{Dq} is the humidity transfer coefficient (see section 3.5).

Under these assumptions of the vertical structure of temperature and specific humidity, the equation (3.2.1) is integrated in the model with respect to z from $z = \hat{h}_b$ to $z = \hat{H}_{tr}$ [that gives the prognostic equation for $\hat{T}(\hat{h}_b)$] and from $z = \hat{H}_{tr}$ to $z = \hat{H}_{top}$, where $\hat{H}_{top} \approx 35$ km is the upper boundary of the atmosphere in the model (that gives the prognostic equation for lapse rate $\hat{\Gamma}_{st}$ in the stratosphere or equivalently for the mean mass-weighted temperature of the stratosphere $\hat{T}_{st,m}$). Equation (3.2.2) is integrated in the same limits with respect to z that gives the prognostic equations for $\hat{q}_v(\hat{h}_b)$ and for the index of exponent $\hat{\beta}_{st}$ in the formula for $\hat{q}_v(z)$ in the stratosphere

$$\hat{q}_v(z)|_{z > \hat{H}_{tr}} = \hat{q}_v(\hat{H}_{tr}) \exp \left\{ - \hat{\beta}_{st} z'' \right\} , \quad (3.2.25)$$

where ($z'' = z - \hat{H}_{tr}$) or equivalently for the mass-weighted specific humidity in the stratosphere $\hat{q}_{v,sm}$.

As to the equations for temperature and specific humidity in the boundary layer, the standard procedure of scale and magnitude analysis of terms in equation (3.2.1) for the boundary layer conditions (see, e.g., Zilitinkevitch, 1970) gives the following equation for \hat{T} in this part of the atmosphere:

$$c_v \frac{\partial}{\partial z} (\overline{w'T'} \hat{\rho}) - \hat{Q}_{H,Z} = 0 , \quad (3.2.26)$$

where

$$\hat{Q}_{H,Z} = c_p \frac{\partial}{\partial z} \left[k_{zT} \hat{\rho} \frac{\partial \hat{\theta}_e}{\partial z} \right] . \quad (3.2.27)$$

The expression for $\overline{w'T'}$ in the boundary layer can be obtained from (3.2.16) using the common

assumptions made in the investigations of BL: (1) $\frac{\partial \hat{\rho}}{\partial \theta} \sim \frac{\partial \hat{\rho}}{\partial \lambda} \ll \frac{\partial \hat{\rho}}{\partial z}$, (2) $\hat{\rho} \sim$

$\rho_0 [1 - \alpha_0 (\hat{T} - T_0)]$ where $T_0 = \text{const}$, $\alpha_0 = 1/T_0$, (3) $\hat{Q}_{PH} = Q'_{PH} = 0$ (Zilitinkevitch, 1970; Deardorff, 1972).

As a result the term $\overline{w'T'}$ in equation (3.2.26) is written in the form

$$\overline{T'w'} = K_{TZ}^b \hat{\rho} \frac{\partial \hat{T}}{\partial z} , \quad (3.2.28)$$

where

$$K_{TZ}^b = \frac{\alpha_0 \gamma \hat{\rho}}{\hat{\rho}^2 g} K_{\rho z} \frac{\hat{T}(h_b) - \hat{T}(0)}{\hat{h}_b} \quad (3.2.29)$$

$$\gamma = c_p/c_v .$$

Except in the rare case of boundary layer temperature inversion on the $(\hat{L}, \hat{\tau})$ temporal/spatial scale,

the quantity K_{TZ}^b in (3.2.29) is less than zero due to $\hat{T}(\hat{h}_b) < \hat{T}(0)$.

Combining (3.2.26) to (3.2.29) one can obtain

$$\frac{\partial}{\partial z} F_{H,Z}^{\text{eff}} = 0 , \quad (3.2.30)$$

where

$$F_{H,Z}^{\text{eff}} = c_v K_{TZ}^b \hat{\rho} \frac{\partial \hat{T}}{\partial z} - c_p k_{zT} \hat{\rho} \frac{\partial \hat{\theta}_e}{\partial z} . \quad (3.2.31)$$

Using the same procedure, equation (3.2.2) in the boundary layer can be written in the form

$$\frac{\partial}{\partial z} F_{v,z}^{\text{eff}} = 0 \quad . \quad (3.2.32)$$

In equation (3.2.32)

$$F_{v,z}^{\text{eff}} = K_{qz}^b \hat{\rho} \frac{\partial \hat{q}_v}{\partial z} - k_{zq} \hat{\rho} \frac{\partial \hat{q}_v}{\partial z} \quad (3.2.33)$$

$$K_{qz}^b = - \frac{\alpha_0 \gamma \hat{\rho} \hat{f}}{\hat{\rho} g} \frac{\hat{T}(\hat{h}_b) - \hat{T}(0)}{\hat{h}_b} K_{Tz}^b \quad , \quad (3.2.34)$$

where \hat{f} is relative humidity.

Under usual boundary layer temperature stratification, $K_{qz}^b < 0$ when $\hat{T}(\hat{h}_b) < \hat{T}(0)$ [see (3.2.29) for K_{Tz}^b].

Equations (3.2.30) and (3.2.32) give the standard formulation of the problem of temperature and water vapor vertical distribution in the BL. Together with the boundary conditions for temperature and specific humidity at the surface (or, more exactly, in the surface layer, see section 3.6), they provide the linkage between the equations for $\hat{T}(\hat{h}_b)$ and $\hat{q}(\hat{h}_b)$, on the one hand, and the equations for the surface temperature of ocean or land and for soil moisture, on the other hand (see sections 3.4 and 3.5). The natural condition of continuity of temperature, specific humidity, and total vertical fluxes of heat and moisture at $z = \hat{h}_b$ is adopted in the model. The linkage between the vertically integrated tropospheric and stratospheric equations for temperature and specific humidity is provided by using the condition of continuity of the same variables at $z = \hat{H}_r$. In vertically integrated equations for stratospheric temperature and specific humidity, heat and moisture vertical fluxes due to convection and turbulent diffusion are equal to zero at $z = \hat{H}_{top}$. To provide continuity of vertical heat and moisture fluxes at $z = \hat{h}_b$ the "jump" of coefficients of vertical small-scale and mesoscale "turbulent"

heat and moisture transfer k_{zT} , k_{zq} is adopted in the model (Moeng and Randall, 1984; Wyngaard and Le Mone, 1980). At $z = \hat{H}_{top}$, these coefficients are considered to be equal to zero. At $z = \hat{H}_r$ the vertical small-scale and mesoscale "turbulent" fluxes of all substances, except water vapor, are considered to be equal to zero.

Vertically integrated equations (3.2.1) and (3.2.2) include the terms $\int_{\hat{h}_s(\hat{H}_r)}^{\hat{H}_r(\hat{H}_{top})} \nabla \cdot \hat{V} \hat{T} \hat{\rho} dz$ and

$\int_{\hat{h}_s(\hat{H}_r)}^{\hat{H}_r(\hat{H}_{top})} \nabla \cdot \hat{V} \hat{q}_v \hat{\rho} dz$, respectively. Corresponding formulae for \hat{v} and \hat{u} in these terms are obtained

in the model using equations (3.2.3) to (3.2.4) under some simplifications reflecting universal features of \hat{u} and \hat{v} fields in the above-mentioned large-scale vertical layers at high and middle latitudes and in equatorial regions. Namely, in the free atmosphere of high and middle latitudes using the standard method of scale and magnitude analysis of terms (see, e.g., Pedlosky, 1979), one can omit the left-hand sides as well as the two last terms on the right-hand sides of equations (3.2.3), (3.2.4).

This brings one to the so-called geostrophic balance formulae for \hat{u} and \hat{v} [the first and the second terms on the right-hand sides of equations (3.2.3) and (3.2.4)], so that in this part of the atmosphere \hat{u} and \hat{v} can be written in the form

$$\frac{\partial \hat{u}}{\partial z} \Big|_{\hat{H}_r, z \geq \hat{h}_s} \approx \hat{u}_T(\hat{h}_s) ; \quad \frac{\partial \hat{u}}{\partial z} \Big|_{z > \hat{H}_r} \approx \hat{u}_T(\hat{H}_r) \quad (3.2.35a)$$

$$\frac{\partial \hat{v}}{\partial z} \Big|_{\hat{H}_r, z \geq \hat{h}_s} \approx \hat{v}_T(\hat{h}_s) ; \quad \frac{\partial \hat{v}}{\partial z} \Big|_{z > \hat{H}_r} \approx \hat{v}_T(\hat{H}_r) \quad , \quad (3.2.35b)$$

where \hat{u}_T and \hat{v}_T are the components of thermal wind (see, e.g. Pedlosky, 1979). As shown in equations (3.2.35a) and (3.2.35b), the vertical profiles of \hat{u} and \hat{v} are linear with respect to z in free troposphere and stratosphere.

In the boundary layer of high and middle latitudes the terms \hat{F}_{uz} and \hat{F}_{vz} should be added to the first and the second terms on the right-hand sides of equations (3.2.3) and (3.2.4), respectively. This gives the Ekman formulation of boundary layer wind speed problem, except that k_{zu} and k_{zv} are determined in the model from the turbulent kinetic energy balance equation (Petoukhov, 1991). The boundary conditions for the Ekman problem in the model are as follows:

$$\begin{aligned} \hat{u}_-(\hat{h}_b) &= \hat{u}_+(\hat{h}_b) \\ \hat{v}_-(\hat{h}_b) &= \hat{v}_+(\hat{h}_b) \\ \frac{\partial \hat{u}}{\partial z} \Big|_{\hat{h}_b} &= \hat{u}_T(\hat{h}_b) \quad , \\ \frac{\partial \hat{v}}{\partial z} \Big|_{\hat{h}_b} &= \hat{v}_T(\hat{h}_b) \end{aligned} \quad (3.2.36)$$

where $\hat{u}_-(\hat{h}_b)$, $\hat{v}_-(\hat{h}_b)$, $\frac{\partial \hat{u}}{\partial z} \Big|_{\hat{h}_b}$, and $\frac{\partial \hat{v}}{\partial z} \Big|_{\hat{h}_b}$ are \hat{u} and \hat{v} components of wind and $\frac{\partial \hat{u}}{\partial z}$, $\frac{\partial \hat{v}}{\partial z}$ at the top of the boundary layer and $\hat{u}_+(h_b)$, $\hat{v}_+(h_b)$ are \hat{u} and \hat{v} components of wind at the bottom of free troposphere. So far the solution of Ekman problem includes, as the parameters, the quantities $\hat{u}_T(\hat{h}_b)$, $\hat{v}_T(\hat{h}_b)$, $\hat{u}_+(\hat{h}_b)$, and $\hat{v}_+(\hat{h}_b)$, the first two being the functions of temperature field at the bottom of free atmosphere and the second two being "free" parameters of the Ekman problem. To close the system the following expressions are used

$$\begin{aligned} k_{zu} \hat{\rho} \frac{\partial \hat{u}}{\partial z} \Big|_{z=\hat{h}_s} &= c_{Du} \hat{\rho} |\hat{U}| \hat{u} \Big|_{z=\hat{h}_s} \\ k_{zv} \hat{\rho} \frac{\partial \hat{v}}{\partial z} \Big|_{z=\hat{h}_s} &= c_{Dv} \hat{\rho} |\hat{U}| \hat{v} \Big|_{z=\hat{h}_s} \quad , \end{aligned} \quad (3.2.37)$$

which are the lower boundary conditions for \hat{u} and \hat{v} components in the boundary layer. Here \hat{h}_s is the height of the surface layer. The corresponding formula for \hat{h}_s used in the model is taken from (Zilitinkevitch, 1970). The module of surface wind velocity $|\hat{U}|$ is described in the model as follows:

$$|\hat{U}| = \left(\hat{u}^2 + \hat{v}^2 + \overline{u'^2} + \overline{v'^2} \right)^{1/2} \Big|_{z=\hat{h}_i} . \quad (3.2.38)$$

Drag coefficients c_{Du} and c_{Dv} in equation (3.2.37) are functions of bulk Richardson number and of surface roughness length (see sections 3.5.1 and 3.5.2). It is supposed that $c_{Du} = c_{Dv} = c_D$. In the equatorial free atmosphere the evaluation of magnitude of terms in equations (3.2.3) and (3.2.4) gives

$$\frac{\partial}{\partial z} \hat{w} \hat{u} \hat{\rho} + \nabla_{\theta} \hat{v} \hat{u} \hat{\rho} = -f \hat{\rho} \hat{v} + \hat{F}_{u\theta} + \hat{F}_{uz} \quad (3.2.39)$$

$$\frac{\partial}{\partial z} \hat{w} \hat{v} \hat{\rho} + \nabla_{\theta} \hat{v}^2 \hat{\rho} = f \hat{\rho} \hat{u} - \frac{1}{a} \frac{\partial \hat{p}}{\partial \theta} + F_{v\theta} + \hat{F}_{vz} . \quad (3.2.40)$$

The continuity equation (3.2.7) for this region using the analogous scale and magnitude analysis can be written in the form

$$\nabla_{\theta} \hat{\rho} \hat{v} + \frac{\partial}{\partial z} \hat{\rho} \hat{w} = 0 . \quad (3.2.41)$$

In equations (3.2.39) to (3.2.41) $\hat{\rho}$ is described by (3.2.20). The term $\frac{1}{a} \frac{\partial \hat{p}}{\partial \theta}$ in equation (3.2.40)

using equation (3.2.6) in which the second item on the right-hand side can be omitted in equatorial regions due to small "penetrability" of the equatorial belt for the synoptic eddies (see, e.g., Pedlosky, 1979), can be written in the form (Petoukhov, 1991):

$$\frac{1}{a} \frac{\partial \hat{p}}{\partial \theta} = \frac{1}{a} \frac{\partial \hat{T}}{\partial \theta} \hat{R} \hat{\rho} 2 \left[1 - \frac{\hat{T}}{T_0} \right] . \quad (3.2.42)$$

In equation (3.2.42) the following approximation for $\hat{\rho}$ is commonly applied to convectively active layers (equatorial free atmosphere is one of the most active convective layers):

$$\hat{\rho} = \rho_0 e^{-z/H_0} \left[1 - \alpha_0 (\hat{T} - T_0) \right], \quad (3.2.43)$$

where $H_0 = RT_0/g$.

Substituting equation (3.2.41) to (3.2.43) for equations (3.2.39) and (3.2.40) gives

$$\int_z^\infty \nabla_\theta \hat{\rho} \hat{v} dz \frac{\partial \hat{u}}{\partial z} + \hat{\rho} \hat{v} \nabla_\theta \hat{u} = -f \hat{\rho} \hat{v} + \hat{\rho} \frac{\partial}{a \sin \theta \partial \theta} \left[k_{\theta u} \frac{\partial \hat{u}}{a \partial \theta} \sin \theta \right] + \frac{\partial}{\partial z} \left[k_{zu} \hat{\rho} \frac{\partial \hat{u}}{\partial z} \right] \quad (3.2.44)$$

$$\int_z^\infty \nabla_\theta \hat{\rho} \hat{v} dz \frac{\partial \hat{v}}{\partial z} + \hat{\rho} \hat{v} \nabla_\theta \hat{v} = f \hat{\rho} \hat{u} - \frac{1}{a} \frac{\partial \hat{T}}{\partial \theta} \hat{R} \hat{\rho} 2 \left[1 - \frac{\hat{T}}{T_0} \right] + \frac{\partial}{a \sin \theta \partial \theta} \left[k_{\theta v} \frac{\partial \hat{v}}{a \partial \theta} \sin \theta \right] + \frac{\partial}{\partial z} \left[k_{zv} \hat{\rho} \frac{\partial \hat{v}}{\partial z} \right]. \quad (3.2.45)$$

In equations (3.2.44) and (3.2.45) the upper boundary condition $\hat{w}|_{\hat{H}_{top}} = 0$ is used and, taking into account equation (3.2.20) and assuming \hat{v} to be confined at the infinity, the upper limits of integration \hat{H}_{top} in the first items on the left-hand side of equations (3.2.44) and (3.2.45) are replaced by infinity. Using the linear dependence of \hat{T} on z in troposphere and stratosphere and taking into account equation (3.2.20) the solution to equation (3.2.44) and (3.2.45) in these layers can be written as follows:

$$\hat{v} = \hat{v}_{1,(st)} + \hat{v}_{2,(st)} \cdot z \quad (3.2.46)$$

$$\hat{u} = \hat{u}_{1,(st)} + \hat{u}_{2,(st)} \cdot z \quad (3.2.47)$$

providing the quantities $k_{\theta u}$, $k_{\theta v}$ and k_{zu} , k_{zv} (we assume $k_{\theta u} = k_{\theta v} = k_H$, $k_{zu} = k_{zv} = k_z$) are written in the form

$$\begin{aligned} k_H &= k_{H1,t(st)} + k_{H2,t(st)}Z \\ k_z &= k_{z1,t(st)} + k_{z2,t(st)}Z \end{aligned} \quad (3.2.48)$$

where $\hat{u}_{1,t(st)}$, $\hat{u}_{2,t(st)}$, $\hat{v}_{1,t(st)}$, $\hat{v}_{2,t(st)}$, $k_{H1,t(st)}$, $k_{H2,t(st)}$, $k_{z1,t(st)}$, $k_{z2,t(st)}$ are functions of λ and θ , lower indices t and st refer to troposphere and stratosphere, respectively.

The boundary conditions on θ for \hat{u}_1 , \hat{v}_1 , \hat{u}_2 , \hat{v}_2 at $\varphi = \pm\varphi_e$ where $\varphi = \frac{\pi}{2} - \theta$ and φ_e is the

width of the equatorial dynamical belt (Dobryshman, 1980), are

$$\begin{aligned} \hat{u}_1 &= \hat{u}_1|_- \\ \hat{u}_2 &= \hat{u}_2|_- \\ \hat{v}_1 &= \hat{v}_1|_- \\ \hat{v}_2 &= \hat{v}_2|_- \end{aligned} \quad (3.2.49)$$

where $\hat{u}_1|_-$, $\hat{u}_2|_-$, $\hat{v}_1|_-$, and $\hat{v}_2|_-$ are corresponding parameters of linear (with respect to z) expansion formulae for \hat{u} and \hat{v} in middle latitudes under $\varphi \rightarrow \pm\varphi_e$ [see equations (3.2.34) and (3.2.35) and corresponding text]. The lower indices t and st are omitted in (3.2.49) for brevity. Substituting equations (3.2.46) to (3.2.49) for equation (3.2.44) and (3.2.45) give six nonlinear ordinary equations of the second order with respect to θ for six functions u_1 , u_2 , v_1 , v_2 , k_{H1} , and k_{H2} in troposphere and stratosphere. The boundary conditions for k_{H1} and k_{H2} in both layers (troposphere and stratosphere) are set in the model at the equator:

$$\begin{aligned} k_{H1}|_{\theta=\frac{\pi}{2}} &= k_{H1,e} \\ k_{H2}|_{\theta=\frac{\pi}{2}} &= k_{H2,e} \end{aligned} \quad (3.2.50)$$

As to the parameters $k_{z1,t}$, $k_{z1,st}$, $k_{z2,t}$, $k_{z2,st}$, the following conditions are used in the model

$$\begin{aligned} k_{z,t} + k_{z,t} \hat{H}_{tr} &= k_{z,st} + k_{z,st} \hat{H}_{tr} \\ k_{z,st} + k_{z,st} \hat{H}_{top} &= 0 \end{aligned} \quad (3.2.51)$$

The other two conditions applied to these four parameters are the conditions of continuity of \hat{u} and \hat{v} at $z = \hat{H}_{tr}$. With some minor simplifications the analytical solution to problems (3.2.44) and (3.2.45) in equatorial troposphere and stratosphere is obtained in Petoukhov (1991), which is used in the global version of the model. In equatorial boundary layer, applying scale and magnitude analysis of terms one can reduce equations (3.2.39) and (3.2.40) to

$$\hat{w} \hat{\rho} \frac{\partial \hat{u}}{\partial z} = -f \hat{\rho} \hat{v} + \hat{F}_{uz} \quad (3.2.52)$$

$$\hat{w} \hat{\rho} \frac{\partial \hat{v}}{\partial z} = -f \hat{\rho} \hat{u} - \frac{1}{a} \frac{\partial \hat{p}}{\partial \theta} + \hat{F}_{vz} \quad (3.2.53)$$

The quantity \hat{w} in equations (3.2.52) and (3.2.53) is specified in the model as follows

$$\hat{w} = w_1 z + w_2 z^2 \quad (3.2.54)$$

This gives $\hat{w} = 0$ at $z = 0$. The quantities w_1 , w_2 (which are functions of λ and θ) are determined in the model by the conditions of continuity of large-scale vertical velocity and its derivative with respect to z at $z = \hat{h}_b$.

Taking into account equations (3.2.54) and (3.2.42) one comes to boundary layer problems (3.2.52) and (3.2.53) for \hat{u} and \hat{v} under boundary conditions (3.2.37) and \hat{u} and \hat{v} continuity at $z = \hat{h}_b$. The systems (3.2.52) and (3.2.53), being added by kinetic turbulent energy balance equation for $k_{zu} = k_{zv} = k_z$ in the boundary layer [with corresponding boundary conditions of k_z continuity at $z = \hat{h}_s$ and neutral stability formula for k_z at $z = \hat{h}_b$ (Zilitinkevitch, 1970; Deardorff, 1972)] give

the solution to \hat{u} and \hat{v} in the equatorial boundary layer.

Let us note that taking into account equations (3.2.15) and equation (3.2.20), equations (3.2.8) to (3.2.11) give the so-called diffusion approximation for corresponding synoptic cross-correlation functions. The utilization in the model of the universal vertical structure of atmospheric temperature and humidity allows us to simplify to a great extent the procedure of radiative and cumulus convection processes computation (Petoukhov, 1991). This assumption, $(\hat{L}, \hat{\tau})$ averaging, and vertical integration of the equations for temperature and specific humidity, as well as proximity of \hat{u} and \hat{v} to thermal wind approximation in free atmosphere of high and middle latitudes, noticeably shorten the turnaround time of the model due to possibility of having relatively large time steps ($\approx 1 \div 3$ days) without violation of CFL criteria when using the explicit numerical schemes.

3.3. Oceanic component

The basic equations of the model for the long-term large-scale oceanic component deduced from the set of primitive equations using $(\hat{L}, \hat{\tau})$ average and scale and magnitude analysis are as follows (Petoukhov, 1991):

$$\frac{\partial \hat{T}_0}{\partial t} + \frac{1}{a \sin \theta} \frac{\partial \hat{u}_0 \hat{T}_0}{\partial \lambda} + \frac{\partial \hat{v}_0 \hat{T}_0 \sin \theta}{a \sin \theta \partial \theta} + \frac{\partial \hat{w}_0 \hat{T}_0}{\partial z} = k_{HTO} \Delta_H \hat{T}_0 + k_{ZTO} \frac{\partial^2 \hat{T}_0}{\partial z^2} \quad (3.3.1)$$

$$\frac{\partial \hat{S}_0}{\partial t} + \frac{1}{a \sin \theta} \frac{\partial \hat{u}_0 \hat{S}_0}{\partial \lambda} + \frac{\partial \hat{v}_0 \hat{S}_0 \sin \theta}{a \sin \theta \partial \theta} + \frac{\partial \hat{w}_0 \hat{S}_0}{\partial z} = k_{HSO} \Delta_H \hat{S}_0 + k_{ZSO} \frac{\partial^2 \hat{S}_0}{\partial z^2} \quad (3.3.2)$$

$$f \hat{v}_0 = - \frac{1}{\rho_0^0} \frac{\partial \hat{p}_0}{a \sin \theta \partial \lambda} - \frac{1}{a \sin \theta} \frac{\partial \overline{u'^2}}{\partial \lambda} - \frac{\partial (\hat{u}_0 \hat{v}_0 + \overline{u'_0 v'_0}) \sin \theta}{a \sin \theta \partial \theta} - \frac{\partial \hat{u}_0 \hat{w}_0}{\partial z} + k_{HUO} \Delta_H \hat{u}_0 + k_{zuo} \frac{\partial^2 \hat{u}_0}{\partial z^2} \quad (3.3.3)$$

$$-f\hat{u}_0 = -\frac{1}{\rho_0^0} \frac{\partial \hat{\rho}_0}{a \partial \theta} - \frac{1}{a \sin \theta} \frac{\partial (\hat{u}_0 \hat{v}_0 + \overline{u_0' v_0'})}{\partial \lambda} - \frac{1}{a} \frac{\partial \overline{v'^2}}{\partial \theta} - \frac{\partial \hat{v}_0 \hat{w}_0}{\partial z} + k_{Hv0} \Delta_H \hat{v}_0 + k_{zv0} \frac{\partial^2 \hat{v}_0}{\partial z^2} \quad (3.3.4)$$

$$\frac{\partial \hat{\rho}_0}{\partial z} = \hat{\rho}_0 g \quad (3.3.5)$$

$$\frac{1}{a \sin \theta} \frac{\partial \hat{u}_0}{\partial \lambda} + \frac{1}{a \sin \theta} \frac{\partial}{\partial \theta} (\hat{v}_0 \sin \theta) + \frac{\partial \hat{w}_0}{\partial z} = 0 \quad (3.3.6)$$

$$\hat{\rho}_0 = \hat{\rho}_0(\hat{r}_0, \hat{S}_0) \quad (3.3.7)$$

In equations (3.3.1) to (3.3.7) all designations are analogous to those of atmospheric box, but with lower index "0." \hat{S}_0 stands for salinity, Δ_H is the horizontal Laplacian on the sphere with radius $r = a$, $k_{HTO} = k_{HSO} = k_{HO}^{TS}$, $k_{ZTO} = k_{ZSO} = k_{ZO}^{TS}$, $k_{Hu0} = k_{Hv0} = k_{HO}$, $k_{zu0} = k_{zv0} = k_{zO}$. The equations for $\overline{u'^2}$, $\overline{v'^2}$ and $\overline{u_0' v_0'}$ in equations (3.3.1) to (3.3.7) using the same method as in atmospheric module can be written in the form (Petoukhov, 1991):

$$\overline{u'^2} = c_{u0} K_{u0} \left[\frac{\partial \hat{u}_0}{\partial z} \right]^2 \quad (3.3.8)$$

$$\overline{v'^2} = c_{v0} K_{v0} \left[\frac{\partial \hat{v}_0}{\partial z} \right]^2 \quad (3.3.9)$$

$$\overline{u_0' v_0'} = c_{uv0} K_{uv0} \left[\frac{1}{a \sin \theta} \overline{u'^2} \frac{\partial \hat{v}_0}{\partial \lambda} + \frac{1}{a} \overline{v'^2} \frac{\partial \hat{u}_0}{\partial \theta} \right] \quad (3.3.10)$$

In equations (3.3.8) to (3.3.10) $c_{u0} > 0$, $c_{v0} > 0$, and $c_{uv0} > 0$ are dimensionless functions of λ , θ , and z of the order of unity and K_{u0} , K_{v0} , and K_{uv0} are as follows (Petoukhov, 1991):

$$K_{u0} = K_{v0} = \frac{K_{z0}}{2k_{HO}/\hat{L}_{HO}^2 + k_{zO}/\hat{L}_{zO}^2} \quad (3.3.11)$$

$$K_{w0} = - \left(2k_{z0} / L_{z0}^2 \right)^{-1}$$

$$K_{z0} = (H^0 RO^0)^2 (L_{Ro}^0)^{-1} (\hat{u}_0^2 + \hat{v}_0^2)^{1/2}$$

$$L_{HO} = L_{Ro}^0, L_{z0} = H^0 RO^0$$

where H^0 , RO^0 , and L_{Ro}^0 are, scale height, Rossby number, and Rossby deformation radius for the ocean at high and middle latitudes (Pedlosky, 1979). In the equatorial belt RO^0 and L_{Ro}^0 are represented by corresponding equatorial values (Pedlosky, 1979).

The set of basic equations (3.3.3), (3.3.4), and (3.3.6) for \hat{u}_0 , \hat{v}_0 , and \hat{w}_0 are considered in the model separately in typical oceanic regions: open ocean below the mixed layer and above the bottom layer with subdivision of seasonal and main thermocline, mixed layer, bottom layer, and littoral ocean with the same vertical subdivision. All these regions are considered outside the equatorial belt and within it. Corresponding standard simplifications of equations (3.3.3), (3.3.4), and (3.3.6) for each region are adopted (Pedlosky, 1979; Holland, 1977; Kamenkovitch, 1973; Kraus and Turner, 1967; Kitaigorodsky and Miropolsky, 1970; Needler, 1967, 1971), with "sewing" of the solutions at the vertical and horizontal boundaries (Petoukhov, 1991). The important assumption used in this procedure is the supposition about universal vertical structure of \hat{T}_0 and \hat{S}_0 in the above-mentioned vertical layers.

The temperature profile is supposed to be isothermal in the mixed layer (with the depth described by Kraus and Turner (1967)), self-similar in the seasonal thermocline (Kitaigorodsky and Miropolsky, 1970), Needler-type in the main thermocline (Needler, 1967, 1971), self-similar in the bottom layer (Kamenkovitch, 1973). The depths of the boundary between seasonal and main thermoclines and of the top of the bottom layer are described in the model by corresponding universal formulae obtained by technique of scale analysis (Kamenkovitch, 1973). The equations (3.3.1) and (3.3.2) are integrated in the model with respect to z in the limits of the vertical layers. This procedure gives the working

nonstationary equations of the model for the temperature and salinity in the mixed layer and at the top of the main thermocline \hat{T}_{om} , \hat{S}_{om} , \hat{T}_{ot} , and \hat{S}_{ot} (Petoukhov, 1991). This vertical integration noticeably reduces the turnaround time of the model.

The equation for the thickness of sea ice (\hat{I}) used in the model is similar to the corresponding equation of the Manabe and Bryan (1972) model. The single distinction is that the model under consideration describes separately the processes of sea ice advection due to large-scale and synoptic-scale movements and that the leads formation is parameterized in the model in terms of ice thickness (\hat{I}) at each mesh (Petoukhov and Manuilova, 1984; Petoukhov, 1991).

3.4. Land component

The land surface temperature \hat{T}_l is calculated in the model using the standard equation of surface temperature balance (see, e.g., Manabe, and Bryan, 1972). For computation of soil moisture the two-layer model is used based on BATS scheme (Dickinson *et al.*, 1986). Eight vegetation/land-cover types (VLCT) are represented in the model: desert, tundra, grass, crop/mixed farming, shrub, mixed woodland, deciduous forest and evergreen forest/rainforest. The geographical distribution of these vegetation/land-cover types at the model resolution follows one used in the BATS scheme. Each model mesh was assigned a dominant type of VLCT. The fraction of bare soil were determined using corresponding BATS parameterization. Eight soil types (STs) was taken into account. The geographical distribution of the STs was set using the same sources of information as in the BATS scheme, but with much more sketchy (according to model resolution) details and less subdivisions into soil types (BATS scheme explores 18 VLCT and 12 ST classes). Sensible heat flux, evaporation, evapotranspiration, surface run-offs and in-soil water transfer were computed using BATS parameterizations (Dickinson *et al.*, 1986).

3.5. Linkage of climate components

The linkage between atmospheric, oceanic, and land components is realized in the model by surface fluxes of radiation, evaporation (evapotranspiration in vegetation-covered regions) rainfall, sensible heat, and momentum.

3.5.1. Atmosphere and ocean

Oceanic surface is treated as a blackbody radiator in thermal range of spectrum. The ocean albedo is a function of solar zenith angle and wind speed as specified by Cox and Munk (1956). The surface fluxes of momentum, heat, and water vapor are computed in the model using a drag law parameterization (Deardorff, 1967). The drag coefficient (c_D), as has already been mentioned, is a function of the drag coefficient for neutral stability (c_{DN}) and the bulk Richardson number (Ri) for the surface layer (Deardorff, 1968). The quantity c_{DN} is a function of roughness length, which in turn is a function of oceanic surface air wind speed (Garrat, 1977).

The heat and humidity transfer coefficients (c_{DT} and c_{Dq}) are functions of c_D and Ri in accordance with Deardorff (1968) parameterization obtained from the Monin-Oboukhov similarity relations. The roughness length of sea ice is taken from Doronin (1969).

As has already been pointed out, the module of surface air wind speed entering the drag law parameterizations is described in the model as follows:

$$|U| = \left(\hat{u}^2 + \overline{u'^2} + \hat{v}^2 + \overline{v'^2} \right)^{1/2} \Big|_{z=0} , \quad (3.5.1)$$

so that the regions with high synoptic activity (i.e., with high values of $\overline{u'^2}$ and $\overline{v'^2}$) make a pronounced contribution to ocean-atmosphere (and land-atmosphere) energy exchange.

3.5.2. Atmosphere and land

Land surface in thermal range of spectrum is black radiator. The albedo of the land surfaces is computed in the model using BATS parameterizations for bare/snow-covered soil and vegetation/snow covered soil albedos at the model resolution with the above-mentioned (see Section 3.4) land surface subdivisions with respect to VLCTs and STs. The surface fluxes of momentum, heat, and water vapor are computed in the model using the same drag law parameterizations as in oceanic module. The surface roughness lengths for bare soil, and snow and vegetation/snow covered surfaces are taken from BATS paper as well as the other parameters of formulae describing surface sensible heat flux, momentum flux, evaporation/evapotranspiration, and in-soil water transfer, (see Table 5.3 of WP1).

No orography of the land surface is taken into account in IAP 2.5-DSCM, except the Antarctic ice sheet, for which corresponding heat and snow/ice mass balance equations are used (Mokhov *et al.*, 1983; Petoukhov, 1991). The main features of the 2.5-DSCM are described in Table 3. 1.

3.6. Present status of the model

At present the model is able to analyze the Northern Hemisphere with strongly simplified geographical distribution of the coastline represented by segments of parallels and meridians (see Figures 4.1-4.20). Salinity is prescribed in the current version of the model. The vertical distribution of small-scale turbulent coefficients of heat, humidity, and momentum transfer k_z , k_{zT} , k_{zq} in the atmospheric boundary layer are approximated by analytical formulae using corresponding results of computations of k_z , k_{zT} , k_{zq} for unstable, neutral, and stable stratification of BL, represented in Zilitinkevitch, (1970). Due to its hemispheric character and relatively large spatial steps (see Table 3.1), the current version of the model does not allow for detailed resolution of the equatorial belt and the littoral ocean. Taking this into account, the additional simplification have been adopted in the atmospheric and oceanic dynamical modules of the present version. Namely, \hat{u} and \hat{v} components are represented by formulae (3.2.34), (3.2.35) in the free atmosphere as a whole with the replacement of f , L_{Ro} , and Ro

by f_e , $L_{RO,e}$, and Ro_e in equatorial belt (Pedlosky, 1979). In the atmospheric boundary layer the Ekman model for the \hat{u} and \hat{v} components is used but with k_z being described by the above-mentioned analytical formulae using results of Zilitinkevitch (1970), and with f replaced by f_e in the equatorial belt. The oceanic dynamical fields \hat{u}_0 , \hat{v}_0 , and \hat{w}_0 are represented in the present version by the sum of the barotropic (Munk, 1950) component (built on zonally averaged wind stress), the component due to the zonally averaged overturning stream function (Petoukhov, 1991), the polar downwelling and middle/high latitude upwelling (in terms of zonally averaged oceanic temperature, salinity, wind stress), the Ekman component, and the geostrophic component with f_z replaced by f_e in the equatorial belt. The Munk and overturning stream function formulae describing the corresponding parts of \hat{u}_0 , \hat{v}_0 , and \hat{w}_0 components are improved, in comparison with the usual description, by introducing the synoptic component influence, according to equations (3.3.8) to (3.3.10). The BATS scheme is adapted to geographical distribution and spatial resolution of the current simplified version of the model.

At present a modified global version with realistic geography (see Figure A1.1 of Appendix 1) and a spatial resolution of $12^\circ \times 4.5^\circ$ (for the atmospheric component) and $6^\circ \times 4.5^\circ$ (for the land and oceanic component) is under development with separate consideration of equatorial and middle/high latitude regions as have been described in sections 3.2 to 3.5 and with oceanic module (MIOM, see Appendix 2) described in terms of isopycnal coordinates (Ganopolski, 1991), including prognostic salinity equation. The sea ice module is being improved by incorporating a more realistic scheme of ice (and leads) formation, ice hummocking, and advection. For more details of the improvement, see Chapter 5 and Appendices 1 and 2 of this paper.

4. Model Results

This chapter contains a description of the results obtained from the current version of the model.

4.1. Overview of results

The figures are grouped into three parts (Table 4.1): simulation of present climate (indicated by "1xCO₂"), equilibrium response to a doubling of CO₂ ("2xCO₂"), and time dependent experiment ("Scenario").

Table 4.1. Overview of model results.

	1xCO₂
<i>Fig. 4.1</i>	Zonal mean surface air temperature.
<i>Fig. 4.2</i>	Zonal mean stratospheric temperature.
<i>Fig. 4.3</i>	Zonal mean surface air specific humidity.
<i>Fig. 4.4</i>	Zonal mean evaporation.
<i>Fig. 4.5</i>	Zonal mean precipitation.
<i>Fig. 4.6</i>	Zonal mean meridional heat transport in the atmosphere.
<i>Fig. 4.7</i>	Zonal mean heat transport in the ocean.
<i>Fig. 4.8</i>	Zonal mean planetary albedo.
<i>Fig. 4.9</i>	Zonal mean flux of outgoing long-wave radiation.
<i>Fig. 4.10</i>	Zonal mean total cloud amount.
<i>Fig. 4.11</i>	Zonal mean temperature synoptic variance in the atmosphere.
<i>Fig. 4.12</i>	Zonal mean specific humidity synoptic variance.
<i>Fig. 4.13</i>	Surface air temperature.
<i>Fig. 4.14</i>	Precipitation.
<i>Fig. 4.15</i>	Ocean surface temperature.
	2xCO₂
<i>Fig. 4.16</i>	2xCO ₂ - 1xCO ₂ zonal mean surface air temperature difference.
<i>Fig. 4.17</i>	2xCO ₂ - 1xCO ₂ zonal mean stratospheric temperature difference.
<i>Fig. 4.18</i>	2xCO ₂ - 1xCO ₂ zonal mean precipitation difference.
<i>Fig. 4.19</i>	Geographical distribution of 2xCO ₂ - 1xCO ₂ precipitation difference.
	Scenario
<i>Fig. 4.20</i>	1990 IPCC Scenario A of CO ₂ -equivalent concentration (1985-2084).
<i>Fig. 4.21</i>	Transient response of surface air temperature (Scenario A).

4.2. Simulation of present climate

Figure 4.1 shows the present climate latitudinal distribution of zonally averaged temperature at $z = \hat{h}_s$ (i.e., at Stephenson screen level) for February and July in the model and as derived from observational data (Oort and Rasmusson, 1971) at $\hat{p} = 1000 \mu b$. The term "present climate" refers to the past 10-year average of the model results after 100 years of integration starting from the initial state corresponding to present climate annually and zonally averaged empirical values of climatic variables. Figure 4.2 demonstrates the latitudinal course of present climate mass-weighted zonal temperature of the stratosphere in the model in comparison with empirical data taken from Makhover (1983) for the same months. In Figure 4.3 the zonal specific humidity meridional profile in the model at $z = \hat{h}_s$ is given for winter and summer as well as corresponding values obtained from present climate observations at $\hat{p} = 1000 \mu b$ (Oort and Rasmusson, 1971). As shown in the figures, the model results are in satisfactory agreement with empirical data.

Zonal mean precipitation and evaporation data obtained in the model, as well as corresponding empirical data, for February and July are depicted in Figures 4.4 and 4.5. The model results describe rather well the equatorial and middle latitude maxima of rainfall, summer minimum of evaporation at $\varphi \sim 45^\circ \div 50^\circ N$, and subtropical minimum of precipitation. The equatorial maxima of rainfall and evaporation in the model are deposited at the equator for both winter and summer, whereas the real distribution of these variables exposes the periodic seasonal shift of these maxima from the Northern Hemisphere to the Southern Hemisphere and vice versa (see, e.g., Houghton *et al.*, 1990). This shortcoming of the current version is connected mainly with its hemispheric character and will be overcome in modified global version, in which the intertropical convergence zone (ICZ) will be able to transfer from one hemisphere to another.

Figure 4.6 shows the mass-weighted zonally averaged atmospheric meridional heat flux due to a synoptic component in the model in comparison with observational data from Oort and Rasmusson (1971). The model results are in rather good agreement with empirical estimations.

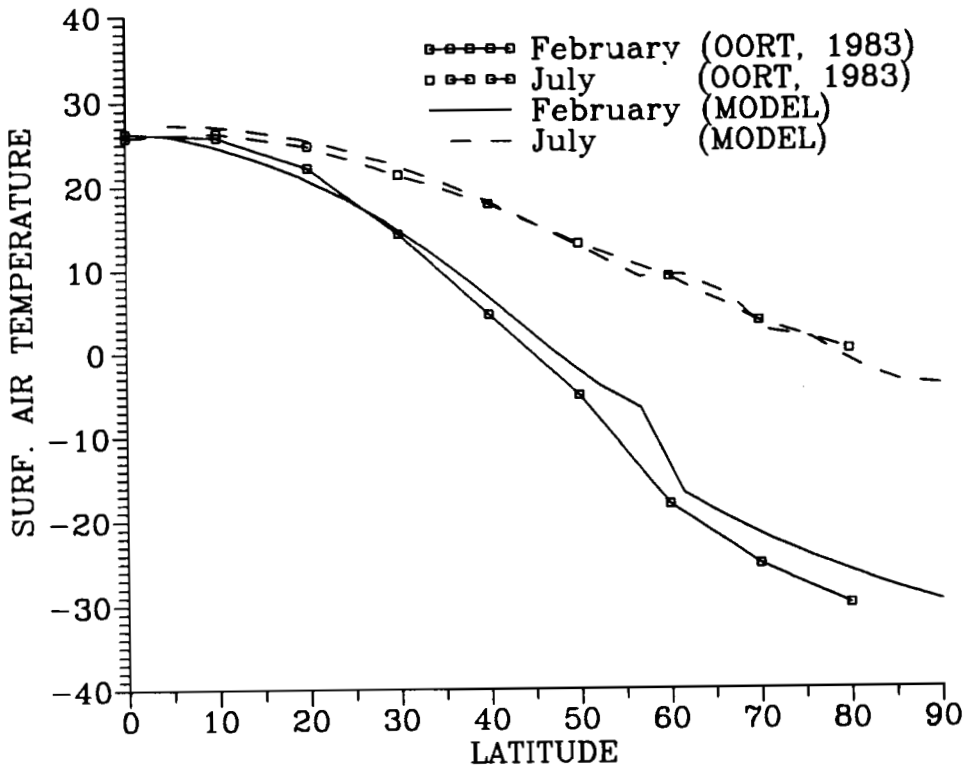


Figure 4.1. Zonal mean surface air temperature of the atmosphere ($^{\circ}\text{C}$) for February and July in the model and as derived from observations.

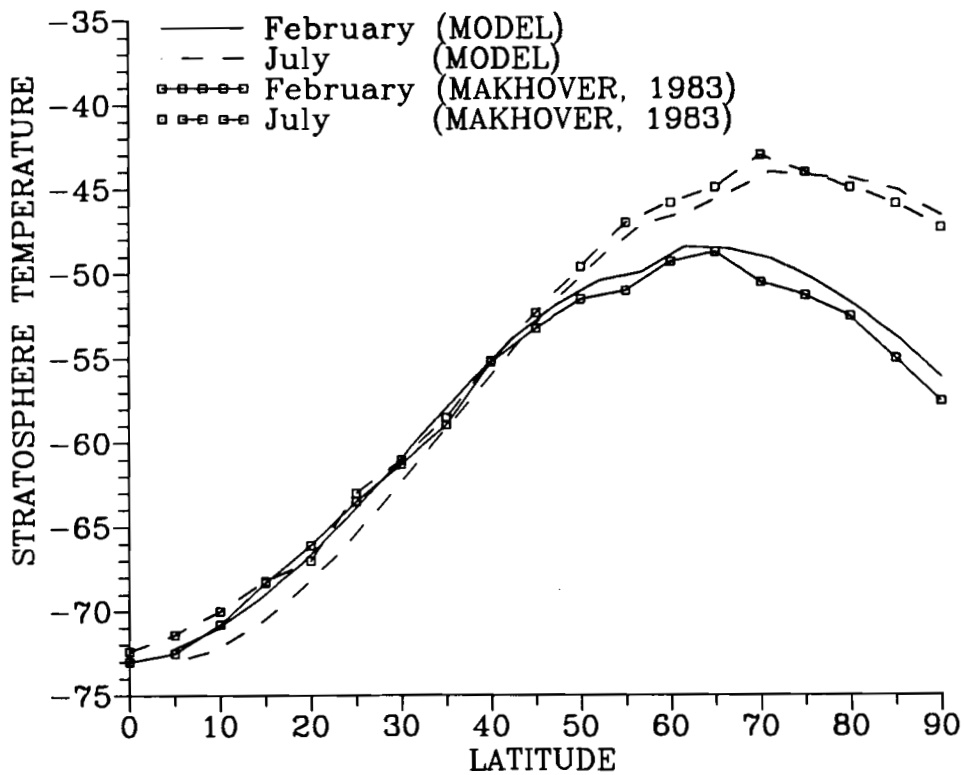


Figure 4.2. Model zonal mean mass-weighted temperature of the stratosphere ($^{\circ}\text{C}$) for February and July in comparison with observational data.

Total oceanic meridional heat transport in the model are shown in Figure 4.7. Taking into account the range of uncertainty of present empirical data on this variable the model results can be considered satisfactory.

Components of the net radiation balance at the top of the atmosphere and zonal mean cloud amount in the model are depicted in Figures 4.8, 4.9, and 4.10. Except for the warm season in polar regions, for which a discrepancy between model results and empirical data is noticeable (this is closely connected with the polar cirrus clouds problem, see, e.g., Ou and Liou, 1984; Feigelson (ed.), 1989), the model, even in its current simplified version, describes the seasonal and latitudinal courses of these important climate variables with rather high accuracy.

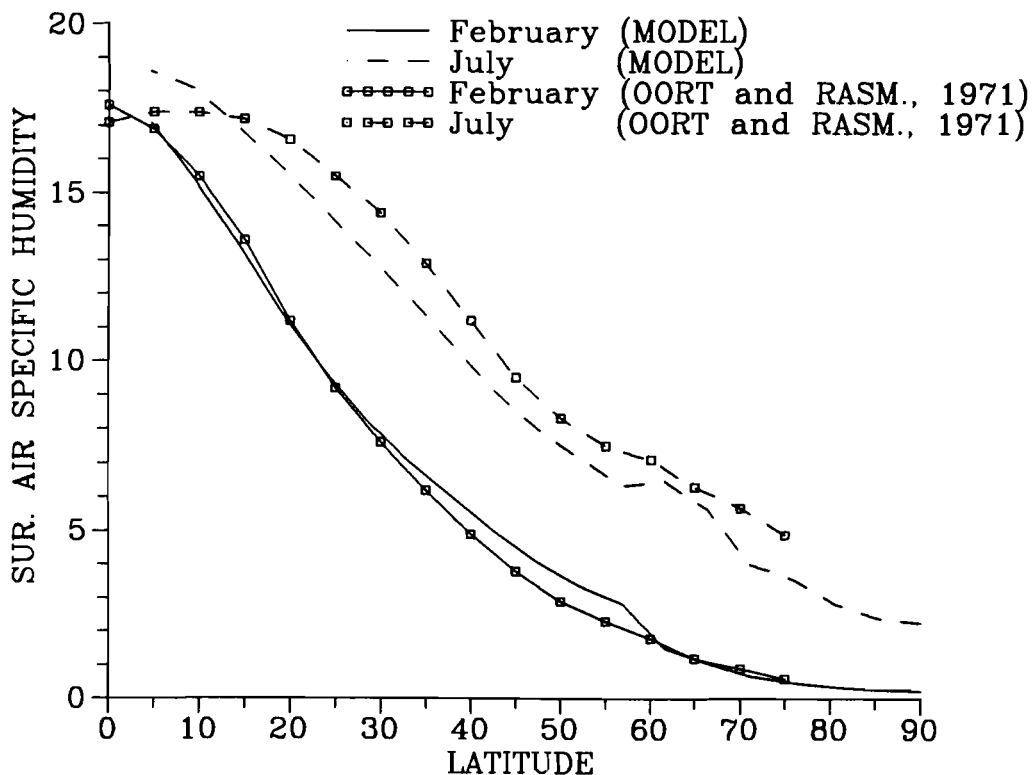


Figure 4.3. Zonal mean surface air specific humidity (g/kg) for February and July in the model and corresponding empirical data from Oort and Rasmusson (1971).

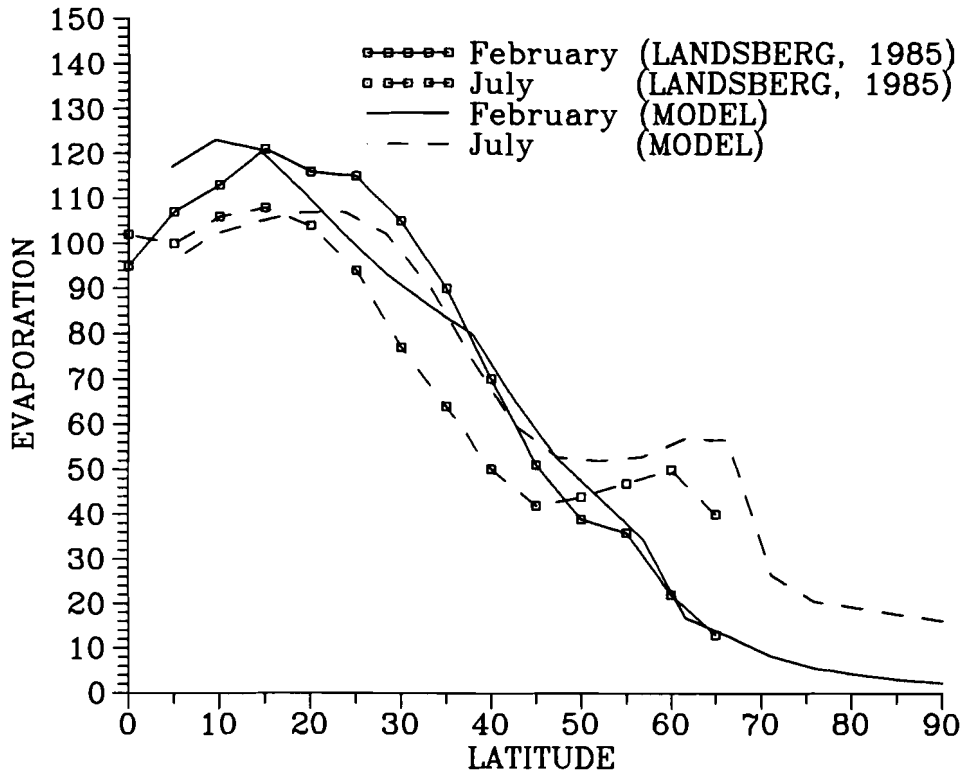


Figure 4.4. Zonal mean evaporation (mm/month) for February and July in the model in comparison with observations.

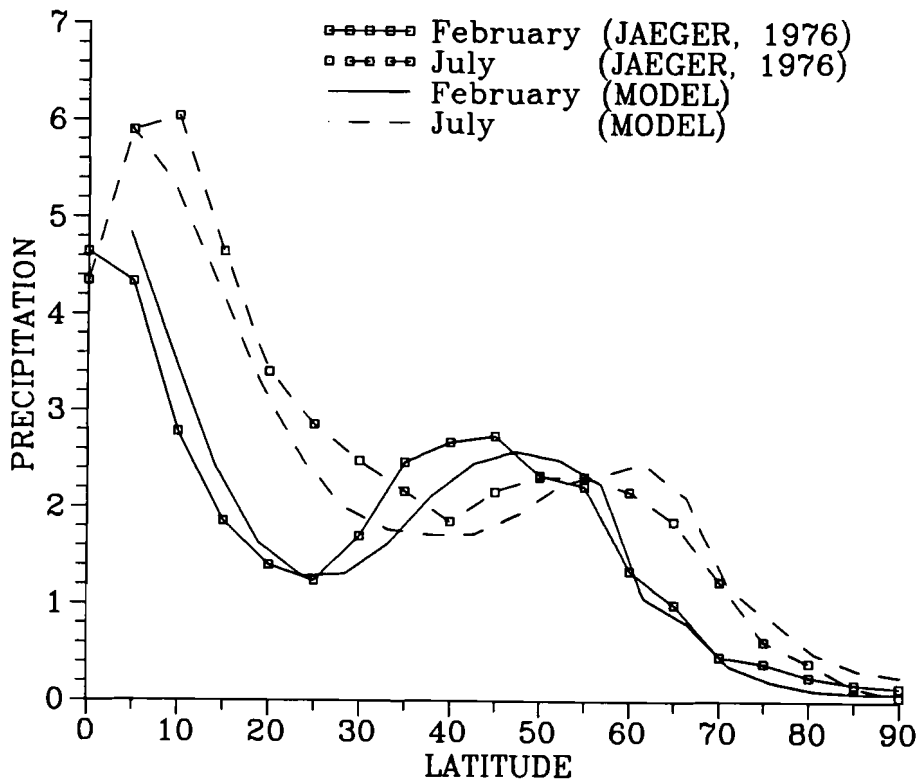


Figure 4.5. Zonal mean precipitation (mm/day) for February and July in the model and corresponding empirical data.

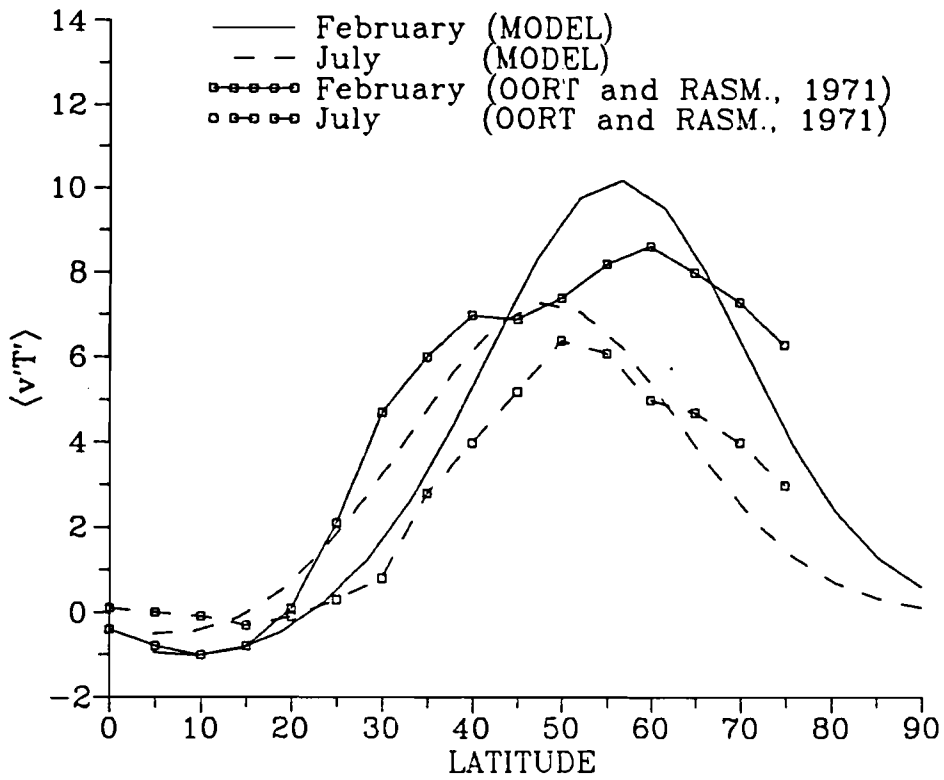


Figure 4.6. Zonally averaged mass-weighted meridional heat transport in the atmosphere (C° m/sec) due to transient eddies for February and July in the model and corresponding empirical data from Oort and Rasmusson (1971).

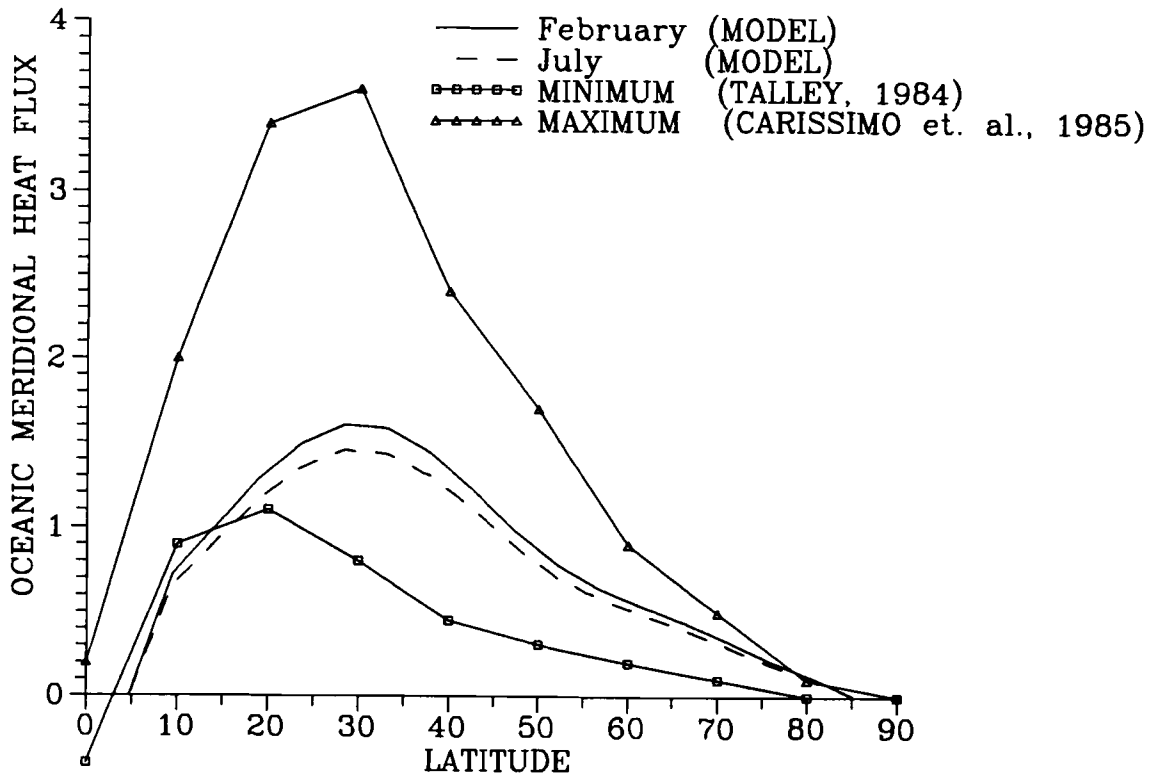


Figure 4.7. Total meridional heat transport in the ocean. (PW) in the model (February and July) and current maximum and minimum empirical estimations (mean annual) of this quantity.

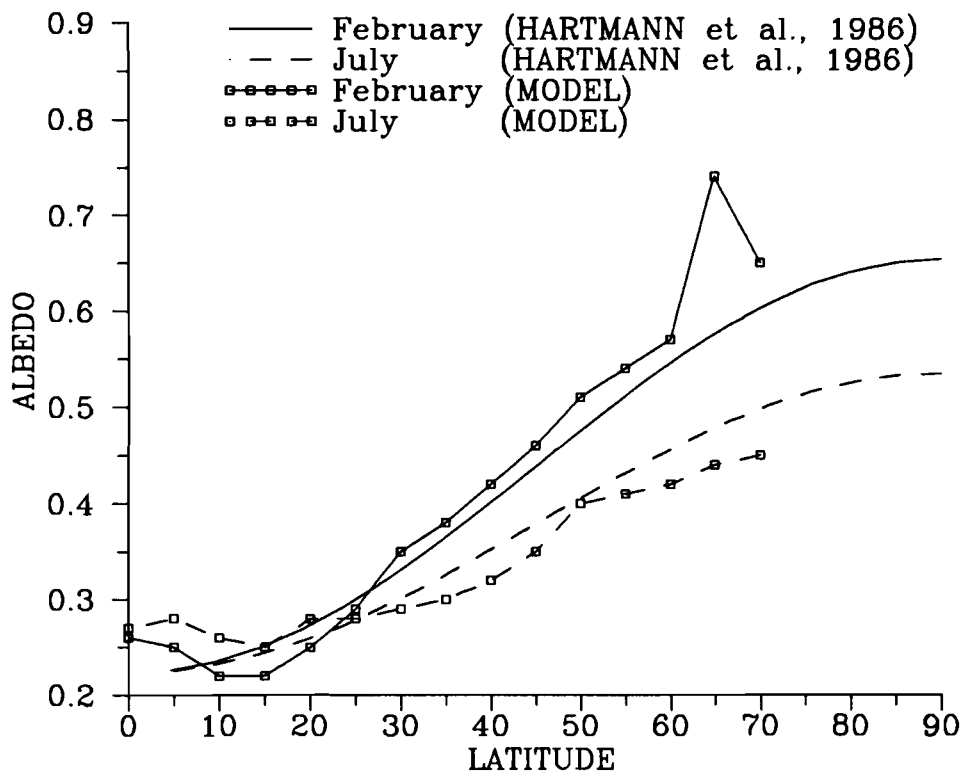


Figure 4.8. Zonal mean planetary albedo for February and July in the model in comparison with satellite data.

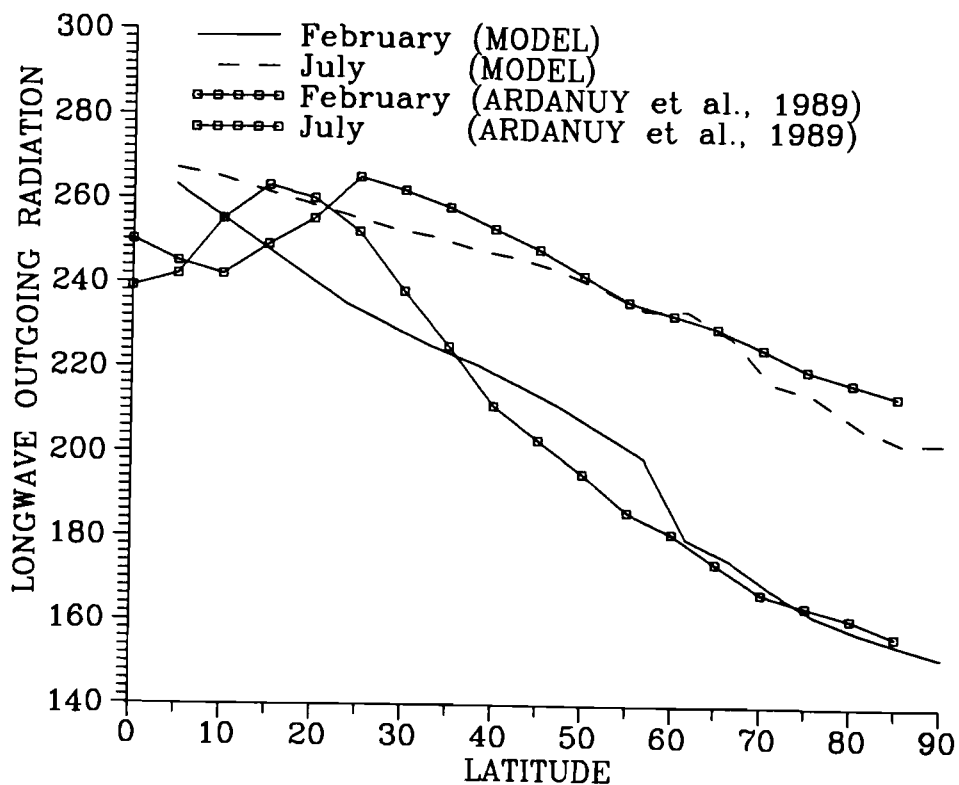


Figure 4.9. Zonal mean flux of long-wave outgoing radiation (w/m^2) for February and July in the model and as derived from satellite data.

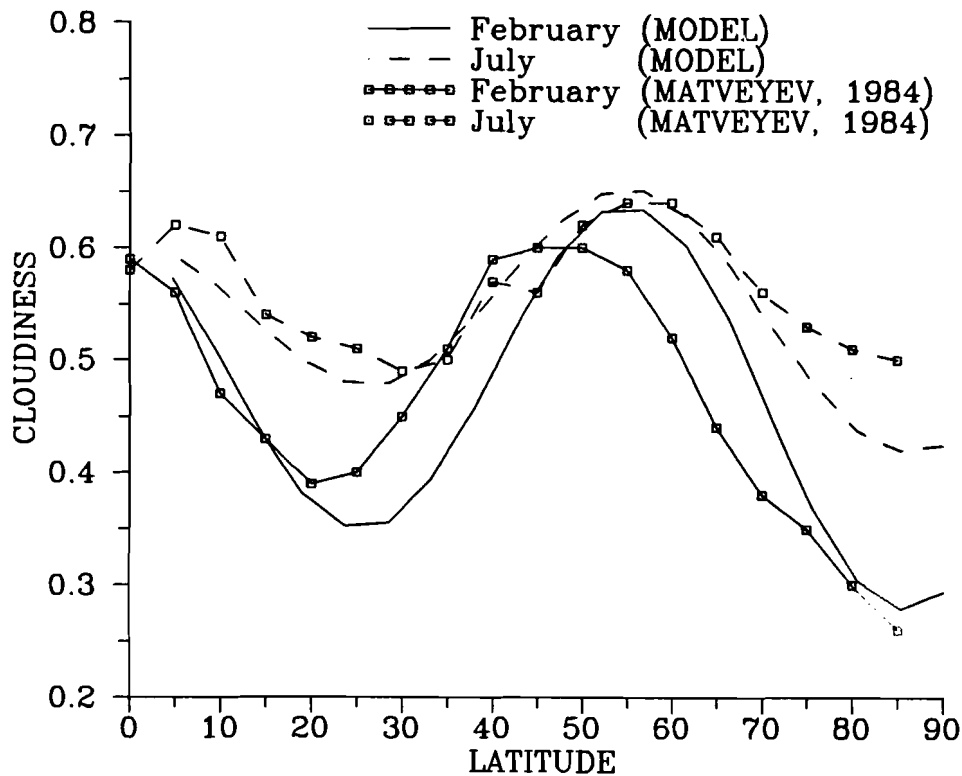


Figure 4.10. Zonal mean total cloud amount for February and July in the model in comparison with empirical data.

As has already been mentioned, one of the specific features of the dynamical-statistical model under consideration is the explicit description of auto- and cross-correlation functions of synoptic component. Figures 4.11 and 4.12 give the examples of computations of two auto-correlation functions (mass-weighted $\overline{T'^2}$ and surface air $\overline{q'^2}$) for February and July (zonal average) in the model and as derived from observations (Oort and Rasmusson, 1971).

In Figures 4.13 to 4.15 the geographical distribution of some basic atmospheric and oceanic climatic fields are represented. The results depicted in Figures 4.13 to 4.15 can be, of course, considered only illustrative ones (due to the highly simplified geographical structure of ocean/land distribution in the current version of the model), although some of the important features of the real climatic system are reflected, at least qualitatively. For example, Siberian and Greenland quasi-stationary anticyclones in surface air temperature (see Figure 4.13), and the Sahara minimum of precipitation (Figure 4.14).

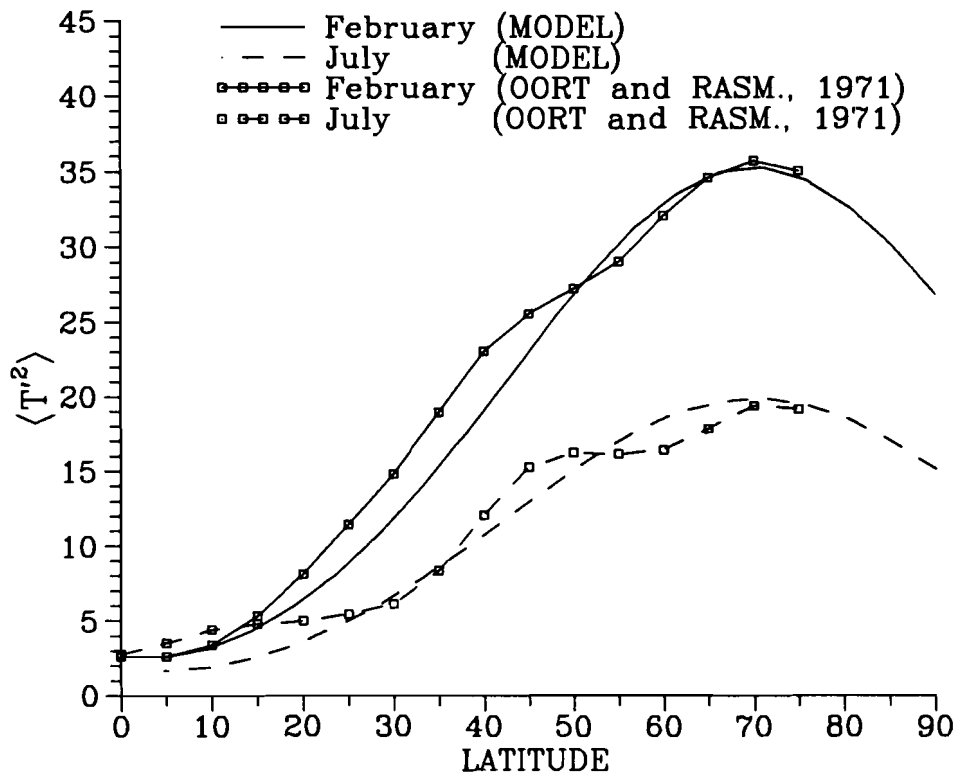


Figure 4.11. Zonally averaged mass-weighted synoptic variance of the atmospheric temperature ($^{\circ}\text{C}^2$) for February and July [model and empirical data from Oort and Rasmusson, (1971)].

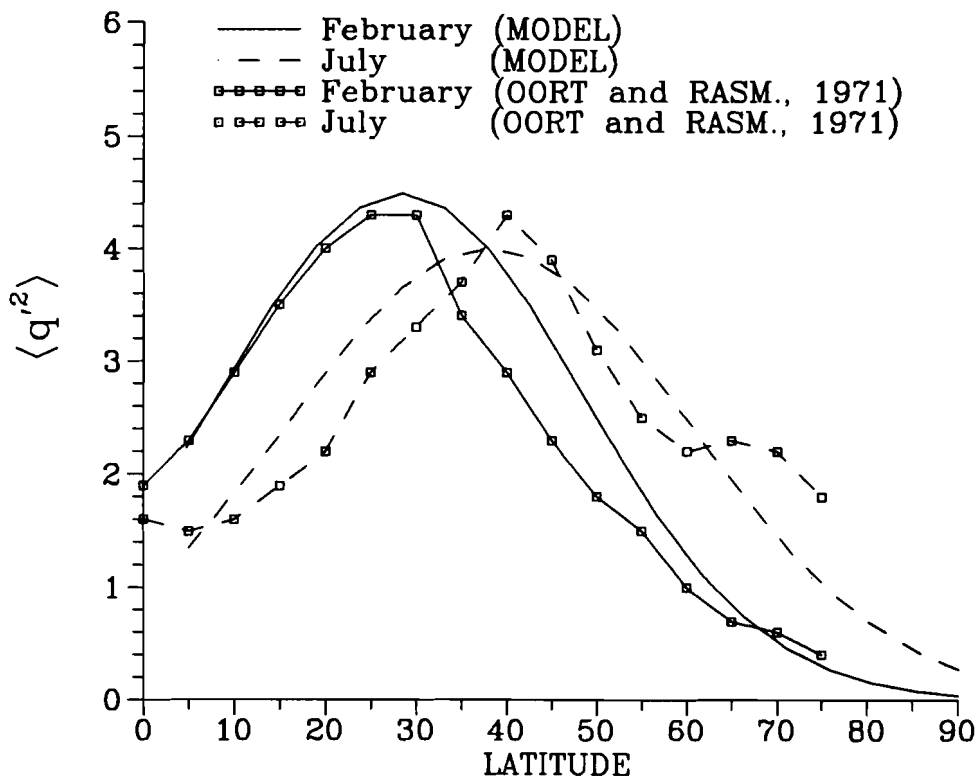


Figure 4.12. Zonally averaged synoptic variance of surface air specific humidity [$(\text{g}/\text{kg})^2$] for February and July in the model in comparison with empirical data from Oort and Rasmusson (1971).

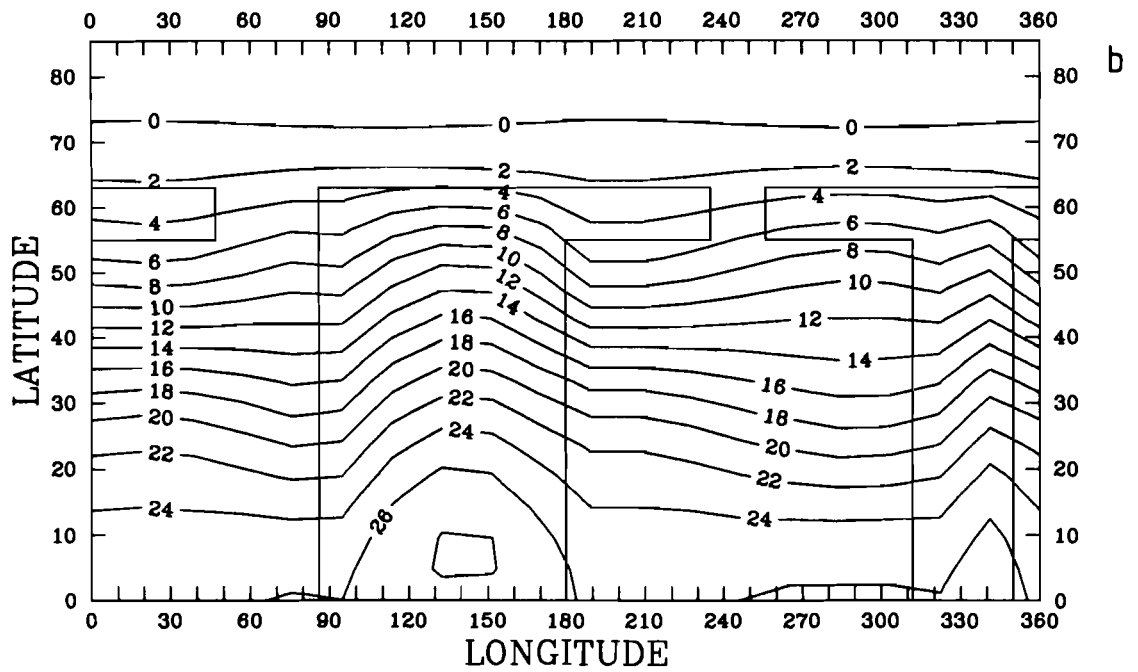
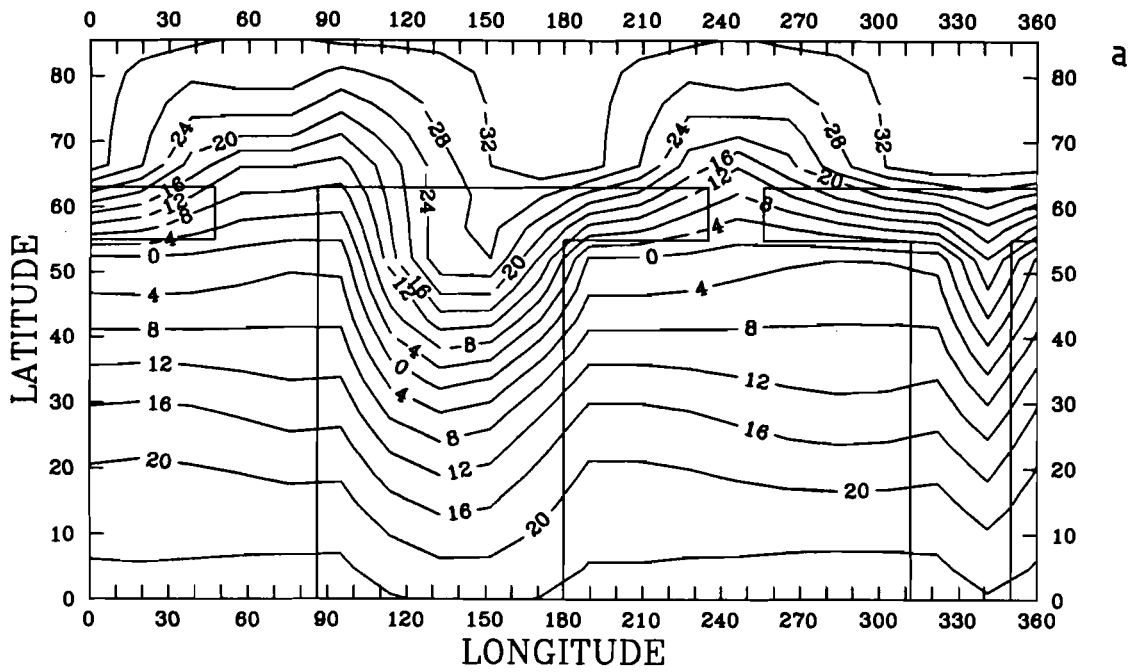


Figure 4.13. Surface air temperature of the atmosphere ($^{\circ}\text{C}$) in the model for February (a) and July (b).

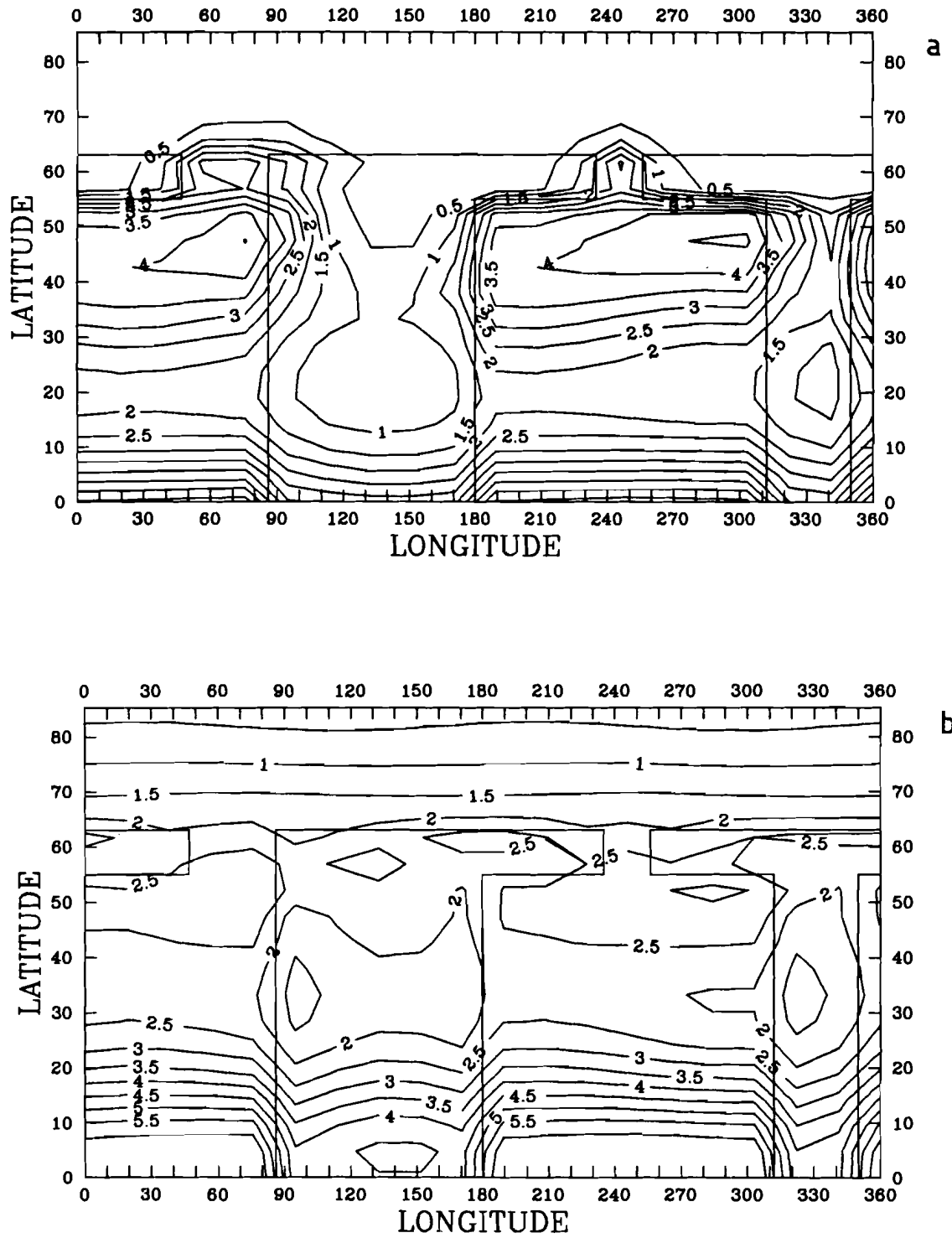


Figure 4.14. Precipitation (mm/day) for February (a) and July (b), model.

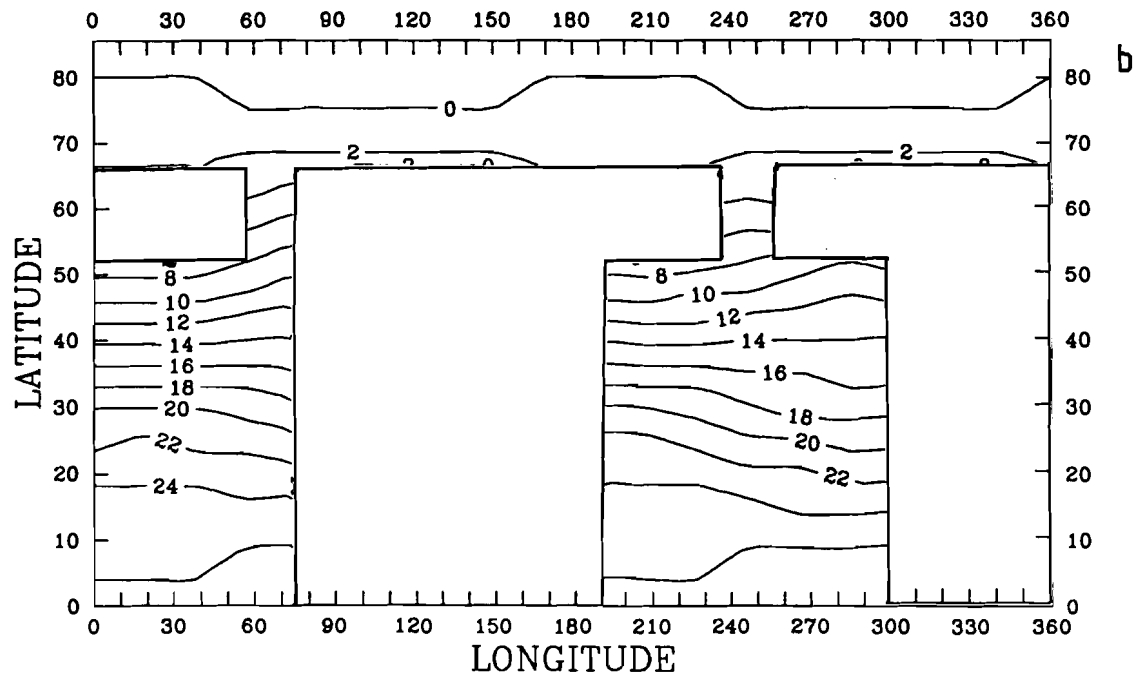
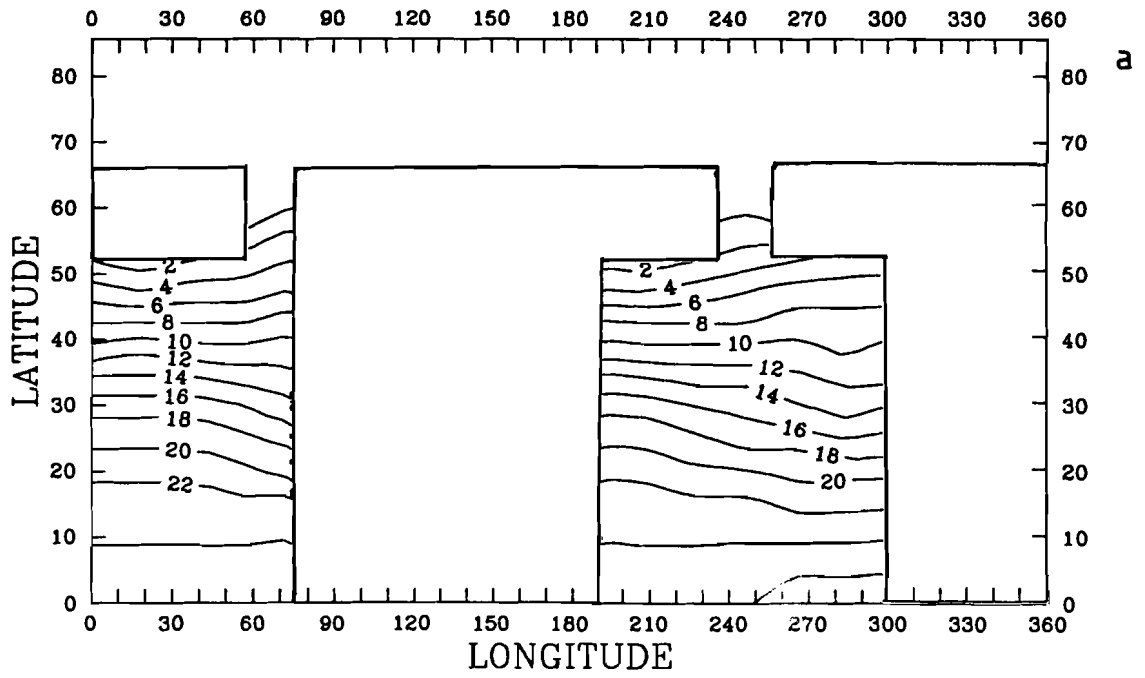


Figure 4.15. Ocean surface temperature (°C) for February (a) and July (b), model.

4.3. Equilibrium response to a doubling of CO₂ content in the atmosphere

Figures 4.16 to 4.19 illustrate the results of an equilibrium climate response to an instantaneous doubling of CO₂ in the atmosphere. The term "equilibrium response" refers to the past 10-year average of the model results after 100 years of integration starting from present climate conditions. Also given are the corresponding results of GCMs (GFDL and MPI) runs. Taking into account noticeable a discrepancy between GCMs results, the model under consideration, as shown in Figures 4.16 to 4.19, can apparently be used as one of the appropriate (informative and computer-efficient) tools for investigations the problem of the possible greenhouse effect.

4.4. Time dependent run

In Figure 4.20 the model result is depicted of hemispherically averaged temperature transient response to gradual time dependent increase of greenhouse gas content in the atmosphere according to the 1990 IPCC scenario A, shown in Figure 4.21. The analogous result of the MPI run is given for comparison. The results of the computations are in rather good agreement, except for the first three decades; this difference seems to be connected with the problem of "cold start" in MPI GCM (see Cubasch *et al.*, 1991) and with the hemispherical character of the present version of 2.5-DSCM.

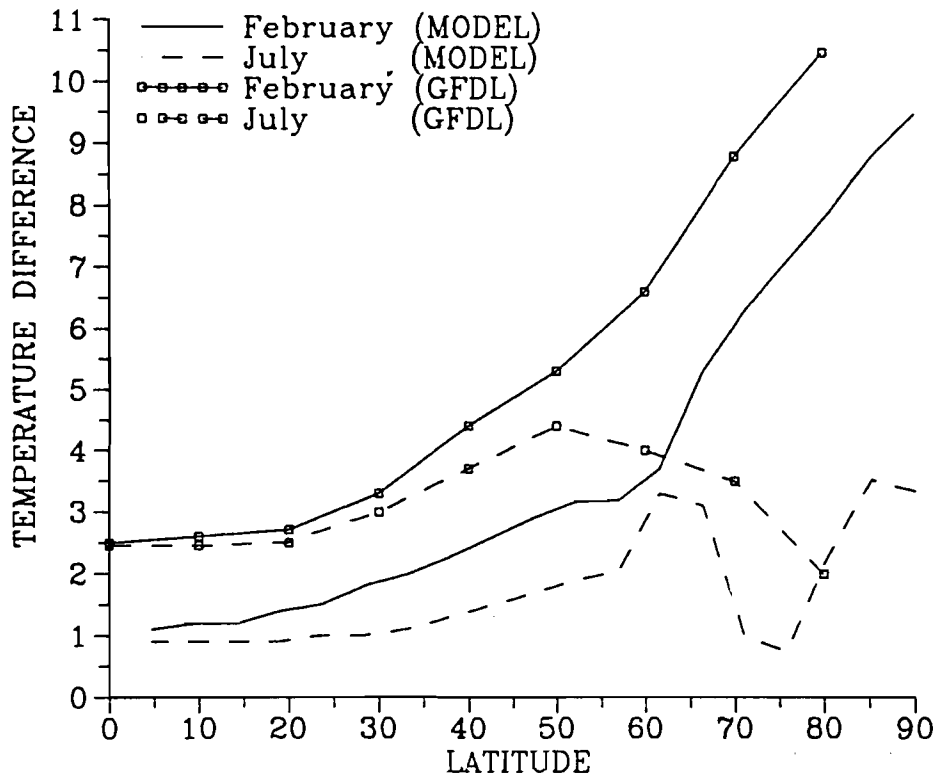


Figure 4.16. $2 \times \text{CO}_2 - 1 \times \text{CO}_2$ zonally averaged surface air temperature difference ($^{\circ}\text{C}$) for February and July in the model and responding results of GFDL runs (Manabe *et al.*, 1992).

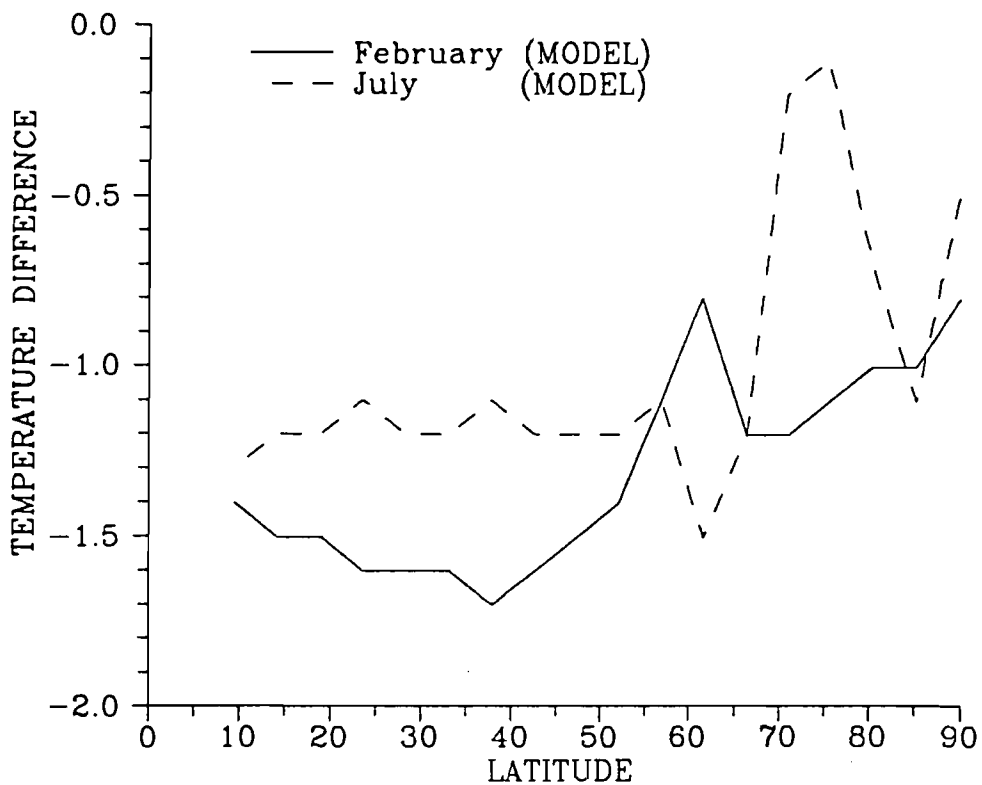


Figure 4.17. $2 \times \text{CO}_2 - 1 \times \text{CO}_2$, zonal mean mass-weighted stratospheric temperature difference ($^{\circ}\text{C}$) for February and July, model.

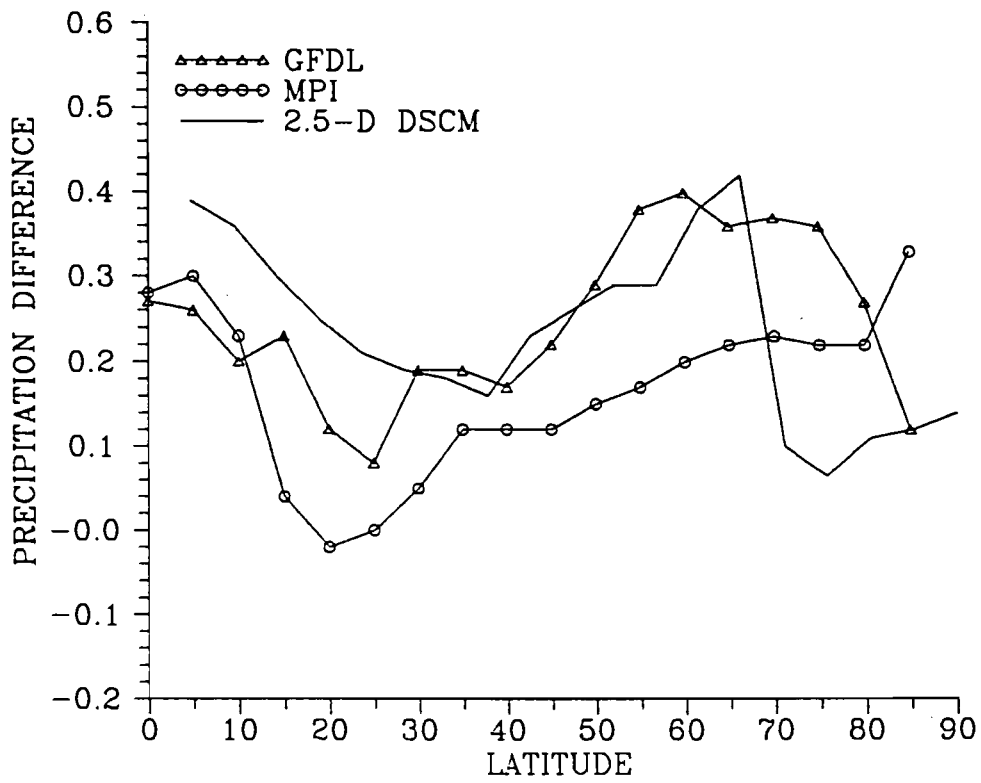


Figure 4.18. $2 \times \text{CO}_2 - 1 \times \text{CO}_2$, mean annual zonally averaged precipitation difference (mm/day) in the model in comparison with corresponding results of GFDL runs (Manabe *et al.*, 1991, 1992) and MPI (Roeckner, private communication).

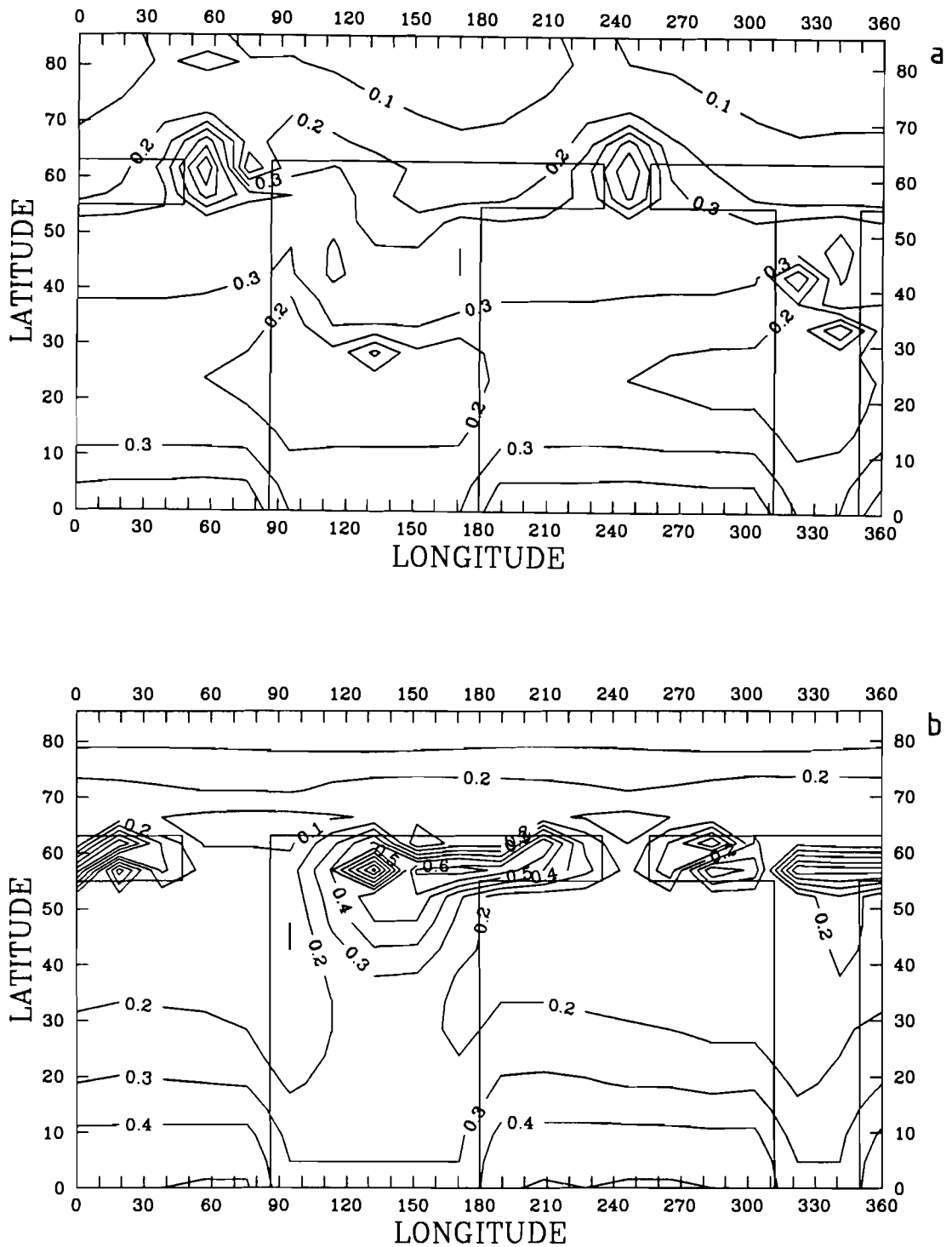


Figure 4.19. Geographical distribution of $2 \times \text{CO}_2 - 1 \times \text{CO}_2$ precipitation difference (mm/day) for February (a) and July (b), model.

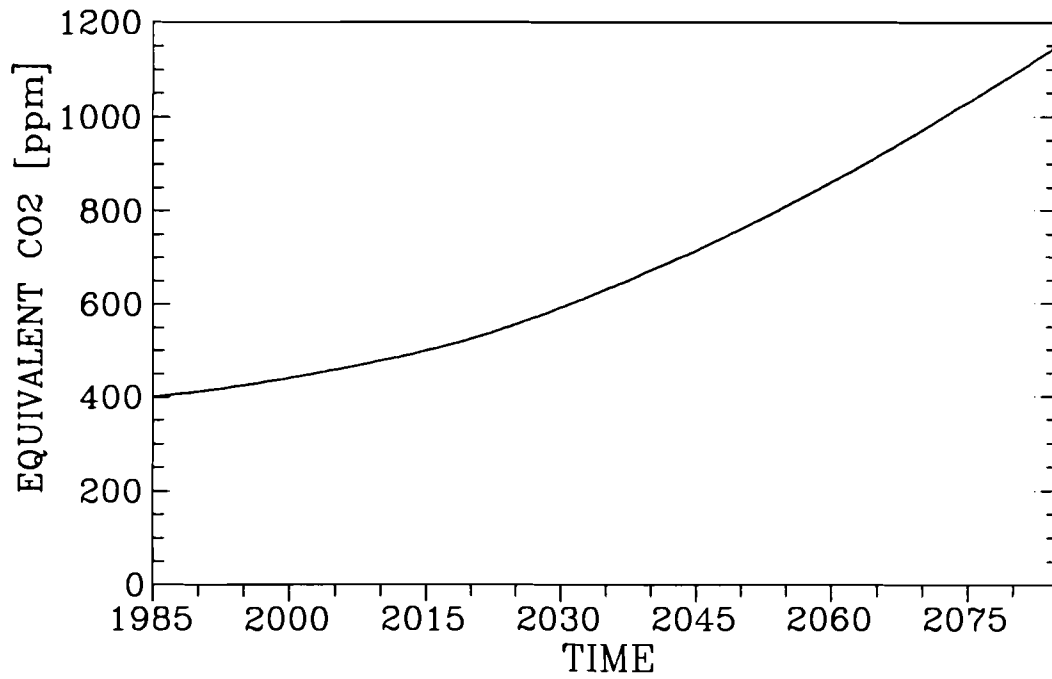


Figure 4.20. CO₂ equivalent concentration for the 1990 IPCC Scenario A (Cubasch, et al., 1991).

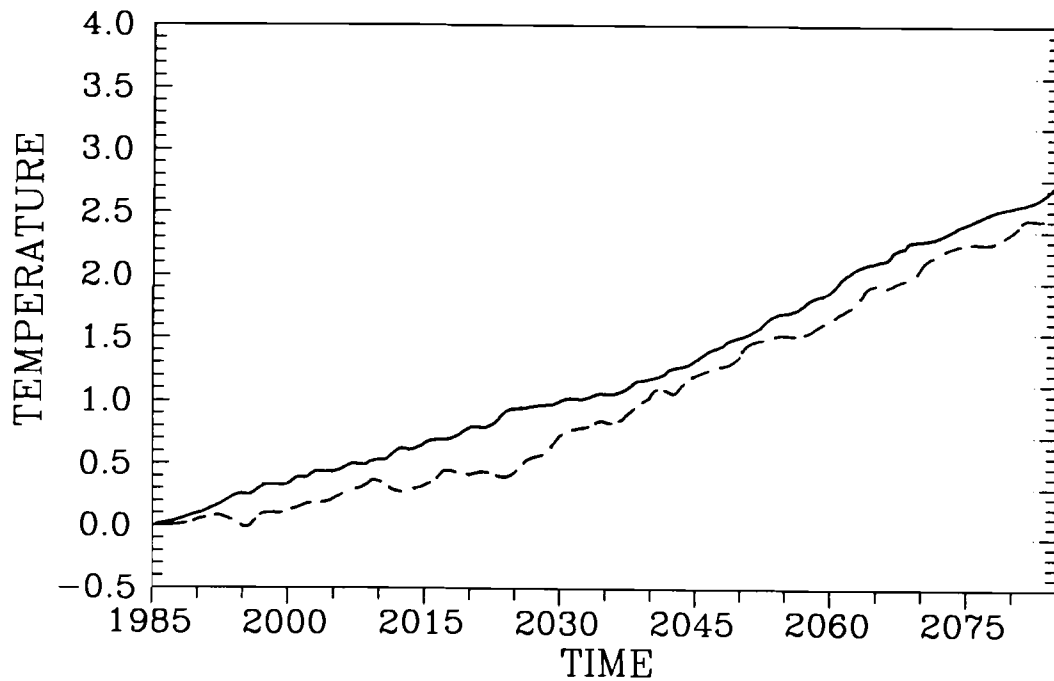


Figure 4.21. Time-dependent evolution of hemispherically averaged surface air temperature, (°C) in the model for the 1990 IPCC Scenario A in comparison with the MPI results for the globally averaged temperature (Cubasch *et al.*, 1991).

5. Multilayer Isopycnal Largescale Ocean Model

The present ocean model called **MILE** (**M**ultilayer **I**sopycnal **L**argescale **O**cean **E**an model) is designed for the simulations of large-scale and long-term ocean processes. The model has the same set of prognostic variables as traditional oceanic GCMs, but it is much faster that allows to use MILE as a part of integrated model of climate change. The model was originally developed at Computing Center of the Russian Academy of Sciences. The previous version of this model was described in Ganopolski (1991).

5.1 Physical background

There is a number of empirical evidences and models results suggesting that the large-scale oceanic currents are quasi-isopycnal, i.e. oceanic water masses move practically along surfaces of constant density, while mixing across isopycnal surface is very slow. It is one of the reasons, why isopycnal coordinates (ICs), where density is used as a vertical coordinate instead of depth, seem to be more appropriate for the oceanic modelling than traditional Cartesian (Z-) coordinates. The other advantage of ICs is that this coordinates allow to describe isopycnal and diapycnal mixing separately, thus excluding impact of lateral diffusion on diapycnal mixing as it takes place in Z-coordinates models. In addition, ICs have the ability to adopt their spatial resolution to vertical density gradients and, thus, one can expect that ICs should be more effective in reproducing of oceanic density structure. At the same time, application of ICs is more complex and creates many technical problems, especially with definition of boundary conditions. That is why before recently ICs were of limited use for oceanic modelling. But now encouraging results in development of ICs models are obtained. Two OGCMs, based on ICs already published, namely Miami University model (Bleck et al., 1989, 1992) and Hamburg OPYC model (Oberhuber 1993a,b).

The other important feature of large-scale oceanic processes is that velocity field is in close geostrophic balance. It means that nonstationar and nonlinear terms in dynamical equations are relatively small (they are important only for mesoscale processes and in narrow equatorial zone). This fact allows to simplify dynamical equations and exclude the terms responsible for fast internal oceanic

gravity waves. That, in turn, allows to increase significantly time step of integration and reduce the computational cost of model run. The use of simplify dynamical equations instead of primitive ones leads to some limitation of the model, but for many purposes this approach is quite justified. The MPI large-scale OGCM (Maier-Reimer et al., 1987) is the example of successful application of this type of models for oceanographic and climatic studies.

The oceanic model MILE described below represents the first attempt to design the global scale model of the ocean climate, based on isopycnal coordinates and quasi-geostrophic approach.

5.2 Model description

The ocean is represented in the model by a set of N vertically uniform layers with thickness h_i , potential temperature T_i , salinity S_i , and current velocity u_i (see Figure 5.1). The two upper layers represent the active ocean layer, that is directly subjected to the seasonal variability. The layer $i=1$ is the *effective* mixed layer (ML)². The bottom of the second layer coincides with the maximum during an year ML depth. Thus, the second layer occupies the region, which at a given moment lies just below ML, but at least once per year is brought into ML. This layer we call *buffer layer* (BL) for its intermediate nature. The introduction of the BL allows to overcome a problem arising when ML directly interacts with the isopycnal layers (Oberhuber, 1993a; Bleck et. al, 1989, 1992). The BL can disappear when ML deepening, but it immediately restores, when detrainment process (shallowing of ML) begins. It is important, that water, detrained from ML, enters into BL and does not perturbs the density of underlying isopycnal layers.

The layers with numbers $i=3, N-2$ are isopycnal ones, i.e. their potential density $\rho_i = const$. In a given gridpoint only isopycnal layers with the numbers $i \geq k$ can exist, where k has to satisfy the

²) Effective ML depth is determined as the depth of uniform layer with heat capacity equal to the sum of the heat capacities of the ML and seasonal thermocline.

density condition $\rho_k > \rho_2$ (or $\rho_k > \rho_1$, if BL is absent). If this density condition is satisfied also for the layer with the number $k-1$, a new layer comes into existence. To keep reasonable vertical resolution some limitations on layer thickness and depth of the bottom surface are applied. The thickness of any isopycnal layer cannot be less than 5m. The depth of the bottom of the lowermost isopycnal layer has to satisfy condition $Z_{N-2} = \sum_{i=1}^{i=N-2} h_i < Z_{\max} = \min(H/2, 2000\text{m})$.

Two bottom layers ($i=N-1, N$) encompass the ocean water masses lying below the main thermocline ($z > 1-2$ km). There are not any restrictions on the density of these layers, thus characteristics of the deep water masses can take arbitrary values. The thickness of the lowermost layer in contrary is fixed: $h_N = 2/3(H - Z_{\max})$. The thickness of layer $N-1$ is determined as $2/3H - Z_{N-2}$. Such approach allows to have reasonable vertical resolution in deep ocean without significant increasing of the number of isopycnal layers.

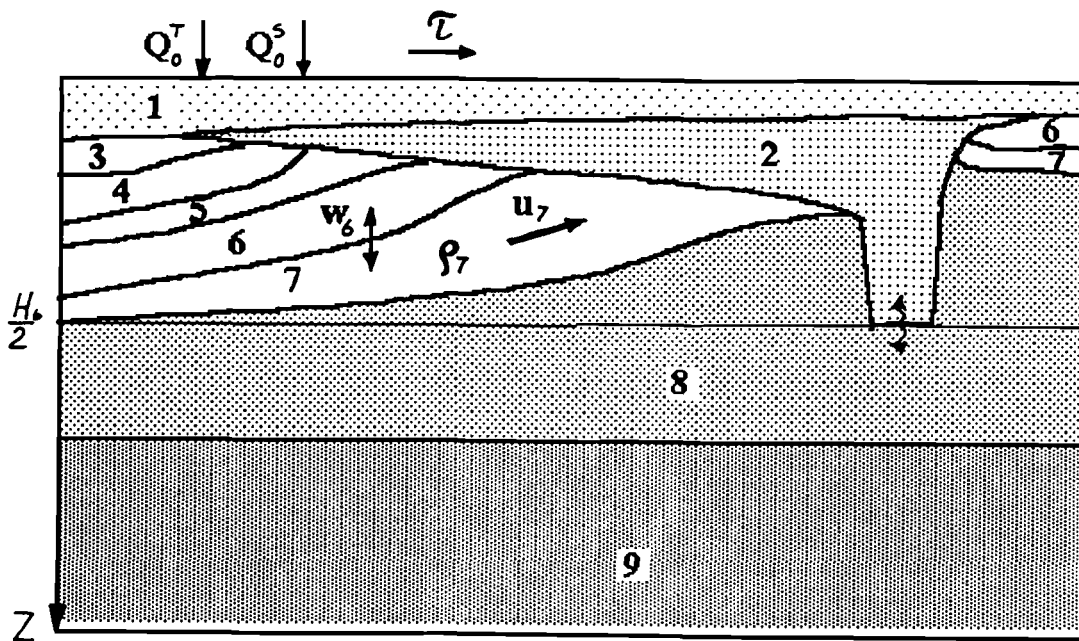


Figure 5.1 The vertical structure of the multilayer isopycnal ocean model.

The model dynamics is described on the basis of linearized stationary equations of the motion. The horizontal component of the current velocity (which is assumed to be equal isopycnal components of velocity in the isopycnal layers) is represented as a sum of baroclinic and barotropic components. For determination of the barotropic components the integral stream function Ψ is introduced

$$\bar{u} = -\frac{1}{Hr} \frac{\partial \Psi}{\partial \varphi}, \quad \bar{v} = \frac{1}{Hr \cos \varphi} \frac{\partial \Psi}{\partial \lambda}. \quad (5.2.1)$$

Following by Sarkisyan (1977) the integral stream function is described by equation

$$A_m \nabla^2 \nabla^2 \Psi - \varepsilon \nabla^2 \Psi = -\frac{1}{\rho_0} \text{curl}_z \tau_0 + \frac{\beta}{\sin \varphi} \frac{\partial \Psi}{\partial \lambda} + \frac{\varepsilon g}{f \rho_0} \int_0^H z \nabla^2 \rho dz + \mathbf{R}, \quad (5.2.2)$$

where A_M is the coefficient of horizontal viscosity, $\varepsilon = (0.5 |f| k_M)^{1/2} H^{-1}$, k_M is the coefficient of vertical viscosity, r the earth radius, H the ocean depth, f the Coriolis parameter, $\beta = df/dy$, ρ_0 is the averaged sea water density, τ_0 the surface wind stress, and \mathbf{R} represents the terms including the horizontal derivations of the ocean depth. In the experiment described below, $H = \text{const}$ and thus $\mathbf{R} = 0$. Boundary conditions for equation (5.2.2) are

$$\Psi|_{\Gamma_m} = C_m, \quad m=1, \dots, M, \quad (5.2.3)$$

where M is the number of separate land domains with the coastlines Γ_m . In case $M > 1$, it is necessary to use additional equations for determination $\Psi_m(t)$ for $m > 1$. (The stream function at the boundary of one land domain can be determined arbitrary, e.g. $\Psi_j = 0$). In the present version of the model we consider two land domain (all continents except Antarctica are combined). The stream function on the boundary of Antarctic is prescribed on the basis of empirical estimations rather than determined from special equation. The introducing of additional equation for determination of streamfunction at the land boundaries is envisaged to be done on the next stage of model development.

The baroclinic components of current velocity $\mathbf{u}'_i = (u'_i, v'_i)$ are described by the equation

$$\rho_o h_i f \times \mathbf{u}'_i = -\nabla p'_i h_i + \tau_{i-1} - \tau_i + \rho_o \nabla_L \cdot (A_m h_i \nabla_L \mathbf{u}_i), \quad (5.2.4)$$

with boundary conditions

$$u'_i|_{\Gamma_m} = 0, \quad m=1,\dots,M$$

where subscript "L" means that the space derivation are determined along a layer rather than horizontally, p'_i is the pressure anomaly, computed by vertical density profile

$$p'(z) = g \left[\int_0^z \rho(z) dz - \frac{1}{H} \int_0^H (H-z) \rho(z) dz \right] \quad (5.2.5)$$

where ρ_s is so-called in situ density related with in situ temperature T_s , salinity and pressure by equation of state

$$\rho_s = \rho_s(T_s, S, p), \quad (5.2.6)$$

where $T_s = T_s(T, S, p)$, $p = \rho g z$.

The friction between i and $i+1$ layers τ_i (for $N > i > 0$) is given by

$$\tau_i = 2k_m \frac{u_i - u_{i+1}}{h_i + h_{i+1}} \quad (5.2.7)$$

and bottom friction is given by

$$\tau_N = C_D \rho_o |u_N| u_N \quad (5.2.8)$$

where C_D is the bottom drag coefficient.

Evolution of the layer's characteristics is described by the following set of equations:

$$\frac{\partial h_i}{\partial t} + \nabla_L (u_i h_i) = w_{i-1} - w_i, \quad (5.2.9)$$

$$\frac{\partial (h_i T_i)}{\partial t} + \nabla_L (u_i h_i T_i) + w_{i-1} T_{i-1}^* - w_i T_i^* = \delta Q_i^T + \nabla_L (A_i h_i \nabla T_i), \quad (5.2.10)$$

$$\frac{\partial (h_i S_i)}{\partial t} + \nabla_L (u_i h_i S_i) + w_{i-1} S_{i-1}^* - w_i S_i^* = \delta Q_i^S + \nabla_L (A_i h_i \nabla S_i), \quad (5.2.11)$$

where T_i^* , S_i^* are the values of temperature and salinity at the boundary between i and $i+1$ layers, A_i the coefficient of isopycnal diffusion, w_i is the relative vertical velocity at the bottom of i th layer, $\delta Q_i^T = q_{i-1}^T - q_i^T$ is the heat (the same for salt) uptake into layer i and q_i^T the heat flux at the bottom of layer i . The fluxes at the ocean surface are determined as follows

$$q_0^T = \frac{1}{c_p \rho_0} [Q_s(1-f_i) + Q_i f_i], \quad q_0^S = -S_0 (P-E+R), \quad (5.2.12)$$

where Q_s is the heat flux at the free ocean surface, Q_i the heat flux through sea ice, f_i the sea ice fraction, c_p the water specific heat capacity, S_0 the surface salinity, P the precipitation, E the evaporation, and R the runoff which is considered as a surface freshwater flux at a given gridpoint. All horizontal fluxes in equations (5.2.9)-(5.2.11) are assumed to be zero on lateral ocean boundaries.

From the boundary condition of the "rigid lid" at the ocean surface and nonpenetration at the bottom it directly follows that $w_0 = w_N = 0$. The value w_1 has the physical sense of entrainment (detrainment) velocity at the ML bottom. For determination of w_1 and the fluxes at the bottom of the ML a modification of Kraus-Turner integral model is used. Following Reasniansky (1976), the equation for entrainment velocity is written in the form

$$C_g F \left(\frac{h_1}{h_e} \right) v_*^3 - \frac{h_1}{2 \rho_0} [C_k B_0 + w_1 g (\rho_1^* - \rho_1)] = 0, \quad (5.2.13)$$

where

$$F\left(\frac{h_1}{h_e}\right) = \max\left(1 - \frac{h_1}{h_e}, 0\right), \quad h_e = \frac{C_g v_*^2}{C_e f},$$

$v_* = C_D^{1/2} u_a$ is the surface friction velocity, C_D the ocean surface drag coefficient, u_a the averaged module of surface wind speed, ρ_1^* the water density below the ML layer, $B_0 = -g(\alpha q_{01} + \beta q_{02})$ is the surface buoyancy flux, $\alpha = \partial \rho / \partial T$, $\beta = \partial \rho / \partial S$, C_g , C_e , C_k are the model parameters. To account for the processes caused by synoptic variability of the surface meteorological conditions, a dependence of coefficient C_g from latitude is introduced following Ganopolski (1988) as

$$C_g = C_g^0 (1 + (\sin \varphi)^2). \quad (5.2.14)$$

In the case of negative surface bouancy flux, the coefficient C_k determines the fraction of buoyancy energy going into entrainment process at the bottom of ML. It was chosen in the form

$$C_k = \begin{cases} 1 & , B_o > 0 \\ C_k^0(1 - 0.001 h_1), & B_o < 0 \end{cases} \quad (5.2.15)$$

Equation (5.2.13) is valid only in the case if $w_1 > 0$ (i.e., entrainment process takes place). If $w_1 < 0$ (detrainment process) formally replacing $\rho_1^* = \rho_1$ in equation (5.2.13) one can derive algebraic expression for equilibrium ML depth. The value of w_1 in this case is determined from equation

$$w_1 = \frac{dh_1}{dt}. \quad (5.2.16)$$

The bottom of the BL was determined above as the maximum ML depth during an year. However this depth can change from year to year. To exclude the jumps of BL depth, the bottom surface of BL is considered not as a fixed one but as a "soft" surface which is attracted to the maximum ML depth $h_{1\max}$ in accordance with the relation

$$w_2 = -(Z_2 - h_{1\max})/t_{rel}, \quad (5.2.17)$$

where $Z_2 = h_1 + h_2$ and t_{rel} is the relaxation time. If the BL is taken up by the ML, then $w_2 = w_1$.

The diapycnal mixing velocity is determined by

$$w_i = -\mu \frac{\alpha \frac{\partial^2 T}{\partial z^2} + \beta \frac{\partial^2 S}{\partial z^2}}{\alpha \frac{\partial T}{\partial z} + \beta \frac{\partial S}{\partial z}} \quad i = k, \dots, N-2. \quad (5.2.18)$$

where μ is the diapycnal diffusion coefficient. In the case of linear equation of state, the formula (5.2.18) turns into the expression for diapycnal velocity given by Huang and Bryan (1987).

The vertical velocity at the upper surface of the lowermost layer can be determined by vertical integration of continuity equation

$$w_{N-1} = - \int_0^{z_{N-1}} \nabla \cdot \mathbf{u}(z) dz = - \sum_{i=1}^{i=N-2} \nabla \cdot (\mathbf{u}_i h_i). \quad (5.2.19)$$

Sea ice model. A sea ice module of the ocean model is based on Semtner (1976) thermodynamic and Hibler (1979) dynamic sea ice models. It describes the time evolution of averaged speed of the ice drift \mathbf{u}_I , sea ice thickness h_I and sea ice fraction f_I :

$$\rho_I h_I \mathbf{f} \times \mathbf{u}_I = \tau_{ia} - \tau_{io} - \rho_I g h_I \nabla H_s + F_I, \quad (5.2.20)$$

$$\frac{\partial h_I}{\partial t} + \nabla \cdot (\mathbf{u}_I h_I) = F_h + \nabla \cdot (A_I \nabla h_I), \quad (5.2.21)$$

$$\frac{\partial f_I}{\partial t} + \nabla \cdot (\mathbf{u}_I f_I) = F_f + \nabla \cdot (A_I \nabla f_I), \quad (5.2.22)$$

where ρ_I is the sea ice density, τ_{ia} the wind stress at the sea ice surface, τ_{io} the stress at the sea ice bottom, H_s the sea surface dynamic height, computed in the model through the vertical profile of water density, F_I the internal sea ice stress, F_h and F_f are the thermodynamical terms computed by the growth rate of ice thickness. Because of the coarse space resolution of the model, the internal ice stress was neglected in the dynamical equation for the sea ice in the present version of the model.

5.3 Numerical methods

Numerical realization of a model in ICs system is more complicated than for traditional multilevel models because ICs are moving (in vertical direction) coordinates with variable number of the layers in given horizontal location. Here we shortly describe the main features of using numerical schemes and approximations.

A shifted B-grid is used for numerical approximation of the spatial derivations. The boundaries of continents are assumed beign coincided with the velocity grid points. In agreement with boundary conditions, the value of stream function and baroclinic velocity are set equal zero in these points.

Equations (5.2.2) for vertically averaged stream function was solved by introducing of vertically averaged vorticity $\omega = \Delta\Psi$ and splitting (5.2.2) into two equations, which are solved iteratively:

$$A_m \nabla^2 \omega - \varepsilon \omega = -\frac{1}{\rho_0} \text{curl}_z \tau_0 + \frac{\beta}{\sin \varphi} \frac{\partial \Psi}{\partial \lambda} + \frac{\varepsilon g}{f \rho_0} \int_0^H z \nabla^2 \rho dz, \quad (5.3.1)$$

$$\nabla^2 \Psi = \omega. \quad (5.3.2)$$

Two different methods are used for solving equation (5.2.4). One is employed for the points locating out of equator and the other one for equatorial rows of grid points. As it was mentioned above, the velocity field out of the narrow equatorial region is in quasi-geostrophic balance. It means that the Coriolis term and horizontal gradient of pressure are the two major terms, while the friction terms are relatively small, except for ML where surface wind stress is also important. It allows to solve equation (5.2.4) iteratively in the form

$$u^{**} f = -\frac{1}{\rho_0} \frac{\partial p^{n-1}}{\partial y} + F_y^*, \quad -v^{**} f = -\frac{1}{\rho_0} \frac{\partial p^{n-1}}{\partial x} + F_x^*, \quad (5.3.3)$$

where F_x, F_y are friction terms. The superscript "n-1" means that the value is taken from the previous time step, "*" means the value from the previous iteration, and "**" means new value.

On the equator the Coriolis term is absent, thus pressure gradient should be compensated by the friction. To solve equation (5.2.4), the so-called "disturbed" dynamical equations (Bryan, 1984) are used:

$$\varepsilon \frac{\partial u'}{\partial t} = -\frac{\partial p}{\partial x} + F_x, \quad \varepsilon \frac{\partial v'}{\partial t} = -\frac{\partial p}{\partial y} + F_y, \quad (5.3.4)$$

where $\varepsilon \ll 1$ is the "disturbed" parameter, that slows down the propagation of the fast equatorial waves. This approach allows to keep time step of integration enough large, while it does not significantly violate current velocity field.

To compute the horizontal density pressure gradient it is necessary to use horizontal density derivation instead of along-layer ones. For this end the values of temperature and salinity are interpolated from the layers onto appropriate horizontal levels such a way to preserve heat and salt contents in the vertical water column.

The explicit scheme with splitting into physical processes is used for numerical solution of equations (5.2.9)-(5.2.11). It is known that one of the main problem connected with using of ICs is the abrupt changes of the layer's thickness. This problem is overcome by applying for solving the advective part of equation (5.2.9) the flux correction transport algorithm, developed by Zalesac (1978). For numerical solution of equations (5.2.10), (5.2.11) the upstream scheme is used with the mass fluxes obtained in solving equation (5.2.9).

The other problem arising in ICs model is the keeping of prescribed density of isopycnal layers. Indeed, if nonlinear equation of state is used, the diapycnal and isopycnal mixing inevitable lead to perturbation of density along the isopycnal layers (see also discussion of this problem in Oberhuber, 1993a and Bleck et al.,1992). Two measures are undertaken to keep reper density and at the same time do not change significantly diapycnal mixing velocity, determined by (5.2.18). First of all, the numerical approximation of the terms w_i and δQ_{ni} are chosen in such form to produce the minimum distortion of the isopycnal layers density. For this end we use the constrain, that in the case of linearized equation of state this approximation should gives **exact** conservation of potential density. For elimination of small deviation of the layer density from reper value, which appear from nonlinearity of the equation of state, additional reallignment of layers structure is applied. The characteristics of every isopycnal layer are recalculated by

$$dh_i = \frac{h_i}{\rho_0} \frac{\rho(T_i, S_i) - \rho_i^*}{\alpha(T_i - T_{i+1}) + \beta(S_i - S_{i+1})}, \quad (5.3.5)$$

$$d(h_i T_i) = dh_i T_{i+1},$$

$$d(h_i S_i) = dh_i S_{i+1}.$$

where dh_i is the changes of layer thickness, and ρ_i^* the reper density of i -th layer. At the end of

every time step the stability of the water column is checked. If density instability arises between two neighboring layers, the procedure of convective adjustment is applied.

The numerical parameters of the model are listed in the Table 5.1.

Table 5.1

Parameters of the Multilayer Isopycnal Ocean Model.

Lateral (isopycnal) viscosity $A_m = 5 \times 10^4 \text{ m}^2/\text{s}$
Vertical (diapycnal) viscosity $k_m = 10^{-3} \text{ m}^2/\text{s}$
Lateral (isopycnal) diffusion $A_i = 2 \times 10^3 \text{ m}^2/\text{s}$
Vertical (diapycnal) diffusion $\mu = 0.8 \times 10^{-4} \text{ m}^2/\text{s}$
Integral models parameters $C_g^0 = 10, C_e = 30, C_k^0 = 0.3$
Ocean depth $H_b = 4000 \text{ m}$
Relaxation parameter $t_{\text{rel}} = 1 \text{ year}$
Space resolution $4.5^\circ(\text{latitude}), 6^\circ(\text{longitde})$
Reper isopycnal layers density $\sigma_i = \rho_i - 1000 = (25.6, 26.2, 26.7, 27.1, 27.5) \quad i=3,7$
Time step $\Delta t = 3 \text{ days}$

5.4 Model results

5.4.1. Description of the numerical experiments

The model was evaluated using the simulations of the world ocean circulation under prescribed meteorological conditions with seasonal course. The used horizontal grid was the same as that envisaged to be used in the coupled climate model ($6^\circ \times 4.5^\circ$). Only two separate land domains were considered: all continents except the Antarctic were linked. The mass transport through Drake Passage was prescribed as 120 Sv. Some parts of the world ocean (such as the Mediterranean Sea, Hudson Bay, and some other seas) were not included in the present version of the ocean model. Surface boundary conditions for temperature and salinity was determined using Newtonian relaxation toward observed seasonal course of sea surface temperature and mean annual observed surface salinity (Levitus, 1982).

$$Q_0^T = k(T_{obs} - T_1), \quad Q_0^S = k(S_{obs} - S_1), \quad (5.4.1)$$

where k is the relaxation parameter. To eliminate the time lag, caused by using of this type of boundary conditions and to obtain correct amplitude of the seasonal variability of surface temperature, observed fields of surface temperature and salinity were slightly modified. Seasonal course of surface wind stress was determined by Hellerman (1982) and averaged module of surface wind from Esbensen and Kushnir (1980). The seasonal course of sea ice distribution was prescribed on the basis of empirical data. The heat flux through sea ice was neglected. The model was run from zonally uniform initial conditions for 1000 years. By the end of integration the ocean achieved the state close to quasi-stationar with global heat uptake less than 0.05 W/m.

5.4.2 Oceanic circulation

There is still a lack of knowledge about 3-dimensional field of the oceanic currents, that complicates the validation of oceanic GCMs. But at least two characteristics can be compared with observations, namely, surface currents field and interhemispheric and interoceanic mass exchange. The last one is not the result of direct measurements, but is estimated on the basis of tracers distribution patterns. The field of the surface and undersurface oceanic currents are shown in Figure 5.2. The model reasonable reproduces all main gyres of surface circulation, but the absolute values current velocity of western boundary currents such as Gulfstream and Kuroshio are underestimated, that is typical for all GCMs with rough space resolution. It is interesting that the model enable even reproduces the equatorial undercurrents (compare Figures 5.2a and 5.2b) and some other features of tropical currents. Some shortcomings are also obvious. In particular, the North Atlantic currents does not penetrate into Arctic basin and Greenland current is very weak. Because of coarse resolution, all coastal upwellings are very weak, while the intensity of equatorial upwelling is overestimated.

It is recognized now, that interoceanic mass exchange (the so-called conveyor belt) is very important feature of present climate. The model investigations of the global scale ocean circulation (e.g. Bryan, 1986; Manabe Stouffer, 1988) show that few different stable (or metastable) patterns of conveyor belt

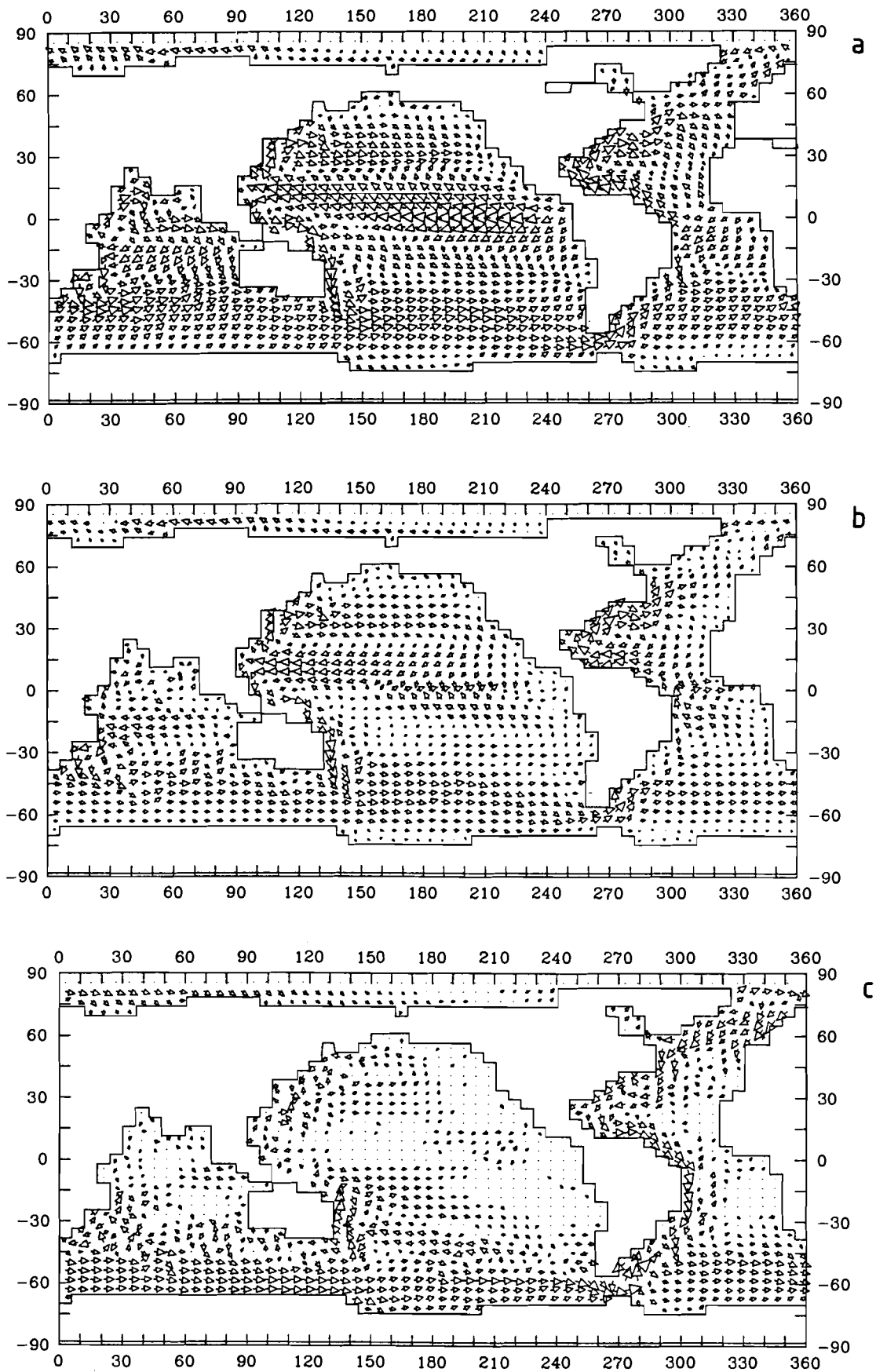


Figure 5.2 Mean annual ocean circulation in the upper mixed layer (a), at the depth 150 m (b), and in the bottom layer (c). Length of velocity vectors is proportional to the square root of the velocity. The vector scale is different for different maps.

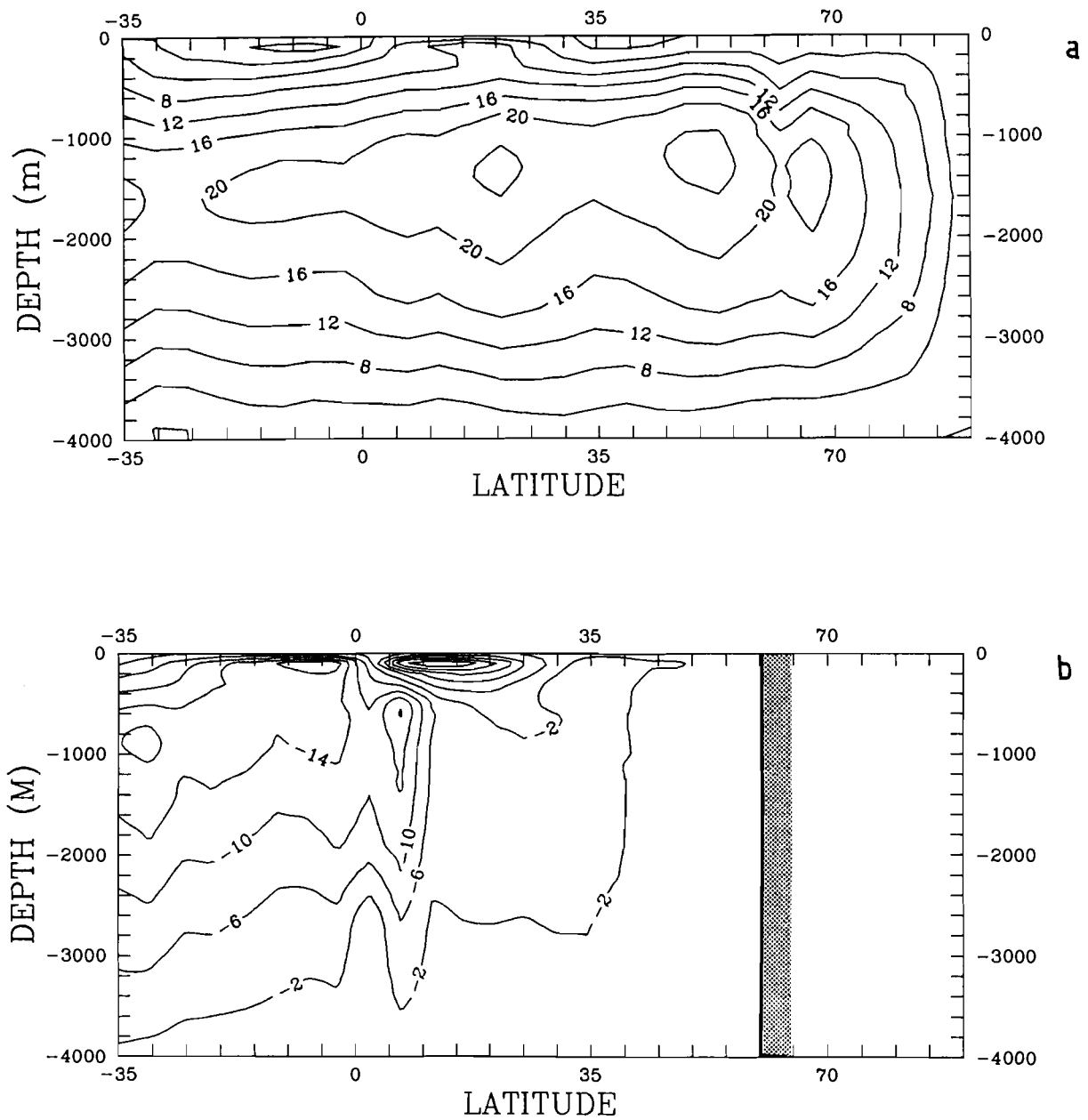


Figure 5.3 The vertical structure of the overturning stream function in the Atlantic ocean (a), and Pacific ocean (b).

can exist even under similar external forcing and, that changes of this forcing can dramatically change the oceanic circulation and, as result, global climate. In this context it is important that our model not only qualitatively (direction) but also quantitative (values of mass fluxes) reproduces zonally averaged circulation (Fig.5.3). The intensity of deep water formation in Northern Atlantic is about 22 Sv ($1\text{Sv}=10^6\text{ m}^3/\text{s}$) that agrees with empirical estimations on the basis of tracers propagation, and with the results of other GCMs simulations. The mass flux on the southern boundary of the Atlantic is about 15 Sv, and approximately the same but with opposite sign on the southern boundary of Pacific. Figure 5.2c, where the currents field in the bottom layer (the depth about 3 km) is shown, presents the bottom part of conveyor belt. The water masses forming in the Northern Atlantic then distribute along western boundary of the ocean to 40 S latitude and then turn eastward and penetrate into Indian and Pacific ocean, first along western boundaries northward, and then propagate eastward with zonal flows. This scheme is in a good agreement with the present concept of interoceanic mass exchange.

5.4.3 Thermohaline structure of the ocean

Because of Newtonian type of boundary condition using in the model for temperature and salinity, these two characteristics at the surface are close to observed. The mean annual temperature distribution at the 500 m depth (approximately the middle of thermocline) is shown in Figure 5.4. Comparison of this field with empirical data of Levitus (1982) shows that the model slightly overestimates the temperature at this horizon, especially in equatorial zone. The vertical section of zonally averaged temperature for individual basins are shown in Figure 5.5. One can see that the model overestimates the temperature in deep layer by 1-2°C and even more in high latitudes. The reason for Arctic basin is clear enough: the absence of real bottom relief in Northern Atlantic leads to more intensive than in reality mass exchange between polar and subpolar part of Atlantic. Comparison of the model temperature field in the southern part of the ocean leads to conclusion, that the model underestimate the intensity of deep water formation near Antarctic, and, as the result, the tongue of cold Antarctic bottom water masses is not pronounced enough.

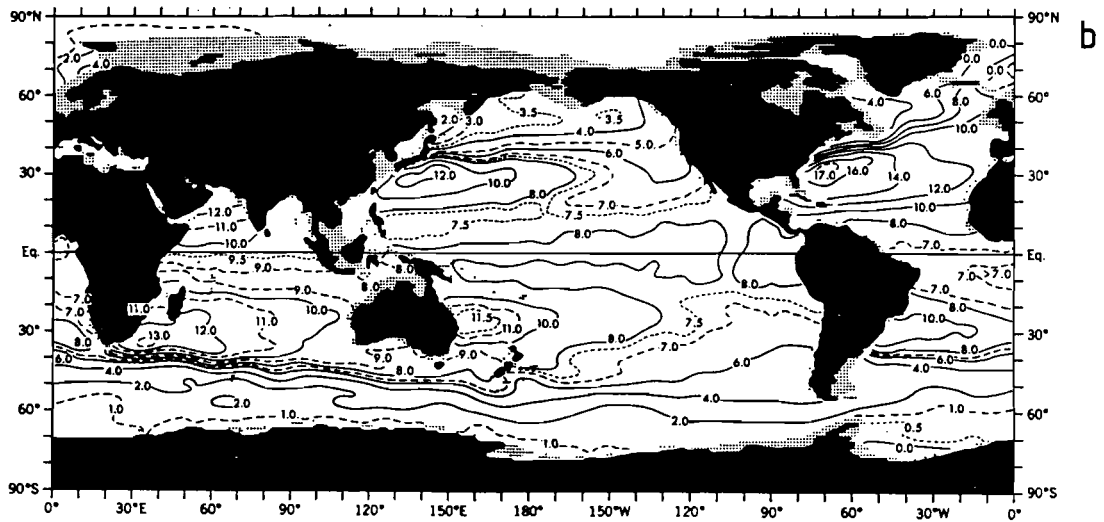
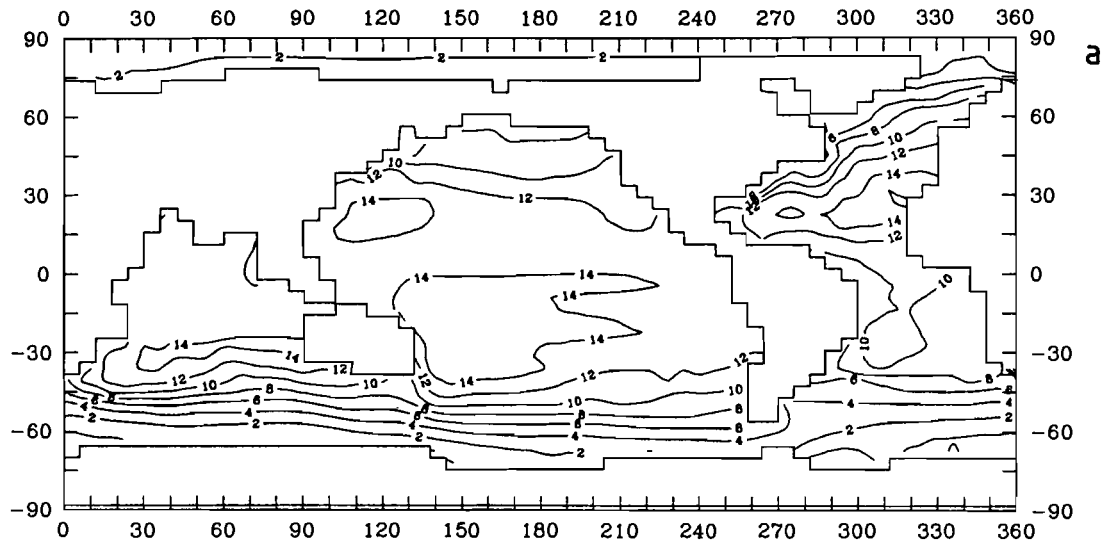


Figure 5.4 Annual mean potential temperature at 500 meters. (a) model, (b) Levitus (1982).

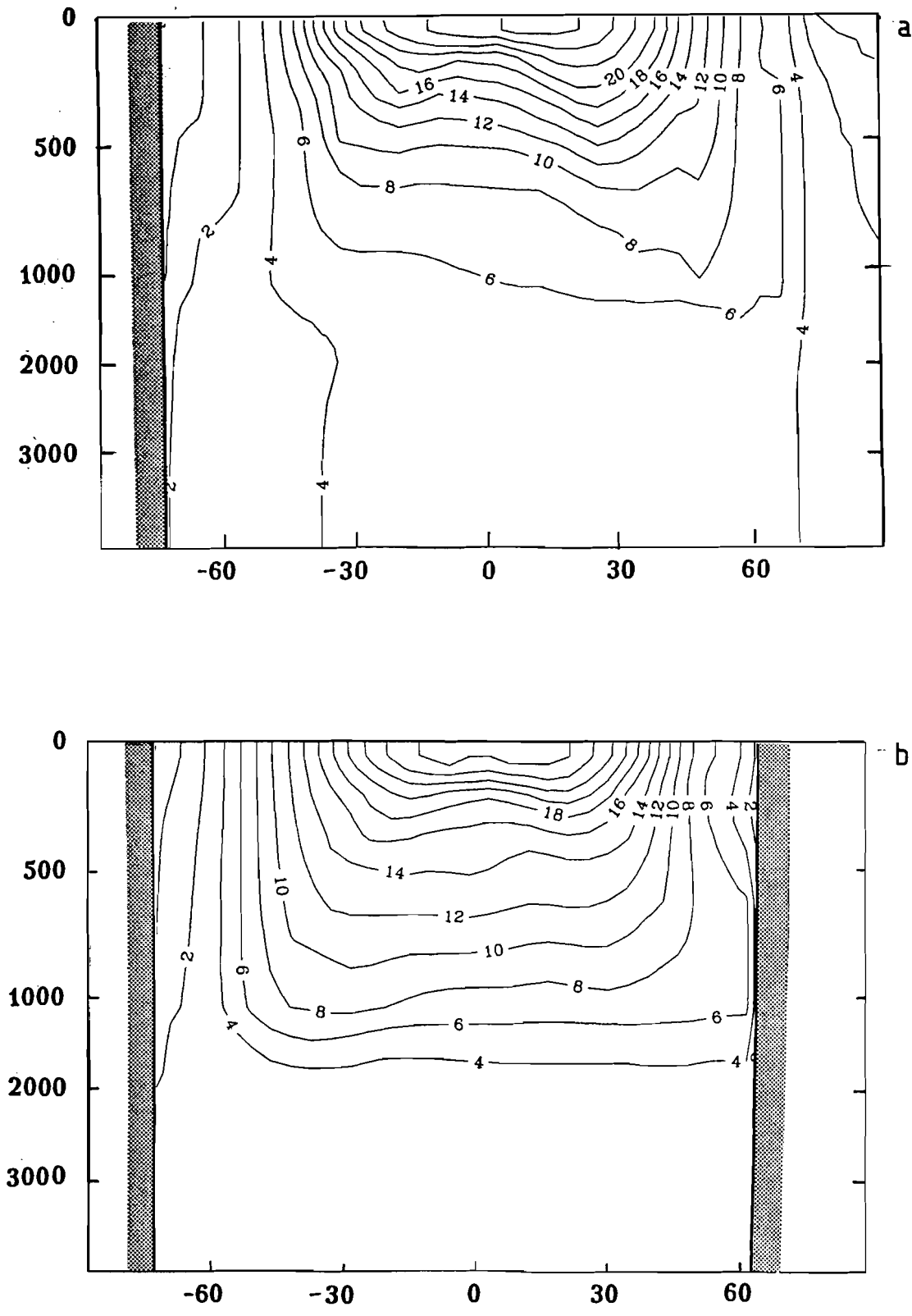


Figure 5.5 The vertical structure of the zonally averaged temperature in the Atlantic ocean (a), and Pacific ocean (b).

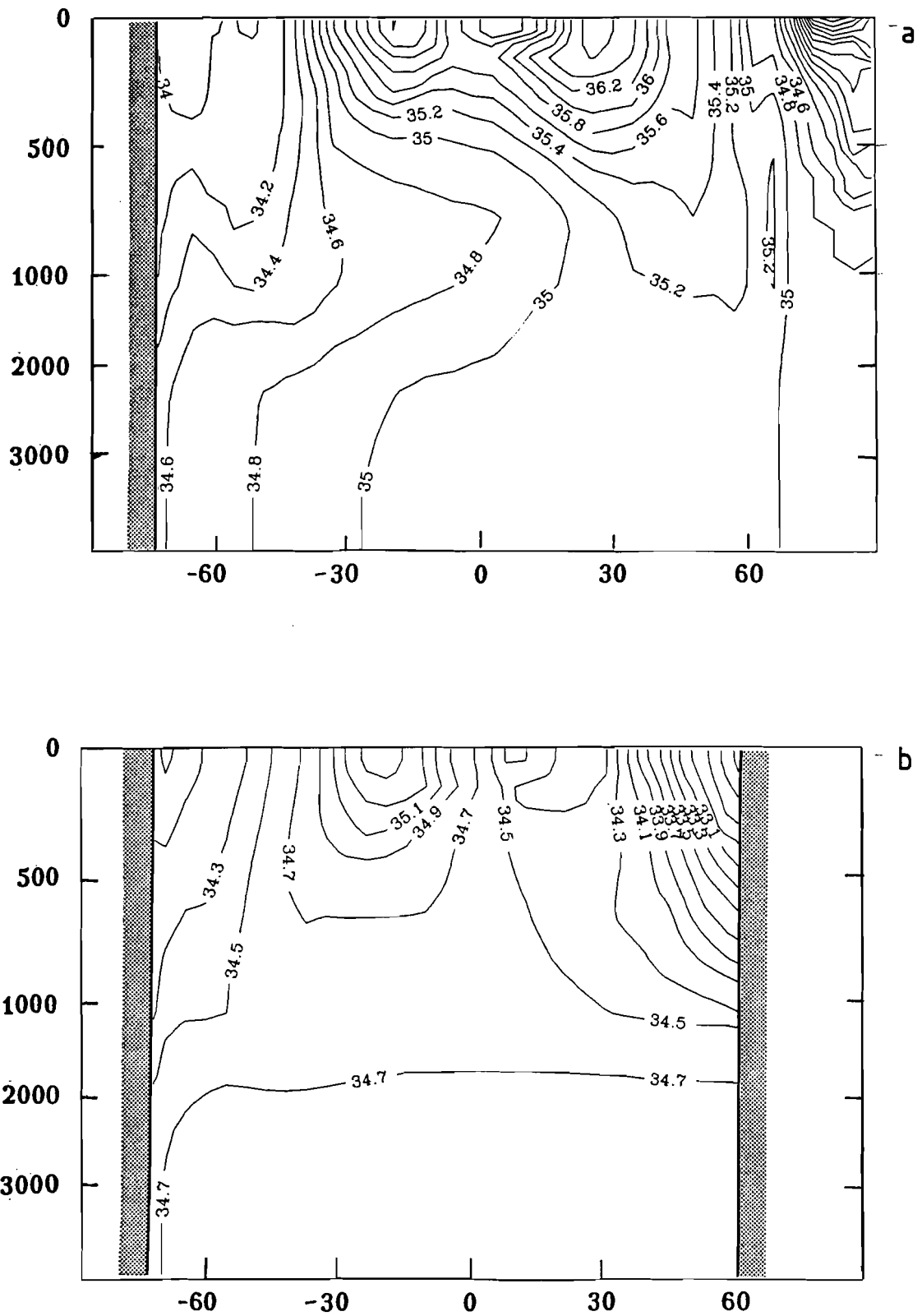


Figure 5.6 The vertical structure of the zonally averaged salinity in the Atlantic ocean (a), and Pacific ocean (b).

Vertical sections of zonally averaged salinity for Atlantic and Pacific are presented in Figure 5.6. The model correctly reproduces the main features of salinity field. It should be emphasized the presence of tongue of intermediate relatively fresh water masses in southern hemisphere at the depth 0.5 - 1 km. This tongue is especially pronounced in Atlantic basin because it overcovers much more salt North Atlantic water masses.

5.4.4 Heat and salt balances

Ocean as a part of climate system plays extremely important role in meridional redistribution of heat. That is why the meridional heat transport in the ocean is one of the major characteristics of the model simulations. The problem of model validation is complicated by the fact that empirical estimations of meridional heat transport in the ocean, obtained by different methods, gives significantly different results. Figure 5.7 shows the results of the model in comparison with empirical estimation of Talley (1984). The maximum heat transport in the northern hemisphere is about 1.5 PW ($1\text{PW} = 10^{15}\text{W}$) and -2.5 PW in Southern. The Atlantic ocean is characterized by positive heat transport for all latitudes with maximum in the northern hemisphere close to 1PW and northward flux through equator is 0.4 Pw.

Space distribution of surface annual net heat fluxes is shown in Figure 5.8. The main regions of oceanic heat release is the Gulfstream and Kuroshio and northern part of Northern Atlantic. The maximum values of heat fluxes here are 100-200 W/m^2 . In the southern hemisphere the distribution of heat fluxes more zonal.

Figure 5.9 shows the zonally averaged model freshwater flux to the ocean in comparison with empirical estimation of Baumgartner and Reichel (1976). One can see that agreement between model results and empirical data in tropics and in the middle latitudes is quite good. In high latitudes of southern hemisphere model freshwater flux is as twice greater than observed. The local minimum of freshwater flux in subpolar region of the northern hemisphere coincides with the region of deep water formation, where much stronger than observed negative freshwater flux (positive salt flux) is necessary to support high surface salinity.

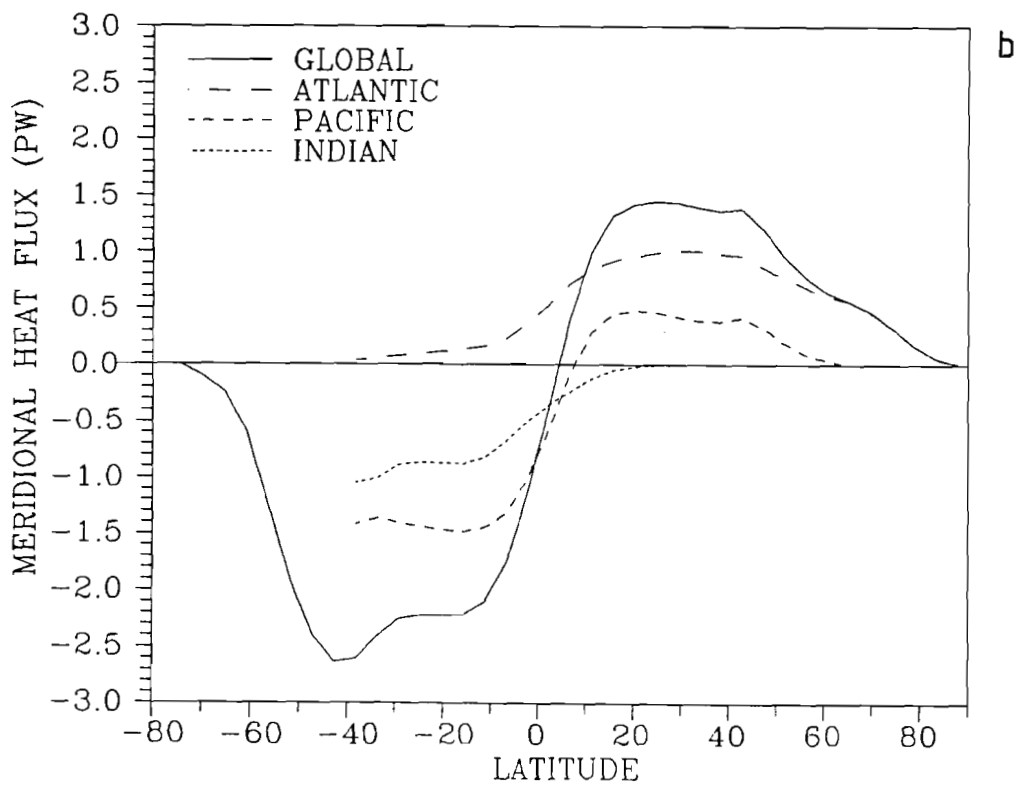
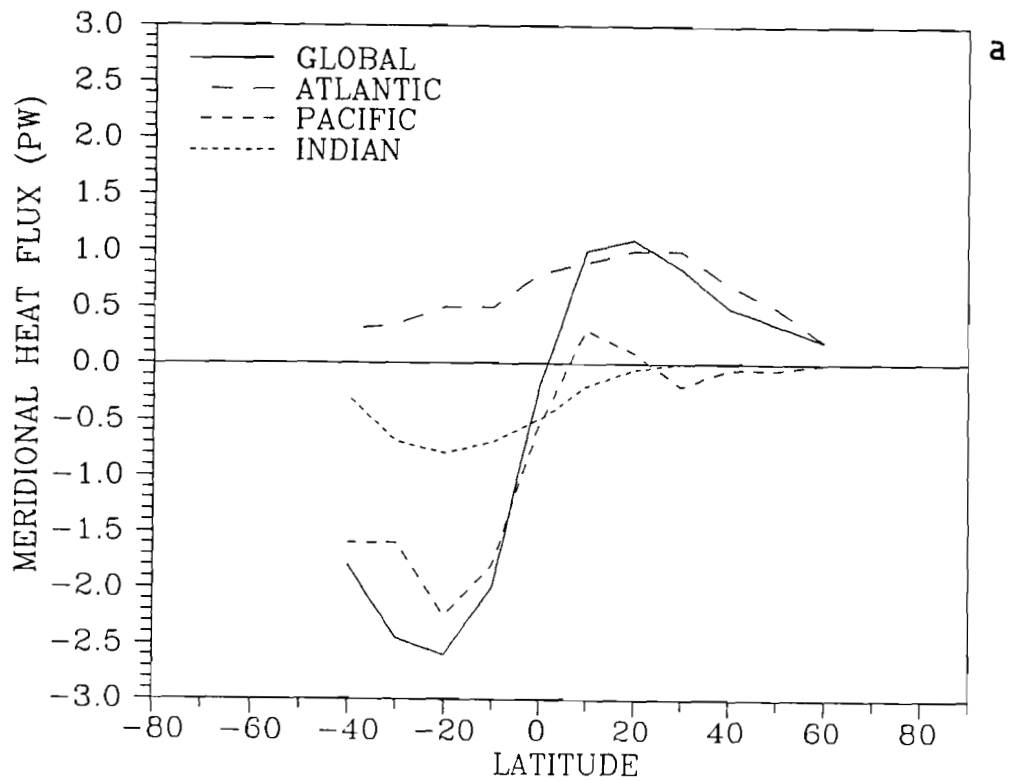


Figure 5.7 Annual mean meridional heat transport in the oceans from the observation (Talley, 1984) (a), and model results (b).

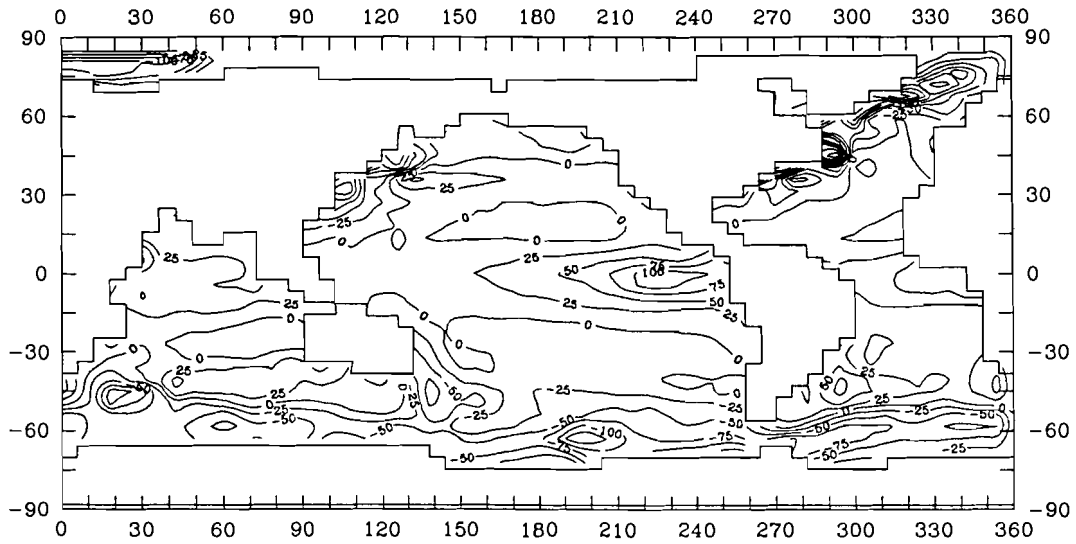


Figure 5.8 Annual mean ocean surface heat flux (W/m^2), positive downward.

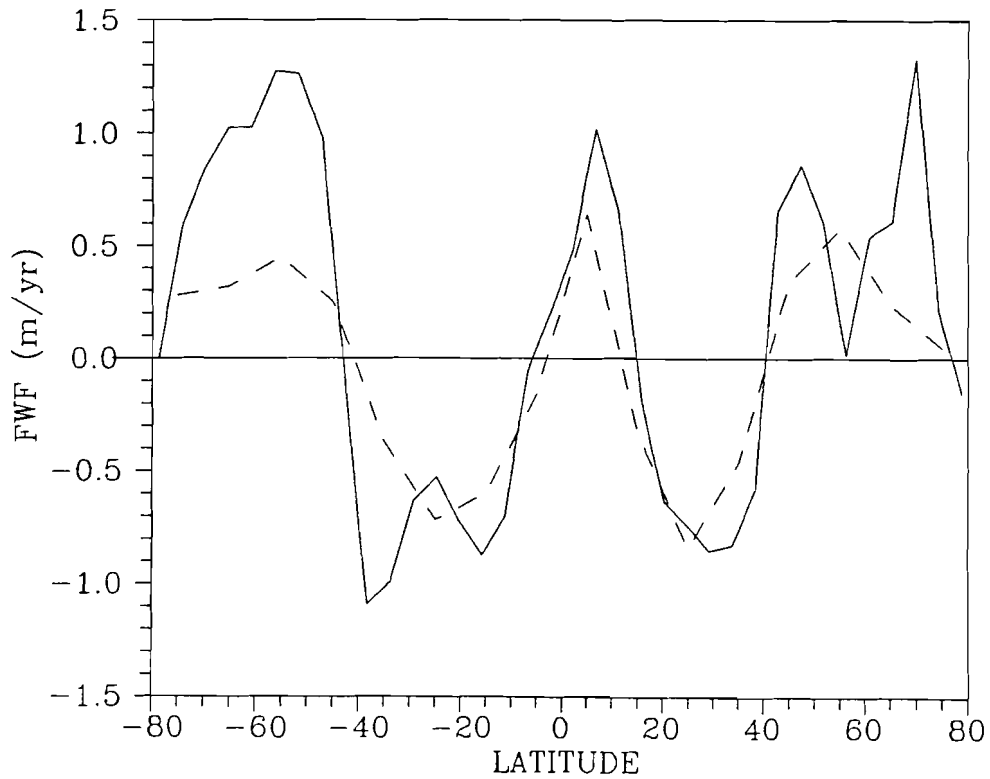


Figure 5.9 Annual mean zonally averaged surface fresh water flux in the model (solid line) and Baumgartner and Reitel (1976) (dashed line).

5.4.5 Tracers distribution

One of the important elements of the model validation is the simulation of different tracers distribution. The radioactive isotope C^{14} is one of commonly used tracers. This isotope has half-life 5730 years. Because it is produced only in atmosphere, its relative (to C^{12}) concentration in the ocean shows the resident time of given water masses, that in turn allows to estimate the intensity of water masses exchange. In contrast, the bomb-produced radiocarbon appeared recently (starting from 1955) and its excess in the upper oceanic layers shows the intensity of short-periodic anomalies penetration into the ocean.

The experiment with radiocarbon was carried out on the basis of the oceanic inorganic carbon cycle model directly embedded into MILE. This model is similar to that described in Maier-Raimer and Hasselmann (1987). After reaching of climate equilibrium, the carbon cycle model was switched on and additional run for 1500 years was made. The initial condition for C^{12} and C^{14} were uniform. The surface fluxes of carbon (S) and radiocarbon (S^{14}) were calculated in the form

$$S = \lambda [(pCO_2)_o - (pCO_2)_a],$$

$$S^{14} = \lambda \left[\left[\frac{C^{14}}{C^{12}} \right]_o (pCO_2)_o - \left[\frac{C^{14}}{C^{12}} \right]_a (pCO_2)_a \right], \quad (5.4.1)$$

where pCO_2 is the partial pressure of carbon dioxide in the ocean ("o") and in the atmosphere ("a"), $\lambda = 0.05 \text{ mol m}^{-2} \text{ a}^{-1} \text{ ppm}^{-1}$ is the bulk coefficient.

After reaching of equilibrium state for carbon distribution, the concentration of atmospheric C^{12} and C^{14} was changed in accordance with empirical observation starting from 1800 (beginning of industrial era). The results of radiocarbon simulations for meridional sections of Atlantic and Pacific ocean corresponding year 1975 in comparison with GEOSECS observations are shown in Fig.5.10 and 5.11. One can see that the model correctly describes the main features of natural radiocarbon distribution (deep ocean) and bomb-produced radiocarbon (upper ocean) as well. For example, the minimum value of radiocarbon in the deep Northern Pacific (the oldest water masses) is about -220 ppm, while

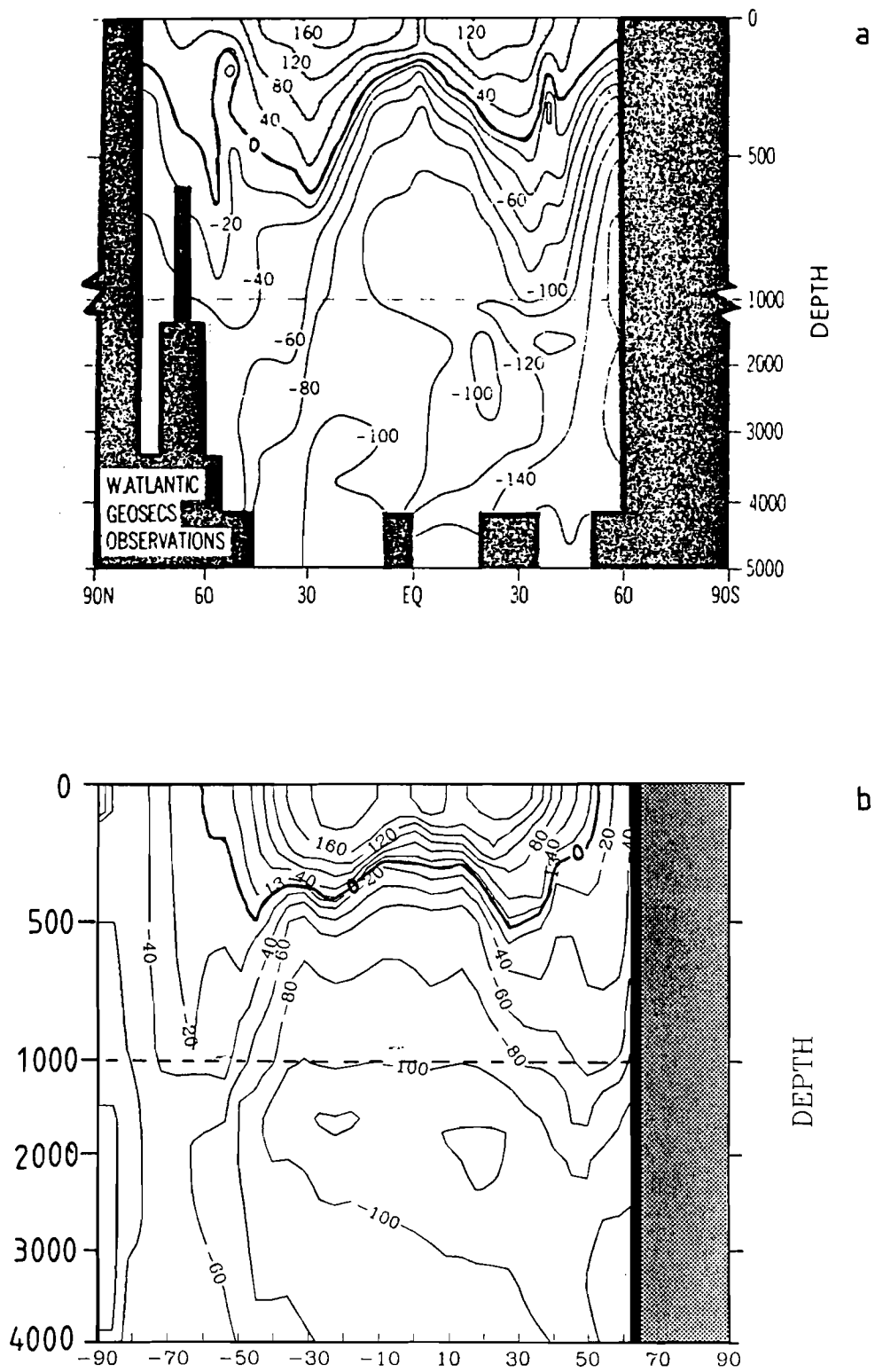


Figure 5.10 Latitude versus depth section of $\Delta^{14}\text{C}$ (per mil) along the western Atlantic GEOSECS track (1974): (top) GEOSECS observations and (bottom) model.

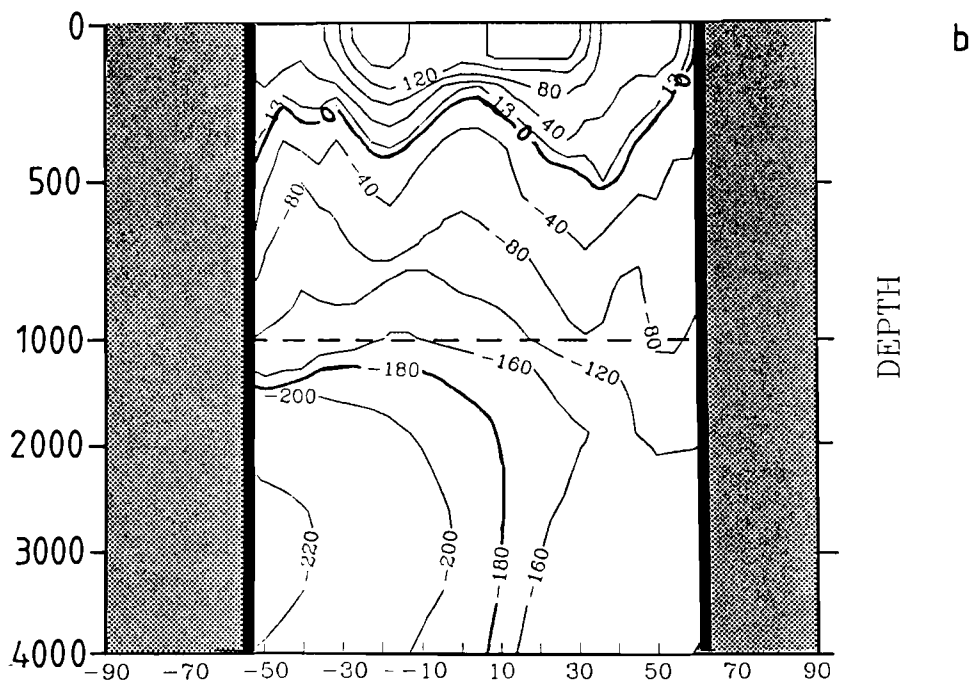
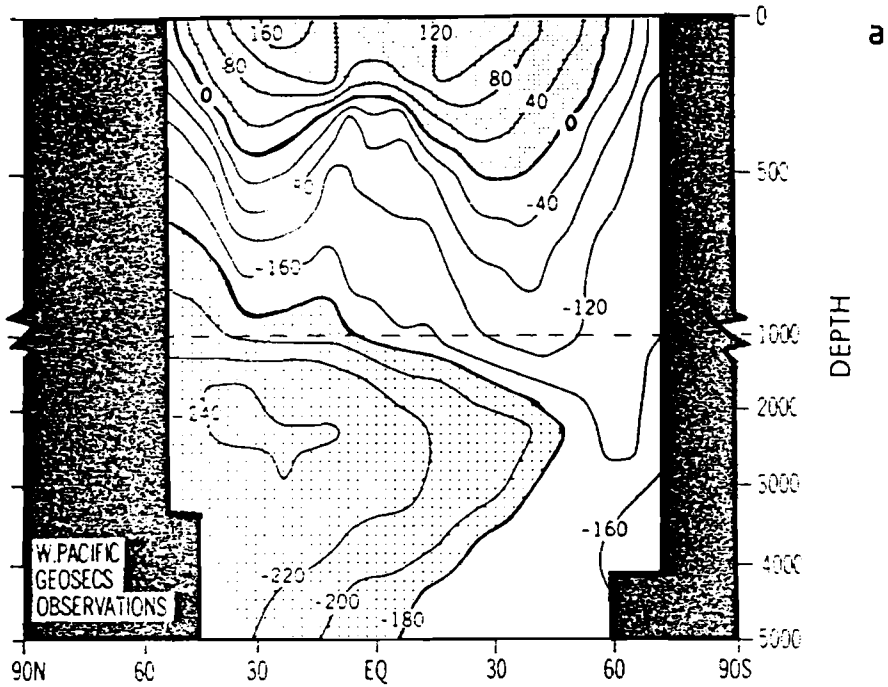


Figure 5.11 Latitude versus depth section of $\Delta^{14}\text{C}$ (per mil) along the western Pacific GEOSECS track (1974): (top) GEOSECS observations and (bottom) model.

observation shows value -240 ppm. Configuration and the depth of zero relative concentration isoline in both oceans reasonable agree with observations. The carbon uptake during last decade (1980-1989) simulated with the model is 2.5 GtC, that falls in the IPCC 1990 estimation range.

Thus tracers experiments give additional support the idea that MILE model describes the main features of oceanic climate characteristics reasonable well and can be used as an oceanic module of a coupled climate model.

**6. Integrated Assessment of Climate Change Impacts on European Forests (ICCF):
A Projected Application to Integrated Modelling of Climate Change Impact**

A study with the above title was the outcome of a 1992 Working Meeting at IIASA. As outlined in Chapter 5 of WP1 the overall objective of the study is to carry out an integrated assessment of the impacts of climate change on the European forests for a variety of greenhouse gas emission scenarios. The study requires a number of models from different disciplines and these models must be modified and linked in an integrated fashion. At the Working Meeting the 2.5 DSCM was considered for describing the climate system. It was decided that the DSCM will be used after various medium-term improvements are introduced (see also Phase 3 of the work schedule presented in section 5.2 of WP1). The improvements will be part of the global version of the DSCM, which reveals a spatial resolution $6^\circ \times 4.5^\circ$ in the atmospheric and land/ocean modules, (for details see Appendix). These improvements are as follows:

- Introduction of the complete BATS scheme. The increased space resolution of the improved DSCM would allow to account for all vegetation and soil types foreseen by the BATS scheme to be taken into account. However, alternative vegetation/land cover/soil schemes (e.g., Sellers *et al.*, 1986; Kowalczyk *et al.*, 1991; Ducoudré *et al.*, 1993) will be discussed as well.
- Introduction of a vegetation succession model. It remains to be decided how vegetation patterns other than European forest ecosystems will be considered in the study. Appropriate vegetation models have been published, for example, by Bogatyrev (1990, 1991), Kellomäki *et al.*, (1992), Venevsky (1992).
- Introduction of the magnitudes of the diurnal cycles with respect to the main atmospheric and land surface climate variables. Among the ecophysiological and forest production models mentioned in Table 5.2 of WP1, BIOMASS is the model with the highest temporal (daily) resolution. It needs to be elucidated whether the above parameterization of the diurnal cycle (following e.g. Saltzmann and Ashe, 1976) will be advantageous to the ecophysiological modelling work of the study.

- Improvement of the DSCM with realistic geography and distribution of surface types will allow for the production of climate-related output information on surface air temperature and specific humidity, precipitation, evaporation, solar fluxes, soil moisture, and temperature, as well as the synoptic and (parameterized) daily variability of these quantities. This output information may serve as input to the ecophysiological and forest production models (BIOMASS, G'DAY, Q, SIMA, TAM; see Table 5.2 of WP1) employed by the ICCF Study. We will make use of a similar superimposing technique as mentioned in Section 5.2 of WP1 for overlaying climate model results over more regional/local observations. The output of the ecophysiological and forest production models, in turn, can then be used to assess the biosphere-climate feedback in the DSCM.

As also stated in Section 5.2 of WP1, at least partly, an important question is: how to account for regions other than Europe and for vegetation other than forests? As an additional alternative to these in the above-mentioned Section, we see the possibility of using a Holdridge type (see, e.g., Leemans, 1990) or time-lag succession vegetation schemes (see, e.g. Bogatyrev, 1990, 1991; Kellomäki *et al.*, 1992) combined with the large-scale soil geochemistry schemes (see, e.g., Krapivin *et al.*, 1982; Tarko *et al.*, 1989). This would allow us to incorporate the parameterization of succession processes with different characteristic time scales depending on ecosystems in the DSCM.

We see several important advantages in linking the DSCM with the hierarchy of the above-mentioned ecophysiological and forest production models. Firstly, the detailed ecophysiological models can be used for validating and improving the understanding of global-scale vegetation and geochemical cycles. Secondly, being interactively linked with the DSCM, these models can help to refine the climate/biosphere response, at least for Europe as a whole.

In the process of developing the DSCM we are planning to pay special attention to investigating the model's sensitivity to uncertainties of vegetation and other parameters and to the uncertainties of climate output information on vegetation processes. The fact that the DSCM is much more computer efficient than GCMs, permits us to produce a great number of sensitivity experiments.

Thus, not only probable, but also sustainable scenarios in respect to the evolution of European forests or, vice versa, the collapse of forest ecosystems can be investigated. Moreover, specific climate-ecosystem behaviors such as bifurcations, instabilities, and large-scale/long-term structural reformations can also be elucidated.

7. Conclusions

The objective of Part II of the Working Paper is twofold: first, to summarize the present status and improved version of the 2.5-DSCM; and, second, to describe the envisaged position of this climate model in the context of an integrated model of climate change. The latter model aims at a holistic approach that helps policy analysts to rapidly assess time-dependent changes in regional ecology, with feedback, resulting from various greenhouse gas emission policies.

Special attention must be paid to the climate module of an integrated model of climate change because it can easily play a dominant role within the integrated model in terms of running time. Attempts were made to facilitate the understanding of the needs of both environmental impact modellers or assessors, on the one hand, and policy analysts, on the other hand. In fact, even among themselves their requirements for an integrated model of climate change can be antagonistic to each other. For example, ecological impact models might require a spatial resolution, which is beyond that of GCMs, and, at the same time, uncertainty in climate model output that can only be satisfied by GCMs or less sophisticated climate models on a coarser resolution scale, while policy experts are essentially asking for the possibility in assessing the impact of a wide variety of emission strategies, i.e., for a quick turnaround time of the integrated model.

For many applications this problem can be solved by creating a set of climate models of graded complexity that are computer-efficient and suitable for a wide variety of policy and impact analyses. As outlined in WP1 two independent approaches, the top-down approach and the bottom-up approach, were identified in regard to the design of the climate module. In our opinion both approaches complement each other; it would be worthwhile pursuing them in parallel. Carefully considering the pros and cons of both approaches, especially the fact that the top-down approach requires frequent access to a GCM, we come to the conclusion that IIASA ought to pursue the bottom-up approach, albeit a somewhat reduced flexibility. The bottom-up approach seems to offer a more restricted choice with respect to diversity of climatic information and its spatial and temporal resolution than the top-down approach. However, this might be compensated for by some advantages of the bottom-up approach, e.g., the somewhat easier implementation of new feedbacks, if appropriate parameterizations

exist or can be derived. The 2-D ZCM (described in WP1) and the 2.5-DSCM are meant for integrated modelling of climate change impacts which makes use of the bottom-up approach. Both climate models are at the upper level of complexity (in terms of spatial and temporal resolutions) out of a set of four climate models that are available or under development at IIASA.

A number of model experiments have been performed which document the present status of the 2.5-DSCM. It simulates today's zonal means of the basic climatic characteristics (temperature, precipitation, evaporation, meridional heat transport, and others) reasonably well and realistically reflects their geographical and seasonal distribution. For a doubling of atmospheric CO₂ the DSCM reveals a climate sensitivity of about 2.5 K and an increase of the hemispherically averaged precipitation rate of about 8%. The climate sensitivity lies within the range estimated by the IPCC (1.5 to 4.5 K) the ratio of precipitation increase to climate sensitivity agrees well with GCM results (Houghton, *et al.*, 1990).

The 100-year integration (1985'-2084) employing IPCC's 1990 (CO₂-equivalent) concentration Scenario A was made. Our results are in rather good agreement with the recently published results of the MPI GCM.

Finally following WP1, Part II of the Working Paper sheds light on applying the DSCM to an Integrated Assessment of Climate Change Impacts on European Forests (ICCF). The respective integrated model comprises a series of models – from policy-oriented accounting tool for greenhouse gas emissions and concentrations to climate model to sequence of dovetailing ecophysiological and forest production models to socioeconomic tools with feedback.

An important feature of the integrated assessment using the 2.5-DSCM is that the ecophysiology of a single plant up to that of aggregated forest ecosystems will be considered. An approach employing the DSCM, in combination with a suitable superimposing technique aiming at bridging the spatial resolution gap between the DSCM, on the one hand, and the ecophysiological and forest production models, on the other hand, is considered.

The main types of information which the DSCM is anticipated to pass on to the ecophysiological and forest production models are surface air temperature and specific humidity, precipitation, evaporation, solar fluxes, soil moisture, and temperature, as well as the synoptic variability and (in terms of parameterized amplitudes) daily cycle of these quantities. This information seems to compliment very well the large-scale information needs of the ecophysiological and forest production models of the ICCF study and thus help to achieve the overall objective of this study.

APPENDIX. The structure of the global-scale coupled climate model and preliminary results

The first step in application of the 2.5-DSCM for the purposes of integrated assessment is the extension of the model to the global scale, including of realistic geography and coupling with multilayer isopycnal ocean model MILE, described in Chapter 5. A global-scale version of the model has the space grid resolution of 4.5° latitude and 6° longitude (see Figure A.1). This space grid allows to resolve the main features of ocean/land distribution and major patterns of surface land types. This space resolution is the same order as used in the most of climatic GCMs. For implementation of MILE as an oceanic module of coupled climate model a few improvements are necessary. They are 1. incorporation of bottom topography and specific description of the shelf zones and internal water basin; 2. parameterization of the mass exchanges through passages which can not be resolved on the space grid but nevertheless are important for heat and salt balances of the oceans.

At the first stage of model development the atmospheric and oceanic models will be linked through the heat and momentum fluxes. The using of fresh-water fluxes computed by atmospheric model needs further improvements. The most of the present GCMs use for climate investigation so-called flux adjustment procedure to exclude climatic trends after coupling atmospheric and oceanic modules. Since justification of implementation of such procedure is not fairly satisfactory, our ultimate objective is to have a completely coupled system without any fluxes adjustment. The time step in the atmospheric module as well as in the oceanic one will be 3 days and both modules will interact synchronously. The estimated computer time requirements for the global version of the model are approximately 1 hour of SPARC-2 station per 3 years of the model integration that is still acceptable for the purposes of integrated assessment studies.

The results of simulation on the base of global scale oceanic GCM MILE are represented in Chapter 5. Here some of the preliminary results of present climate simulations with global scale version of 2.5-D DSCM will be present. The seasonal course of sea surface temperature and sea ice extension were prescribed on the basis of empirical data.

Zonally averaged distribution of surface air temperature for two seasons is shown in Figure A.2 in comparison with empirical data (Landsberg, 1985). One can see that model results are in a reasonable agreement with observations for both seasons and both hemispheres. Geographical distribution of surface air temperature is shown in Figures A.3 and A.4.

Zonally averaged precipitation distribution is shown in Figure A.5. The model correctly describes the location and absolute values of tropical maximum of precipitation and some other important features of precipitation patterns. The most significant discrepancy between model and observation takes place in February in high latitudes of southern hemisphere, where the model underestimates precipitation approximately by a factor of 2. Figure A.6 shows the zonally averaged cloudiness which is close to observed values in both seasons.

Thus, even preliminary results obtained with the global scale DSCM shows the model ability to reproduce important features of present climate reasonably well.

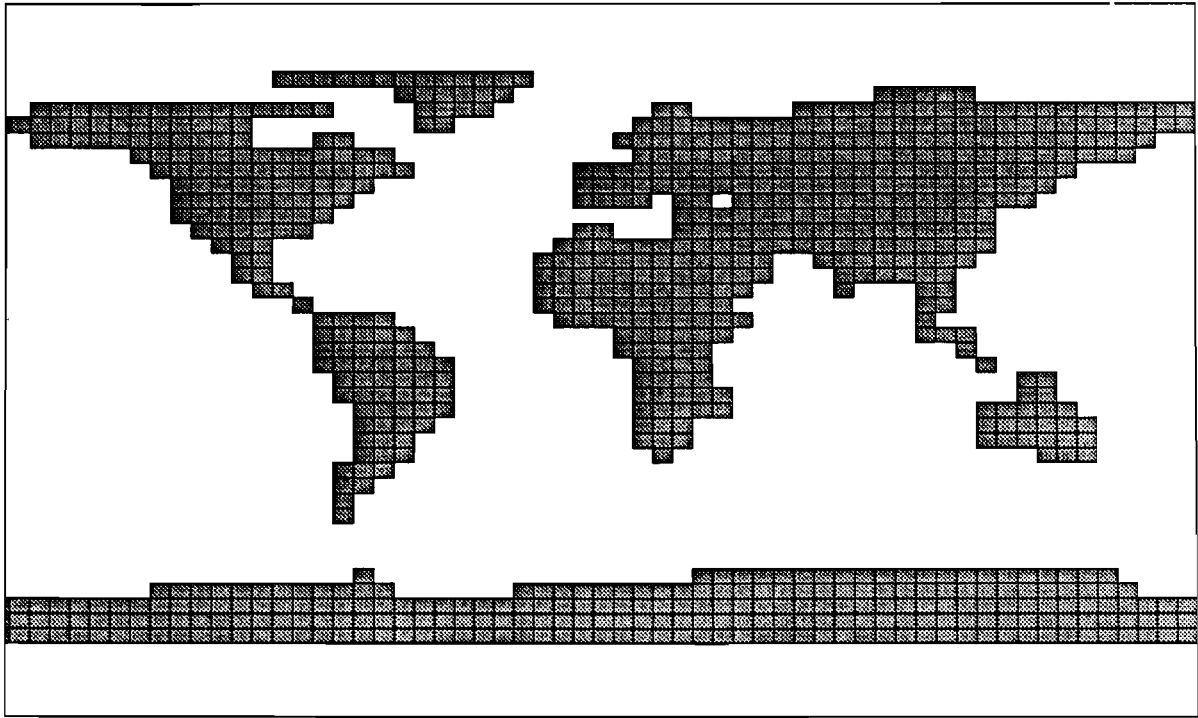


Figure A.1 Grid spacing and geographical land ocean distribution envisaged to be used in the global version of nonzonal climate model.

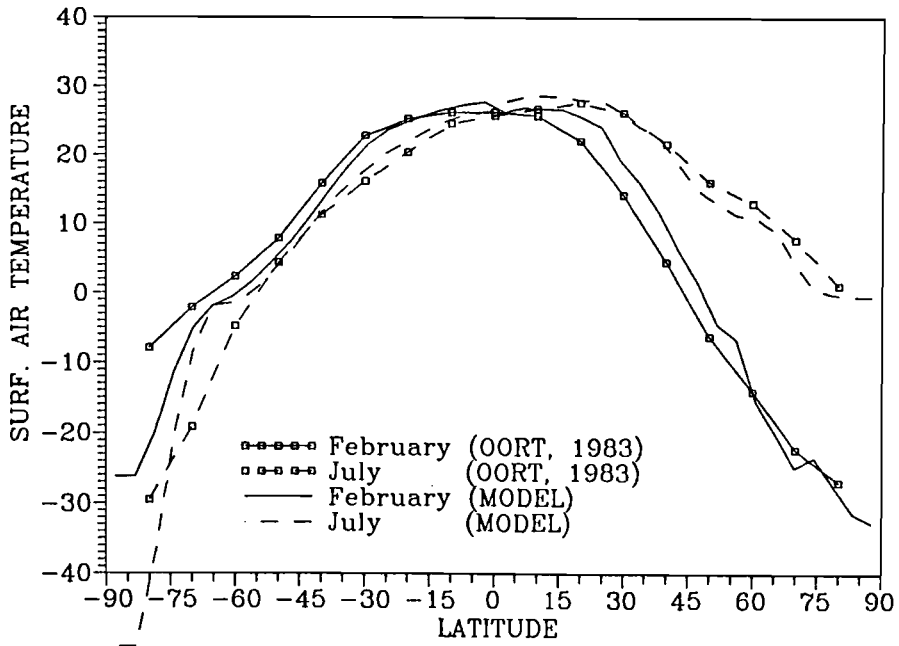
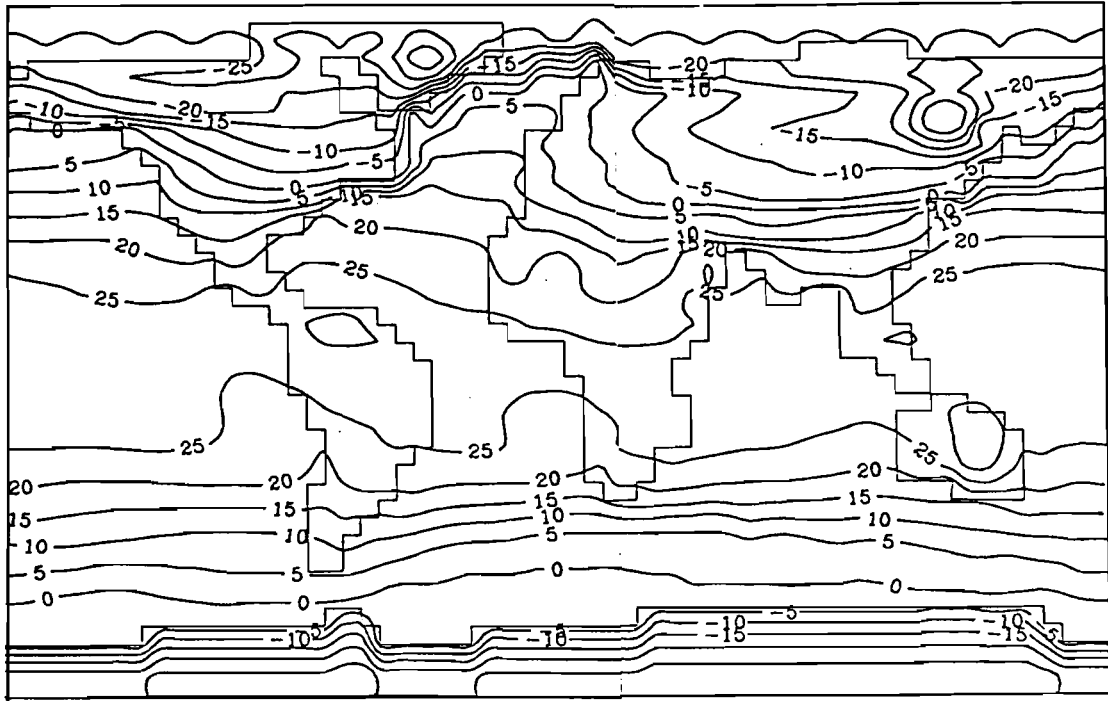
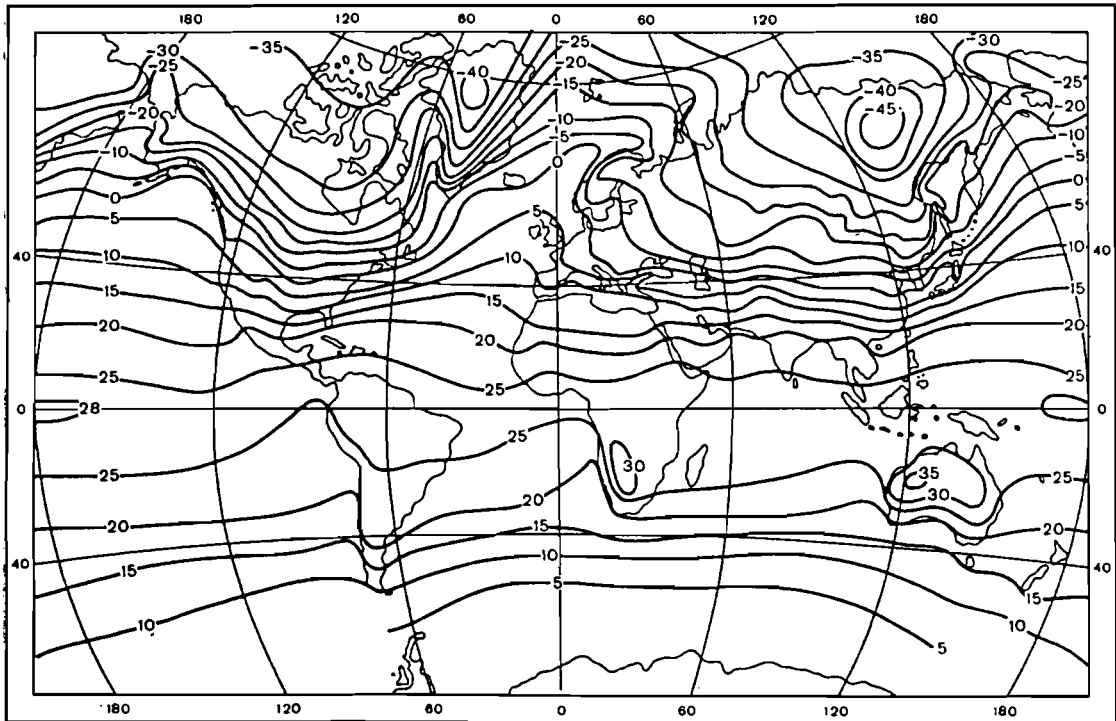


Figure A.2 Zonal mean surface air temperature of the atmosphere (°C) for February and July in the model and as derived from observations.

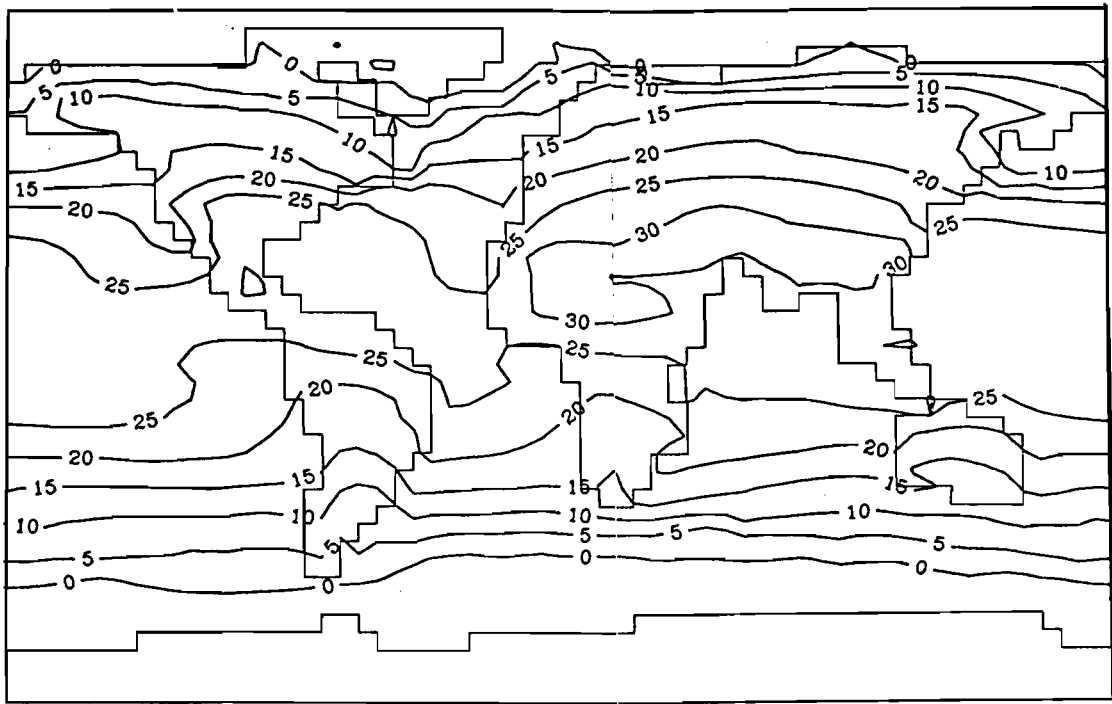


a

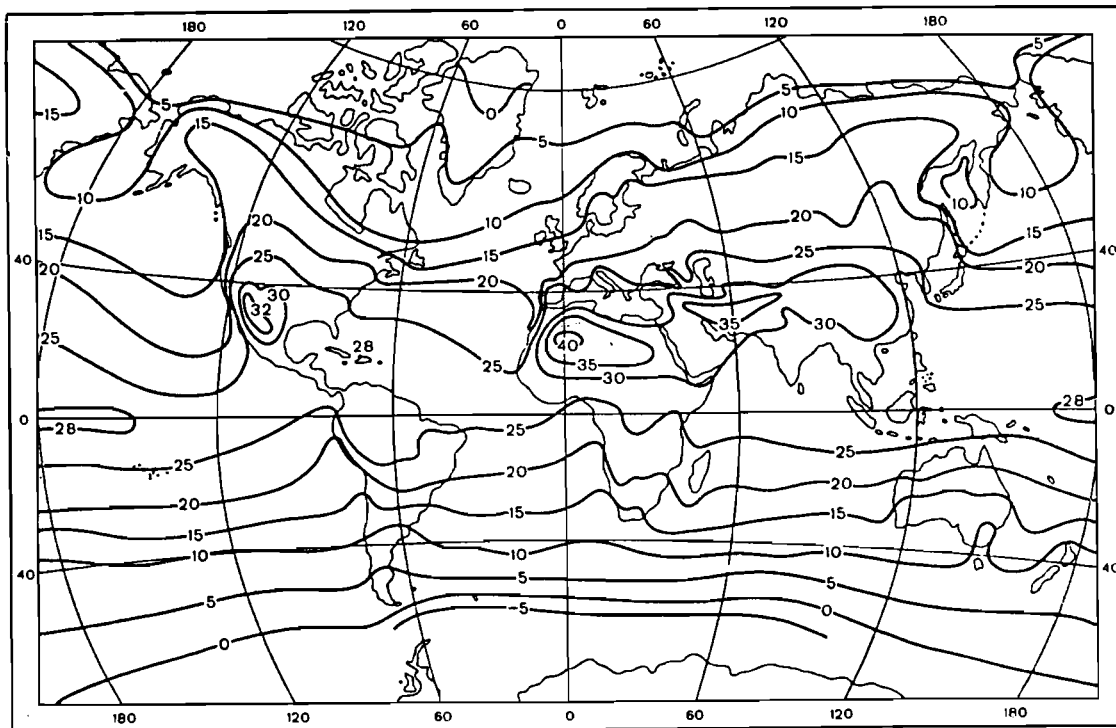


b

Figure A.3 Surface air temperature of the atmosphere ($^{\circ}\text{C}$) in the model (a) and empirical data (b) for February.



a



b

Figure A.4 Surface air temperature of the atmosphere ($^{\circ}\text{C}$) in the model (a) and empirical data (b) for July.

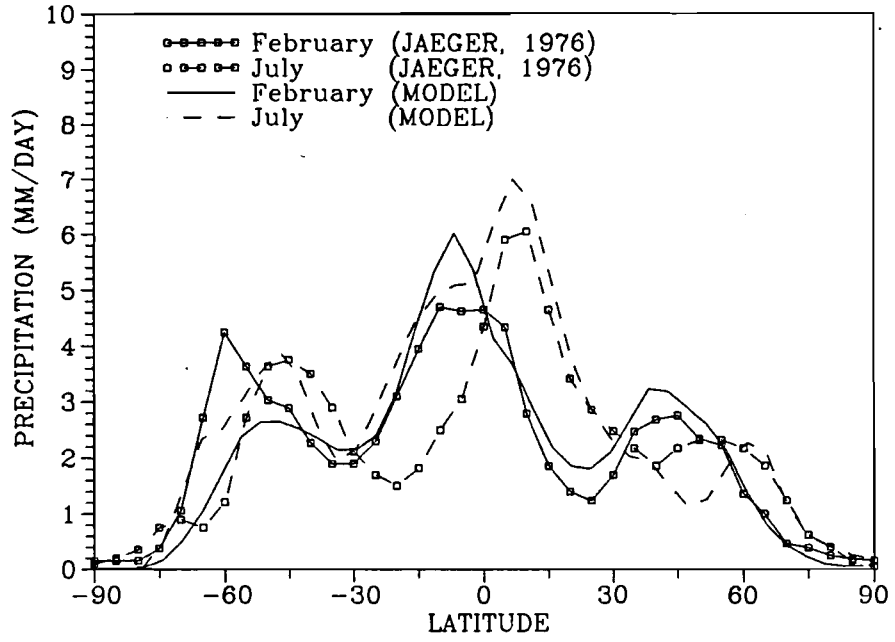


Figure A.5 Zonal mean precipitation (mm/day) for February and July in the model and corresponding empirical data.

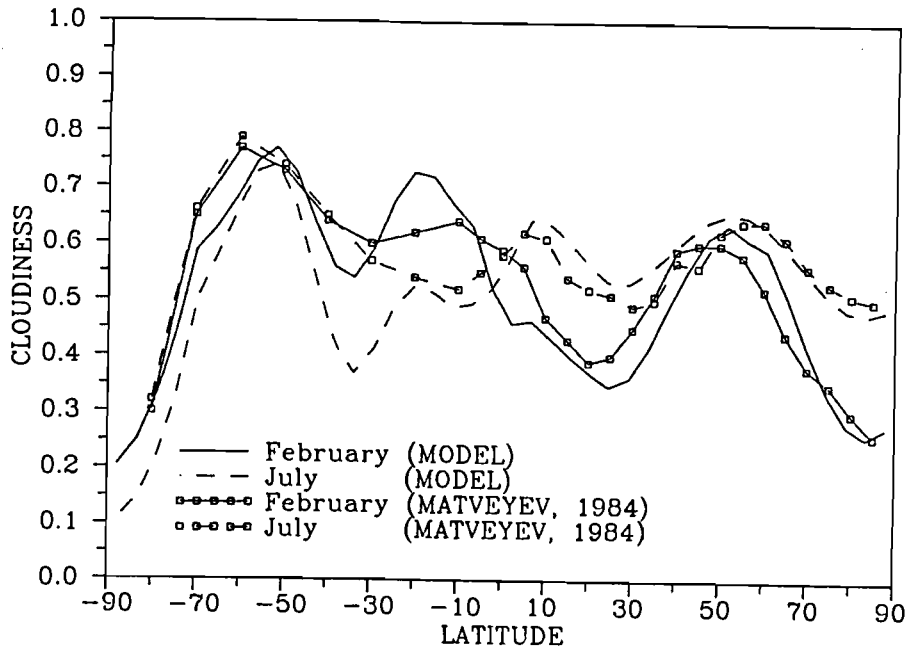


Figure A.6 Zonal mean total cloud amount for February and July in the model in comparison with empirical data.

REFERENCES

- Adem, J., 1964, On the physical basis for the numerical prediction of monthly and seasonal temperature in the troposphere-ocean-continent system, *Mon. Wea. Rev.*, **92**:91-104.
- Ardanuy, P.E., Stowe, L.L., Gruber, A., Weiss, M., and Long, C.S., 1989, Longwave cloud radiative forcing as determined from Numbus-7 observations, *Journal of Climate*, **2**:766-799.
- Baumgartner, A., and Reichel, E., 1975, *The World Water Balance*, Elsevier, 179 pp.
- Betts, A., 1986, A new convective adjustment scheme. Part 1: Observations and theoretical basis. Part 2: Single column tests using GATE wave, BOMEX ATEX and Arctic air mass data sets, *Quart. J. Roy. Meteorol. Soc.*, **112**:677-709.
- Bleck, R., Hanson, H.P., Hu, D., and Kraus E.B., 1989, Mixed-layer-thermocline interaction in a three-dimensional isopycnic coordinate model, *J. Phys. Oceanogr.*, **19**: 1417-1439.
- Bleck, R., Rooth, C., Hu, D., and Smith, L.T., 1992, Salinity-driven thermocline transients in a wind- and thermohaline-forced isopycnic coordinate model of the North Atlantic, *J. Phys. Ocean.*, **22**:1486-1505.
- Bogatyrev, B.G., 1990, Modeling of plant communities dynamics on the tundra-taiga boundary under climate changes, in *Proceedings of the International Symposium Northern forests: State, dynamics, anthropogenic influence*, Moscow, v. iii, p. 12-18 [in Russian, English resume].
- Bryan, F., 1986, High latitude salinity effects and interhemispheric thermohaline circulations. *Nature*, **305**: 301-304.
- Bryan, K., 1984, Accelerating the convergence to equilibrium of ocean-climate models, *J. Phys. Oceanogr.*, **14**: 663-673.
- Budyko, M.I., 1969, The effect of solar radiation variations on the climate of the earth, *Tellus*, **21**:611-619.
- Carissimo, B.C., Oort, A.M., and Vonder Haar, T.H., 1985, Estimating the meridional energy transports in the atmosphere and the ocean, *J. Phys. Oceanogr.*, **15**: 82-91.
- Cox, C., and Munk, W., 1956, Slopes of the sea surface deduced from photographs of the sun glitter, *Bull. Scripps Inst. Oceanogr.*, **6**:401-488.
- Cubasch, U., Hasselmann, K., Höck, H., Maier-Reimer, E., Mikolajewicz, U., Santer, B.D., and Sausen, R., 1991, *Time-dependent Greenhouse Warming Computations with a Coupled Ocean-atmosphere Model*, Max-Planck-Institut für Meteorologie, Hamburg, Report No. 67, ISSN 0937-1060, 18 p.
- Deardorff, J.W., 1967, Empirical dependence of the eddy coefficient for heat upon stability above the lowest 50 m., *J. Appl. Meteor.*, **6**:631-643.
- Deardorff, J.W., 1968, Dependence of air-sea transfer coefficients on bulk stability, *J. Geophys. Res.*, **73**:2549-2557.

- Deardorff, J.W., 1972, Parameterization of the planetary boundary layer for use in general circulation models, *Mon. Wea. Rev.*, **100**(2):93–106.
- Dickinson, R.E., Henderson-Seller, A., Kennedy, P.J., and Wilson, M.F., 1986, Biosphere–Atmosphere Transfer Scheme (BATS) for the NCAR Community Climate Model, NCAR/TN-275+STR, NCAR TECHNICAL NOTE, Boulder, Colorado, 69 p.
- Dobryshman, E.M., 1980, Dynamics of the equatorial atmosphere, *L., Hydrometeoizdat*, 287 p. [in Russian].
- Doronin, Yu.P., 1969, Thermal Interaction of the Atmosphere and the Hydrosphere in the Arctic, Israel Program for Scientific Translations, Jerusalem, 1970, 244 p. [NTIS N71-15668].
- Ducoudré, N.I., Laval, K., and Perrier, A., 1993, SECHIBA, a new set of parameterizations of the hydrolic exchanges at the land-atmosphere interface within the LMD atmospheric general circulation model, *Journal of Climate*, **6**:248–273.
- Dushkin, P.K., Lomonosov, E.G., and Luinin, Yu.N., 1960, A test of numerical humidity, cloudiness and precipitation forecast method using a computer, *Meteorology and Hydrology*, No. 12, p. 3–12 [in Russian].
- Esbensen, S.K., and Y.Kushnir, 1981, The heat budget of the global ocean: an atlas based on estimates from surface marine observations. Climate Research Institute, Oregon State University, Report N 29.
- Feigelson, E.M., ed., 1989, Radiative properties of cirrus clouds, *M., Nauka*, 224 p. [in Russian].
- Ganopolski, A.V., 1988, A role of wind synoptical variability in formation of the vertical thermal structure of the upper ocean layer, *Marine Hydrophysical J.*, N 6: 23-28 [in Russian].
- Ganopolski, A.V., 1991, A multilayer model for the ocean seasonal variability, *Oceanology*, 31: 892-897 [in Russian].
- Garrat, J.R., 1977, Review of drag coefficients over oceans and continents, *Mon. Wea. Rev.*, **105**:915–928.
- Golitsyn, G.S., and Demchenko, P.F., 1980, Statistical properties of a simple energy balance climate model, *Izvestia Acad. Sciences USSR, FAO*, **16**(12):1235–1242 [in Russian].
- Goudriaan, J., and Ketner, P., 1984, A simulation study for the global carbon cycle, including man's impact on the biosphere, *Climate Change*, **6**:167–192.
- Hansen, J., Russel, G., Rind, D., Stone, P., Lacis, A., Lebedeff, S., Ruedy, R., and Travis, L., 1983, Efficient three-dimensional global models for climate studies: Models I and II, *Mon. Wea. Rev.*, **111**(4):609–662.
- Hartmann, D.L., Ramanathan, V., Berrior, A., and Hunt, G.E., 1986, Earth radiation budget data and climate research, *Reviews of Geophysics*, **24**(2):439–468.
- Hasselmann, K., and von Storch, H., 1992, Concept of a Global-Environment-and-Man (GEM) model, Max Planck Institut für Meteorologie, Second International Conference on Modelling of Global Climate Change and Variability, Abstracts, p. 29.

- Hellerman, S. and M. Rosenstein, 1983, Normal monthly wind stress over the world ocean with error estimates, *J. Phys. Oceanogr.*, 13: 1093-1104.
- Hibler W.D., 1979, Dynamic thermodynamic sea ice model, *J. Phys. Ocean.*, 17: 815-846.
- Holdridge, L.R., 1967, *Life zone ecology*, Tropical Science Center, San Jose.
- Holland, W.R., 1977, Ocean general circulation models, *The Sea*, 6(5):3-45.
- Houghton, J.T., Jenkins, G.J., and Ephraums, J.J., eds., 1990, *Climate Change. The IPCC Scientific Assessment*, Cambridge University Press, 365 p.
- Hsiung, J., 1985, Estimates of global oceanic meridional heat transport, *J. Phys. Oceanogr.* 15: 1405-1413.
- Huang, R.X., and Bryan K., 1987, A multilayer model of the thermohaline and wind-driven circulation, *J. Phys. Ocean.*, 17: 1909-1924.
- Hummel, J.R., and Kuhn, W.R., 1981, Comparison of radiative-convective models with constant and pressure-dependent lapse rates, *Tellus*, 33:254-261.
- Jäger, L., 1976, Monatskarten des Niederschlags für die ganze Erde, *Bericht Deutscher Wetterdienst*, 18(139):38.
- Kamenkovitch, V.M., 1973, The principles of the ocean dynamics, L., *Hydrometeoizdat*, 240 p. [in Russian].
- Karol', I.L., and Rozanov, E.V., 1982, Radiative-convective climate models, *Izvestia Acad. Sciences USSR, FAO*, 18(11):1179-1191 [in Russian].
- Kellomäki *et al.*, 1992, A simulation model for the succession of the boreal forest ecosystem, *Silva Fennica*, 26(1):1-18.
- Kitaigorodsky, S.A., and Miropolsky, Yu.Z., 1970, On the theory of the active layer of open ocean, *Izvestia Acad. Sciences USSR, FAO*, 6(2):178-188 [in Russian].
- Kowalczyk, E.A., Garratt, J.R., and Krummel, P.B., 1991, A soil-canopy scheme for use in a numerical model of the atmosphere — 1D stand-alone model, CSIRO, Australia, Technical Paper No. 23, CSIRO division of atmospheric research, 56 p.
- Krapivin, V.F., Sviredjev, Yu.M., and Tarko, A.M., 1982, *Mathematical modelling of the global biospheric processes*, M. Nauka, pp. 272 [In Russian].
- Kraus, E.B., and Turner, J.S., 1967, A one-dimensional model of the seasonal thermocline — II. The general theory and its consequences, *Tellus*, 19(1):98-105.
- Landsberg, H.E., (ed), 1985, *World survey of climatology*, V 1A: *General climatology 1A*, Elsevier, Amsterdam - London - New York - Tokyo, 224 p.
- Leemans, R., 1990, Possible change in natural vegetation patterns due to a global warming. IIASA, Laxenburg, Austria, WP-90-08.

- Lemke, P., 1977, Stochastic climate models. Part 3. Application to zonally averaged models, *Tellus*, **29**(5):387-392.
- Lorenz, E.N., 1967, The nature and theory of the general circulation of the atmosphere, *WMO*, 161p.
- Maier-Reimer, E., and Hasselman, K., 1987, Transport and storage of CO₂ in the ocean - an inorganic ocean-circulation carbon cycle model. *Climate Dynamics*, 2: 63-90.
- Maier-Reimer, E., Hasselman, K., Olbers, D., and Willebrand, J., 1987, An ocean circulation model for climate studies. Techn. Report, Max-Planck-Institut für Meteorologie, Hamburg.
- Makhover, Z.M., 1983, Climatology of the tropopause, *L., Hydrometeoizdat*, 255 p. [In Russian].
- Manabe, S., and Bryan, K., 1972, Climate and ocean circulation, *L., Hydrometeoizdat*, 192 p. [in Russian].
- Manabe, S., Stouffer, 1988, Two stable equilibria of a coupled ocean-atmosphere model, *J. Climate*, **1**:841-866.
- Manabe, S., Stouffer, R.J., Spelman, M.J., and Bryan, K., 1991, Transient response of a coupled ocean-atmosphere model to gradual changes of atmospheric CO₂. Part I: Annual mean response, *J. Climate*, **4**:785-818.
- Manabe, S., Spelman, M.J., and Stouffer, R.J., 1992, Transient responses of a coupled ocean-atmosphere model to gradual changes of atmospheric CO₂. Part II: Seasonal response, *Journal of Climate* **5**:105-126.
- Manuilova, N.I., Mokhov, I.I., and Petoukhov, V.K., 1992, Estimation of the influence of hydrological cycle characteristics on the sensitivity of global climate to anthropogenic impacts, *Meteorology and Hydrology*, No. 1, p. 44-51 [in Russian].
- Matveyev, Yu.L., and Matveyev, L.T., 1984, Physical-statistical analysis of the global cloudiness field, *Izvestia Acad. Nauk USSR, FAO*, 20, No. 11, 1042-1054 [In Russian].
- McMurtrie, R.E. *et al.*, 1992, Modifying existing forest growth models to take account of effects of elevated CO₂, *Aus. J. Bot.*, **40**:657-677.
- Moeng, C.-H., and Randall, D.A., 1984, Problems in simulating the stratocumulus-topped boundary layer with a third order closure model, *J.A.S.*, **41**:1588-1600.
- Mokhov, I.I., and Petoukhov, V.K., 1978, Parameterization of thermal radiation fluxes for climatic models, Preprint of the Institute of Atmospheric Physics of the Academy of Sciences of the USSR, Moscow, No. 3, 34 p. [in Russian].
- Mokhov, I.I., Mokhov, O.I., Petoukhov, V.K., and Khairullin, R.R., 1992, Tendencies of eddy activity trends in the atmosphere under global climate changes, *Izvestia Acad. Russia, FAO*, **28**(1):11-26 [in Russian].
- Mokhov, I.I., Petoukhov, V.K., and Rusin, N.N., 1983, Sensitivity of mass and heat exchange of the Antarctic sheet surface to climatic changes, *Meteorology and Hydrology*, No. 11, p. 53-59 [in Russian].

- Monin, A.S., and Yaglom, A.M., 1965, Statistical hydrodynamics. Part I, M., *Nauka*, 640 p. [in Russian].
- Monin, A.S., and Yaglom, A.M., 1967, Statistical hydrodynamics. Part II, M., *Nauka*, 720 p., [in Russian].
- Munk, W.H., 1950, On the wind-driven ocean circulation, *J. Meteorol.*, **7**(2):79-93.
- Needler, G.T., 1967, A model for thermohaline circulation in an ocean of finite depth, *J. Marine Res.*, **25**(3):329-343.
- Needler, G.T., 1971, Thermocline models with arbitrary barotropic flow, *Deep-Sea Res.*, **18**(9):895-904.
- North, G., 1975, Theory of energy balance climate models, *J. Atmos. Sci.*, **32**:2033-2043.
- Oberhuber, J., 1993a, Simulation of the Atlantic circulation with a coupled sea ice-mixed layer-isopycnal general circulation model. Part I: Model description, *J. Phys. Oceanogr.*, **23**: 808-829.
- Oberhuber, J., 1993b, Simulation of the Atlantic circulation with a coupled sea ice-mixed layer-isopycnal general circulation model. Part I: Model experiment, *J. Phys. Oceanogr.*, **23**: 830-845.
- Oort, A.H., and Rasmusson, E.M., 1971, Atmospheric circulation statistics, NOAA Prof. Pap. 5, Rockville, pp. 323.
- Oort, A.H., 1983, Global atmospheric circulation statistics, 1958-1973, NOAA Prof. Pap. 14, Rockville, pp. 180.
- Ou, S.-C.S., and Liou, K.-N., 1984, A two-dimensional radiation-turbulence climate model. I. Sensitivity to cirrus radiation properties, *J. Atmos. Sci.*, **41**:2289-2309.
- Pedlosky, J., 1979, *Geophysical Fluid Dynamics*, Springer-Verlag, New York, 619 p.
- Petoukhov, V.K., 1976, Zonally averaged model of heat and moisture exchange in atmosphere underlying ocean layer system, *Izvestia Acad. Sciences USSR, FAO*, **12**(11):1130-1142 [in Russian].
- Petoukhov, V.K., 1980, Zonal climatic model of heat and moisture exchange in the atmosphere over underlying layer, in *Physics of the atmosphere and the problem of climate*, G.S. Golitsyn, and A.M. Yaglom, eds., M., *Nauka*, p. 8-41 [in Russian].
- Petoukhov, V.K., 1990, Thermodynamical approach to macroturbulent heat, humidity and momentum transfer description in climatic models, in *Investigations of eddy dynamics, atmospheric energetics and the problem of climate*, E.G. Nikiforov and N.Ph. Romanov, eds., L., *Hydrometeoizdat*, p. 156-171 [in Russian].
- Petoukhov, V.K., 1991, Dynamical-statistical modelling of large-scale climatic processes, Ph.D. B. Leningrad Hydrometeorological Institute, St. Petersburg, 431 p. [in Russian].
- Petoukhov, V.K., and Manuilova, N.I., 1984, Estimation of some climate-forming factors in a simple thermodynamical climate model, *Meteorology and Hydrology*, No. 10, p. 31-37 [in Russian].

- Polglase, P.J., and Wang, Y.P., 1992, Potential CO₂-enhanced carbon storage by the terrestrial biosphere, *Aus. J. Bot.*, **40**:641–656.
- Polyak, I.I., 1975, Numerical methods of observation analysis, *L., Hydrometeoizdat*, 212 p. [in Russian].
- Rasool, S.I., and Schneider, S.H., 1971, Atmospheric carbon dioxide and aerosols: Effects on large increases on global climate, *Science*, **173**:138–141.
- Resnjansky, Yu.D., 1976, Parameterization of dissipation of integral energy in the upper ocean layer, *Izvestia USSR Academy*, 11: 726–733 [In Russian].
- Saltzman, B., 1978, Statistical–dynamical models of the terrestrial climate, *Adv. of Geophys.*, **20**:183–304.
- Saltzman, B., and Ashe, S., 1976, The variance of surface temperature due to diurnal and cyclone-scale forcing, *Tellus*, **28**(4):307–322.
- Sarkisyan, A.S., 1977, Numerical analysis and forecast of sea currents, *Hydrometeoizdat*, 182 p. [in Russian].
- Schlesinger, M.E., Oh, J.-H., and Rosenfeld, D., 1988, A parameterization of the evaporation of rainfall, *Mon. Wea. Rev.*, 116, No. 10, 1887–1895.
- Sellers, P.J., Mintz, Y., Sudy, C., and Dalcher, A., 1986, A Simple Biosphere Model (SiB) for use within general circulation models, *J.A.S.*, **43**(6):505–531.
- Sellers, W.D., 1969, A climate model based on the energy balance of the earth–atmosphere system, *J. Appl. Meteorol.*, **8**(3):392–400.
- Semtner, A.J., 1976, A model for the thermodynamic growth of sea ice in numerical investigations of climate, *J. Phys. Oceanogr.*, 6: 409–425.
- Talley, L.D., 1984, Meridional heat transports in the Pacific Ocean, *J. Phys. Oceanogr.* 14: 231–241.
- Tarasova, T.A., 1992, Evaluation of aerosol and cirrus cloud single scattering albedo using ground-based radiation measurements, Proceedings of International Radiation Symposium, Tallinn, August 1992, p. 10–17.
- Tarasova, T.A., and Feigelson, E.M., 1981, An accounting of aerosol effects in radiative heat exchange, *Izvestia Acad. Sciences USSR, FAO*, **17**(12):1330–1333 [in Russian].
- Tarko, A.M., Bogatyrev, B.G., Kirilenko, A.P., and Udalkina, M.V., 1989, Modelling of the global and regional changes of carbon circle in the biosphere, Preprint of the Computing Center USSR Acad. of Sci., Moscow, pp. 39 [In Russian].
- Veltischev, N.N., Tarasova, T.A., and Frol'kis, V.A., 1990, Practical methods of accounting of solar radiation absorption by water vapor in different radiative schemes, Preprint of the Institute of Atmospheric Physics of the Academy of Sciences of the USSR, Moscow, No. 1, 27 p. [in Russian].

- Venevsky, S.V., 1992: Terrestrial vegetation in Asia as one of possible regulators in climate change. Proceedings of the 8th Conference of the International Society for Ecological Modelling, Kiel, p. 201-211.
- Vinnichenko, N.K., Pinus, N.Z., Schmeter, S.M., and Shur, G.N., 1968, Turbulence in free atmosphere, *L., Hydrometeoizdat*, 336 p. [in Russian].
- Vinnikov, K.Ya., 1986, Sensitivity of climate, *L., Hydrometeivzdat*, 224 p. [in Russian].
- Wyngaard, J.C., and Le Mone, M.A., 1980, Behaviour of the refractive index structure parameter in the entraining convective boundary layer, *J.A.S.*, 37:1573-1585.
- Zilitinkevitch, S.S., 1970, Dynamics of the atmospheric boundary layer, *L., Hydrometeoizdat*, 291 p. [in Russian].
- Zalesak, S., 1979, Fully multidimensional flux-corrected transport algorithms for fluids, *J. Comput. Phys.*, 31: 335-362.